Spring 5-31-2004

Multi-rate access schemes and successive interference cancellation for wireless multimedia MC-CDMA communications

Mizhou Tan
New Jersey Institute of Technology

ABSTRACT

MULTI-RATE ACCESS SCHEMES AND SUCCESSIVE INTERFERENCE CANCELLATION FOR WIRELESS MULTIMEDIA MC-CDMA COMMUNICATIONS

by
Mizhou Tan

To catch up with the fast changes of the information challenges, providing multimedia services has become a very important requirement for future wireless communications. A proper system, capable of supporting multi-rate transmissions as well as handling high quality of service (QoS) requirements in hostile wireless communication environments, should be sought. Multi-carrier CDMA (MC-CDMA), a combination of multi-carrier modulation (MCM) and direct-sequence CDMA (DS-CDMA), appears to be one of the most elegant solutions. In this dissertation, four multi-rate access schemes, termed uncoded fixed spreading length (UFSL), coded fixed spreading length (CFSL), multi-code fixed spreading length (MFSL) and variable spreading length (VSL), are constructed for MC-CDMA. Due to different sub-carrier assignment strategies, they present different properties in spectral utilization efficiency (SUE), rate matching capability, receiver structure and bit-error-rate (BER) performance in correlated Rayleigh fading channels. With these schemes, different information traffic such as voice, video and higher rate data can be transmitted seamlessly through one MC-CDMA infrastructure.

The performance of the multi-rate MC-CDMA is mainly limited by multiple access interference (MAI). For example, in the MFSL MC-CDMA systems, the interference is not only presented among different users, but also among different symbols of the same user transmitted in parallel on different spreading codes. To mitigate this problem, a nonlinear zero-forcing successive interference cancellation (ZF-SIC) receiver and a minimum mean square error SIC (MMSE-SIC) receiver are applied in

the MFSL MC-CDMA systems. It is well known that SIC is sensitive to the receive power distribution. By providing channel state information (CSI) at the receiver and reliable feedback of power distribution from the receiver to the transmitter, SIC can be integrated with power distribution control (PDC), which improves the system capacity significantly.

In this dissertation, the PDC algorithms, under both a short-term power constraint (STPC) and a long-term power constraint (LTPC) are investigated for two different SIC receivers. For the ZF-SIC receiver, the PDC under the equal BER criterion, which ensures the same performance after SIC for all parallel transmit symbols, is first considered. It is found that for a multi-code system, such equal BER PDC is only suboptimal from the viewpoint of minimizing each user's BER, hence, an optimal PDC algorithm is proposed, which significantly outperforms the equal BER PDC, particularly under the STPC and highly-loaded systems. For the MMSE-SIC, the PDC under the equal BER criterion is derived, which cancels interference very effectively, resulting in a performance of a fully-loaded system close to the single user bound (SUB). In comparison to the nonlinear matched-filter SIC (MF-SIC) with the equal BER PDC, studied extensively in the literature, the ZF-SIC and MMSE-SIC with the proposed PDC algorithms present remarkable performance advantage.

Finally, the effect of channel estimation errors (CEE) on the performance of the MMSE-SIC with the equal BER PDC is analyzed. A method of second-order approximation is used to estimate the mean excess MSE (MEMSE) of the parallel transmit symbols, under a given decision order. The approximation accuracy is confirmed by simulation results. Furthermore, it is also interesting to find out that the MMSE-SIC with the equal BER PDC presents significant robustness to CEE.

MULTI-RATE ACCESS SCHEMES AND SUCCESSIVE INTERFERENCE CANCELLATION FOR WIRELESS MULTIMEDIA MC-CDMA COMMUNICATIONS

by
Mizhou Tan

A Dissertation
Submitted to the Faculty of
New Jersey Institute of Technology
in Partial Fulfillment of the Requirements for the Degree of
Doctor of Philosophy in Electrical Engineering

Department of Electrical and Computer Engineering, NJIT

May 2004

APPROVAL PAGE

MULTI-RATE ACCESS SCHEMES AND SUCCESSIVE INTERFERENCE CANCELLATION FOR WIRELESS MULTIMEDIA MC-CDMA COMMUNICATIONS

Mizhou Tan

Dr. Yeheskel Bar-Ness, Dissertation Advisor — Date
Distinguished Professor, Department of Electrical and Computer Engineering, NJIT

Dr. Ali Abdi, Committee Member — Date
Assistant Professor, Department of Electrical and Computer Engineering, NJIT

Dr. Alexander M. Haimovich, Committee Member — Date
Professor, Department of Electrical and Computer Engineering, NJIT

Dr. Zoi-heleni Michalopoulou, Committee Member — Date
Associate Professor, Department of Mathematical Sciences, NJIT

Dr. Laurance B. Milstein, Committee Member — Date
Professor, Department of Electrical and Computer Engineering, UCSD

BIOGRAPHICAL SKETCH

Author: Mizhou Tan

Degree: Doctor of Philosophy

Date: May 2004

Undergraduate and Graduate Education:

- Doctor of Philosophy in Electrical Engineering
  New Jersey Institute of Technology, 2004
- Master of Science in Electrical Engineering
  Sichuan University, Chengdu, Sichuan, P. R. China, 1996
- Bachelor of Science in Electrical Engineering
  Sichuan University, Chengdu, Sichuan, P. R. China, 1993

Major: Electrical Engineering

Presentations and Publications:

Mizhou Tan and Yeheskel Bar-Ness, "Effect of channel estimation errors on the performance of MMSE-SIC with equal BER power control," *submitted to IEEE Vehicular Technology Conference (VTC) 2004-Fall*, March, 2004.

Christian Ibars, Mizhou Tan and Yeheskel Bar-Ness, "Equal SNR power distribution for generalized DFE structures," *submitted to the Seventh International Symposium on Wireless Personal Multimedia Communications (WPMC)*, March, 2004.

Mizhou Tan and Yeheskel Bar-Ness, "Optimal power distribution control for multicode MC-CDMA with zero-forcing successive interference cancellation," *Proc. of IEEE Wireless Communication and Networking Conference (WCNC)*, March, 2004.

Mizhou Tan and Yeheskel Bar-Ness, "Equal BER power distribution control for multicode MC-CDMA with MMSE successive interference cancellation," *to appear in proceeding of IEEE International Conference on Communications (ICC)*, June, 2004.

Mizhou Tan, Christian Ibars and Yeheskel Bar-Ness,"Optimal power distribution control for multicode MC-CDMA with zero-forcing successive interference cancellation," *to appear in the EURASIP Journal on Applied Signal Processing*, March, 2004.

Mizhou Tan and Yeheskel Bar-Ness, "Equal BER power distribution control for uplink MC-CDMA with MMSE successive interference cancellation," *to appear in IEEE Communications Letters*, 2004.

Mizhou Tan, Pingping Zong and Yeheskel Bar-Ness, "Multi-rate access schemes for MC-CDMA," *published in the International Journal of Wireless Personal Communications (WPC)*, vol. 27, pp. 149 –182, 2003.

Mizhou Tan and Yeheskel Bar-Ness, "OFDM peak-to-average power ratio reduction by combined symbol rotation and inversion with reduced complexity," *Proc. of IEEE Global Communications Conference (Globecom)*, San Francisco, California, vol. 2, pp. 605 –610, Dec., 2003.

Mizhou Tan, Christian Ibars and Yeheskel Bar-Ness, "Performance comparison of MC-CDMA and OFDMA with adaptive resource allocation in Infostations," *Proc. of 37th Annual Conference on Information Sciences and Systems (CISS)*, Baltimore, MD, April, 2003.

Christian Ibars, Mizhou Tan and Yeheskel Bar-Ness, "Adaptive transmission for Infostations: a MC-CDMA implementation," *Proc. of Asilomar Conference on Signals, Systems and Computers*, vol. 2, pp. 1223 –1227, Pacific Grove, CA, Nov., 2002.

Mizhou Tan, Christian Ibars and Yeheskel Bar-Ness, "Rate-adaptive convolutional coded fixed spreading length (CCFSL) multi-rate transmission schemes for MC-CDMA ," *Proc. of the Fifth International Symposium on Wireless Personal Multimedia Communications (WPMC)*, vol. 2, pp. 663 –667, Honolulu, HI, Oct., 2002.

Mizhou Tan and Yeheskel Bar-Ness, "Performance comparison of the multi-code fixed spreading length (MFSL) scheme and variable spreading length (VSL) scheme for multi-rate MC-CDMA," *Proc. of IEEE International Symposium on Spread Spectrum Techniques and Applications (ISSSTA)*, vol. 1, pp. 108 –112, Prague, Czech Replublic, Sept., 2002.

Mizhou Tan and Yeheskel Bar-Ness, "Maximum spectral utilization efficiency multi-code FSL scheme for multi-rate MC-CDMA," *Proc. of 3G Wireless*, San Francisco, CA, May, 2002.

Mizhou Tan, Jie Cheng and Yeheskel Bar-Ness, "OFDM peak power reduction by a novel coding scheme with threshold control," *Proc. of IEEE Vehicular Technology Conference (VTC) 2001-Fall*, vol. 2, pp. 669 –672, Atlantic City, NJ, Oct., 2001.

to my dear father

ACKNOWLEDGMENT

This work could not have been accomplished by myself alone. It required guidance, support, understanding and love of so many people. First and foremost, I would like to express my deepest gratitude and respect for my advisor, Dr. Yeheskel Bar-Ness, from whom I learned about quality research and hard work. His guidance and encouragement during my studies were invaluable. Also, I would like to express my sincere appreciation to the members of the dissertation committee: Dr. Larry Milstein, Dr. Alexander Haimovich, Dr. Ali Abdi and Dr. Zoi-heleni Michalopoulou. Their support and insightful comments have improved the quality of this dissertation significantly.

I was lucky to have the friendship of the people in Center for Communications and Signal Processing Research, which made the past few years a very exciting and enjoyable time. Everyone in the center gave me so much assistance, especially when I met difficulties. I would like to express my thanks to Christian Ibars and Jianming Zhu for their unselfish help with my research. Miss Marlene Toeroek, did so many things for me, making my life much happier and easier.

Finally, I would like to dedicate this work to my family for their unconditional love and support, without which, this work could not have been done. Although my dear father could not wait for this day, his wisdom, love and strength will always encourage me to take challenges bravely in the rest of my life.

TABLE OF CONTENTS

TABLE OF CONTENTS
(Continued)

Chapter **Page**

TABLE OF CONTENTS
(Continued)

Chapter **Page**

LIST OF FIGURES

Figure **Page**

LIST OF FIGURES
(Continued)

Figure **Page**

LIST OF FIGURES
(Continued)

Figure **Page**

CHAPTER 1

INTRODUCTION

1.1 Overview

Multimedia service, whose contents increase and differentiate with the changing information challenges, has become an inevitable requirement for wireless communications. For example, the International Mobile Telecommunications in the year 2000 (IMT-2000), corresponding to the third-generation (3G) mobile systems, aims to support at least $144Kbps$ (preferable $384Kbps$ for high-mobility users with wide-area coverage and $2Mbps$ for low-mobility users with local coverage). Moreover, the fourth-generation (4G) systems, planned to be put in service around 2010, must meet the requirement of broadband multimedia services up to 20-$100Mbps$ in downlink and 2-$20Mbps$ in uplink, in any wireless communication environments [1, 2].

Due to the need for flexibility in handling multiple data rates, direct-sequence CDMA (DS-CDMA) was considered as a suitable candidate for supporting multimedia services in wireless communications, with which, different multi-rate access schemes have been studied [3]. Nevertheless, it has been pointed out that DS-CDMA is not a good choice especially for high rate data communications, because of the increased computational complexity of a RAKE receiver and the higher severity of inter-symbol interference (ISI), caused by the multi-path fading channels [4]. That is, the hostile nature of wireless channels, which mainly limits the transmission rate, must be taken into consideration when designing a system supporting multimedia services. Among many techniques, multi-carrier modulation (MCM) appears to be one of the most elegant solutions since by certain system structure, each sub-channel becomes frequency non-selective, which significantly simplifies the receiver design [5, 6].

In recent years, different multiple access schemes based on MCM have been proposed and extensively studied [7–10]. Among them, multi-carrier CDMA (MC-CDMA), a combination of MCM and DS-CDMA, has drawn considerable attentions in both industrial and academic communities [11]. With this system, each transmit symbol is spread by a preassigned signature code and each chip modulates a different sub-carrier (frequency domain spreading), making frequency diversity available to be exploited. By inserting a guard interval (GI) (cyclic prefix) of proper length, the symbol duration can be extended to include the maximum delay spread so that cyclic convolution is enabled and ISI is avoided. Moreover, due to the overlapped sub-carrier spectra (orthogonal), MC-CDMA can achieve higher spectral utilization efficiency (SUE). Also, with the aid of the fast Fourier transform (FFT), discrete-time modulation and demodulation can be easily performed [8, 12]. Due to all these advantages and the flexibility to generate different data rates as with the DS-CDMA, MC-CDMA became very attractive for supporting multimedia services in future wireless communications [13]. In fact, designing multi-rate access schemes for supporting different data rates and ensuring high quality of service (QoS) requirements are the two very important issues in the multi-rate MC-CDMA systems.

1.2 Multi-rate Access Schemes for MC-CDMA

To preserve sub-carrier signals orthogonality, in a single-rate MC-CDMA, the frequency separation of adjacent sub-carriers should be chosen as multiple integers of the signal transmission rate. Therefore, for a multi-rate MC-CDMA, different rate users have different requirements for the frequency spacing of adjacent sub-carriers. The strategies of sub-carrier assignment become very crucial, which should be well handled, not only to protect different signals from inter-carrier interference (ICI) but also to ensure high spectral utilization efficiency (SUE).

With different sub-carrier assignment strategies, four MC-CDMA multi-rate access schemes have been proposed, which can be classified into two categories: the fixed spreading length (FSL) and the variable spreading length (VSL). With the FSL scheme, different rate users share the same set of sub-carriers, while with the VSL scheme, different rate users utilize different sets of sub-carriers. Three different FSL schemes have been studied, which are termed uncoded fixed spreading length (UFSL) [14], coded fixed spreading length (CFSL)[1] [15, 16] and multi-code fixed spreading length (MFSL) [17, 18]. With the UFSL scheme, the frequency spacing of adjacent sub-carriers equals the bandwidth of the highest rate users. To protect different rate signals from ICI, the highest rate should be an integer multiple of any lower rates. Since the frequency separation of adjacent sub-carriers must be at least twice the bandwidth of any lower rate users, the non-overlapped spectra for these users result in a loss of SUE and consequently a reduction in system capacity. To alleviate this problem, the CFSL scheme was proposed, in which the lower rate bits are encoded to become the highest rate, making the multi-rate system equivalent to a single highest rate system. The coding gain achieved compensates for the SUE loss of lower rate users and hence improves their bit-error-rate (BER) performance. This idea was first implemented by a block coding method in a dual-rate system [15]. To achieve better performance, greater flexibility in rate matching and simpler decoder, a rate compatible punctured convolutional (RCPC) coding method was proposed [16]. However, since in both the UFSL and CFSL schemes, the frequency spacing of adjacent sub-carriers equals the bandwidth of the highest rate users, the number of sub-carriers might be limited, especially when a very high rate is supported by the system. To mitigate this disadvantage, the MFSL scheme was proposed, in which the frequency spacing of adjacent sub-carriers equals the bandwidth of the lowest rate

[1]Although the terms uncoded and coded were used, earlier channel error-correcting coding of the data to obtain high performance is possible. In this context, CFSL means to add coding to the lower rate users.

users. With this sub-carrier assignment strategy, maximum SUE can be achieved for all different rate users. To preserve sub-carrier signals orthogonality, a higher rate stream is split into a plurality of the lowest rate substreams, each assigned a different spreading code with the same processing gain. To realize this transformation, any higher rate should be an integer multiple of the lowest rate. Since more sub-carriers are utilized, each user is assigned a longer spreading code with better cross-correlation property, which provides stronger interference suppression capability[2]. Apart from these three FSL schemes, in the VSL scheme, different rate users employ a different set of sub-carriers [19]. Although this scheme ensures high SUE for different rate users, ICI might be produced due to the loss of signals orthogonality between sub-carriers. However, it has been found that by properly selecting the spreading codes, the ICI can be eliminated, which ensures the feasibility of this scheme [13].

Due to different sub-carrier assignment strategies, different receivers are designed for different schemes. Minimum mean square error combining (MMSEC) detection is employed for the purpose of joint energy combining and interference cancellation. The BER performances in correlated Rayleigh fading channels are investigated by both theoretical analysis and simulation results. It is found that compared with other schemes, the MFSL and CFSL schemes present better performance, greater flexibility in rate matching and lower complexity, hence, more appropriate for practical applications.

1.3 Successive Interference Cancellation

The performance of the multi-rate MC-CDMA system is mainly limited by multiple access interference (MAI). In the MFSL MC-CDMA systems, for example, the interference is not only presented among different users but also among different symbols transmitted in parallel on different spreading codes of the same user, which is termed

[2]It is assumed that the length of spreading codes equals the number of sub-carriers in MC-CDMA systems.

alternatively as self interference (SI). Therefore, to ensure high QoS requirements, MAI should be well handled. Among many interference cancellation schemes, successive interference cancellation (SIC) is highly desirable for its ability to increase capacity while maintaining low complexity, its compatibility to existing systems and its simple accommodation to strong error-correcting codes [20]. A zero-forcing (ZF) SIC (ZF-SIC) receiver and a minimum mean square error (MMSE) SIC (MMSE-SIC) receiver, originally proposed for single-rate DS-CDMA systems [21], are applied in the uplink MFSL MC-CDMA systems. With these SIC receivers, parallel symbols transmitted on different spreading codes are detected successively and for each symbol, ZF or MMSE detectors is employed to suppress MAI, taking advantage of Cholesky factorization (CF). It is well known that unlike other detection techniques, SIC is sensitive to the receive power distribution and it favors unequal receive power from different users. However, in a multi-code system, it is customary to let the transmit power of each user be evenly distributed among all its spreading codes, resulting in a loss of the efficiency of SIC. By providing channel state information (CSI) at the receiver and reliable feedback from the receiver to the transmitter, SIC can be integrated with power distribution control (PDC), which improves the system capacity significantly .

Since the integration of SIC and power control became an attractive solution for increasing system capacity, extensive research has been done in this area. Nevertheless, most of the work focused on a single-rate, single-carrier CDMA system with a matched-filter (MF) SIC (MF-SIC) receiver. Equal BER criterion was adopted in many references to derive the power distribution, which is suitable for a system, where all users aim to achieve comparable BER performances [20, 22–24]. In [20], it is shown that when ignoring decision errors, a geometric distribution of the receive power will provide equal BER. In [23], equal BER performance is analyzed for linear SIC[3] in AWGN channel. In [24], with nonlinear SIC, the power distribution for equal BER

[3]With the linear SIC, soft decisions are employed for interference cancellation, while with the non-linear SIC, hard decisions are employed.

is obtained using gradient search considering all error patterns. For a multi-code system, since one higher rate user can be looked upon as several virtual lowest rate users, each assigned with a single spreading code [13], the equal BER PDC is also a reasonable solution, which ensures the same BER after SIC for each virtual lowest rate user. However, from the viewpoint of minimizing the BER of each user, which is the average over all its parallel transmit symbols on different spreading codes, the equal BER is only suboptimal for a multi-code system. This motivates a search of an optimal PDC algorithm. In this dissertation, with the assumption of perfect CSI at the receiver, the PDC algorithms, under both a short-term power constraint (STPC), wherein the transmit power is kept the same for each channel realization, and a long-term power constraint (LTPC), wherein the transmit power is adapted with channel variations [25], are investigated for both SIC receivers. For the ZF-SIC, both equal BER PDC and optimal PDC algorithms are derived [26,27]. As concluded in the literature, the equal BER PDC benefits SIC significantly by increasing the reliability of earlier detected symbols. However, not surprisingly, simulation results show that the optimal PDC significantly outperforms the equal BER PDC, particularly under the STPC and highly-loaded systems. For the MMSE-SIC, only equal BER PDC is considered. Even with this suboptimal PDC strategy, interference can be suppressed very effectively, resulting in a performance very close to the single user bound (SUB) when the system is fully-loaded [28, 29]. Moreover, in comparison to the nonlinear MF-SIC with the equal BER PDC, which was extensively studied in the literature, the ZF-SIC and MMSE-SIC receiver integrated with the proposed PDC algorithms present remarkable performance advantage.

In practise, CSI is obtained from estimation, thus, channel estimation errors (CEE) are inevitable. Therefore, the analysis of the robustness of the proposed PDC algorithms with respect to CEE is of great interest and importance [30]. In this dissertation, the analysis of the effect of CEE on the system performance is only

considered for the MMSE-SIC with the equal BER PDC. A method of second-order approximation is applied to estimate the mean excess MSE (MEMSE) of the parallel transmit symbols, under a given decision order [31]. The approximation accuracy is confirmed by simulation results. Furthermore, it is also interesting to find out that the equal BER PDC makes the MMSE-SIC more robust to CEE.

1.4 Thesis Outline

In Chapter 2, following a description of a general multi-rate MC-CDMA system, four multi-rate access schemes are discussed in details. For each scheme, the sub-carrier assignment strategy, the receiver structure and the BER performance analysis are shown. Simulation results are presented for both synchronous downlink and quasi-synchronous uplink MC-CDMA in correlated Rayleigh fading channels.

In Chapter 3, the nonlinear ZF-SIC and MMSE-SIC receivers are applied in the quasi-synchronous uplink MFSL MC-CDMA systems. The SIC algorithms are described and the lower bounds (LBs) of the BER performances are derived for both receivers. Simulation results are presented and compared with the conventional linear ZF and MMSE receivers and the nonlinear MF-SIC receiver.

In Chapter 4 and 5, with the assumption of perfect CSI at the receiver, under both a STPC and a LTPC, the PDC algorithms are proposed for the ZF-SIC and MMSE-SIC receivers, respectively. The LBs are derived for all PDC algorithms and simulation results are presented and compared with the nonlinear MF-SIC receiver with the equal BER PDC proposed in the literature.

In Chapter 6, the effects of CEE on the system performance is considered for the MMSE-SIC receiver with the equal BER PDC. The MEMSE is derived by a method of second-order approximation. The robustness of the MMSE-SIC with the equal BER PDC to CEE is confirmed by both theoretical analysis and simulation results.

Finally, Chapter 7 summaries the contributions of this dissertation.

Through this dissertation, the following notations are used: scalars are unbold lower case or upper case, vectors are bold lower case and matrices are bold upper case; The symbols $(\cdot)^*$,$(\cdot)^T$and $(\cdot)^H$ are conjugate, transpose and Hermitian transpose; $\odot$, $\otimes$, $\mathrm{mod}\,(\cdot)_N$, $\lfloor(\cdot)\rfloor$, $\|\cdot\|_2$ and $\mathrm{diag}\,(\cdot)$ are element-wise multiplication, Kronecker product, modulo-N, floor, vector 2-norm and diagonal matrix operators.

CHAPTER 2

MULTI-RATE ACCESS SCHEMES FOR MC-CDMA

2.1 A General Multi-rate MC-CDMA System

Suppose that the multi-rate users are divided into G groups and the number of users and transmission rate of group g be denoted by $K^{(g)}$and $R^{(g)}$, $(g = 0, 1, \cdots, G-1)$, respectively. Assume that $R^{(g)} = L^{(g)}R^{(0)}$, with $1 = L^{(0)} < L^{(1)} < \cdots < L^{(G-1)}$. Therefore, during the bit duration $T^{(0)} = \frac{1}{R^{(0)}}$ of group 0 users, group g users transmit $L^{(g)}$ bits with bit duration $T^{(g)} = \frac{1}{R^{(g)}} = \frac{T^{(0)}}{L^{(g)}}$. Let the total available bandwidth BW be fixed. If adjacent sub-carriers are separated by Δf , then the total number of sub-carriers is

$$M = (BW - \Delta f)/\Delta f. \tag{2.1}$$

To preserve sub-carrier signals orthogonality, for group g users, Δf should be multiple integers of $\frac{1}{T^{(g)}}$, i.e., $\Delta f = N \cdot \frac{1}{T^{(g)}}, (N = 1, 2, \cdots)$. Therefore, the minimum Δf required equals $1/T^{(g)}$. In such a case, maximum number of sub-carriers can be utilized. The number of sub-carriers and the chip duration of group g are denoted by $M^{(g)}$ and $T_c^{(g)}$, respectively, with

$$T_c^{(g)} = \frac{T^{(g)}}{M^{(g)}}. \tag{2.2}$$

In the multi-rate MC-CDMA, the information bits of each user in group g are replicated into $M^{(g)}$ parallel copies and then each copy is multiplied by a chip of a preassigned signature sequence of length $M^{(g)}$ (frequency domain spreading). To avoid implementing a bank of oscillators with prohibitive complexity, a discrete-time multi-carrier modulation performed by an $M^{(g)}$-point IDFT is applied at the transmitter. Then, after parallel-to-serial (P/S) conversion, a GI (cyclic prefix) of

proper length is inserted between successive OFDM symbols (time domain) to avoid inter-symbol interference (ISI). Finally, following radio frequency (RF) upconversion, the signal $s_k(t)$ is transmitted through the fading channel. At the receiver, after RF downconversion and discarding GIs, the receive (time domain) waveform of the multi-rate MC-CDMA signal can be written as[1]

$$r(t) = \sum_{i=-\infty}^{+\infty} \left[\sum_{g=0}^{G-1} \sum_{s=(i-1)L^{(g)}+1}^{iL^{(g)}} \sum_{k=1}^{K^{(g)}} \sum_{n=1}^{M^{(g)}} a_k^{(g)} b_k^{(g)}(s) \right.$$
$$\left. \sum_{m=1}^{M^{(g)}} h_{k,m}^{(g)} c_{k,m}^{(g)} e^{j2\pi \frac{mn}{M^{(g)}}} P^{(g)}\left(t - \left(sM^{(g)} + n\right) T_c^{(g)}\right) \right] + n(t). \quad (2.3)$$

In this equation, i denotes the i^{th} lowest rate bit interval $\left[(i-1)T^{(0)}, iT^{(0)}\right)$, during which the group g users transmit $L^{(g)}$ higher rate bits. Subscript n denotes the n^{th} sample during the s^{th} higher rate bit interval $\left[(s-1)T^{(g)}, sT^{(g)}\right)$ of group g users and m denotes the m^{th} sub-carrier. $a_k^{(g)}$, $b_k^{(g)}(s) \in [1, -1]$ and $c_{k,m}^{(g)}$ denote the transmit signal amplitude, the s^{th} BPSK-modulated information bit and the m^{th} chip of the spreading code $\mathbf{c}_k^{(g)}$ for the k^{th} user in group g, respectively. The additive white Gaussian noise process $n(t)$ has zero mean and variance σ_n^2. The rectangular pulse shape function in equation (2.3) is defined as,

$$P^{(g)}(t) = \begin{cases} 1 & \left(sM^{(g)} + n - 1\right) T_c^{(g)} \le t \le \left(sM^{(g)} + n\right) T_c^{(g)} \\ 0 & otherwise \end{cases}. \quad (2.4)$$

Corresponding to the worst case of no line-of-sight (LOS) component, a Rayleigh fading channel is considered. By using a cyclic prefix of proper length, frequency-nonselective fading can be obtained over each sub-carrier, and it is assumed that during each OFDM symbol interval the channel is time-invariant. Thus, for the k^{th} user in group g, the channel can be represented by an $\left(M^{(g)} \times 1\right)$ vector $\mathbf{h}_k^{(g)} = \sqrt{q_k^{(g)}}$.

[1]In this equation, $L^{(g)}$ is assumed to be a multiple integer of $L^{(0)}, (g = 0, 1, \cdots, G-1)$ for convenience. However, it is not necessary in the CFSL scheme.

$\left[h_{k,1}^{(g)}, h_{k,2}^{(g)}, \cdots, h_{k,M^{(g)}}^{(g)}\right]^T$, where $q_k^{(g)}$ denotes the path loss of the k^{th} user in group g between the transmitter and the receiver (For simplicity, different users are assumed to undergo the same path loss, which equals 1.); $h_{k,m}^{(g)}$ $\left(m = 1, 2, \cdots, M^{(g)}\right)$ represents the fading over the m^{th} sub-carrier which is a complex Gaussian random variable with unit variance. Furthermore, due to the proximity and partial overlap of signal spectrum, correlated fading on different sub-carriers is considered. The correlation between two sub-carriers depends on the channel delay spread and the frequency separation between them, which is given by the spaced-frequency correlation function $\rho(\Delta f_{mn})$. In a wide-sense stationary uncorrelated scattering (WSSUS) channel, $\rho(\Delta f_{mn})$ is derived using the Fourier transform of the exponentially decaying power-delay profile of the channel [32,33], which can be expressed as

$$\rho(\Delta f_{mn}) = \frac{1 - j2\pi\tau_d \Delta f_{mn}}{1 + (2\pi\tau_d \Delta f_{mn})^2}, \tag{2.5}$$

where τ_d is the rms channel delay spread, defined as the square root of the second central moment of the channel's power-delay profile, and Δf_{mn} is the frequency separation between the m^{th} and n^{th} sub-carrier.

Both synchronous downlink and quasi-synchronous uplink transmissions[2] are considered. Notice that in the downlink, different rate users experience the same fading channel, while in the uplink, different rate users experience different channels, assumed independently, identical distributed (i.i.d.).

2.2 Uncoded Fixed Spreading Length (UFSL) Scheme

2.2.1 Sub-carrier Assignment

With the UFSL scheme, all different rate users share the same set of sub-carriers, whose frequency separation equals the bandwidth of the highest rate users. Therefore

[2]In a quasi-synchronous uplink MC-CDMA system, the symbol GI is designed to be larger than the maximum receive time offset. After discarding it at the receiver, the quasi-synchronous system can be analyzed as a synchronous system.

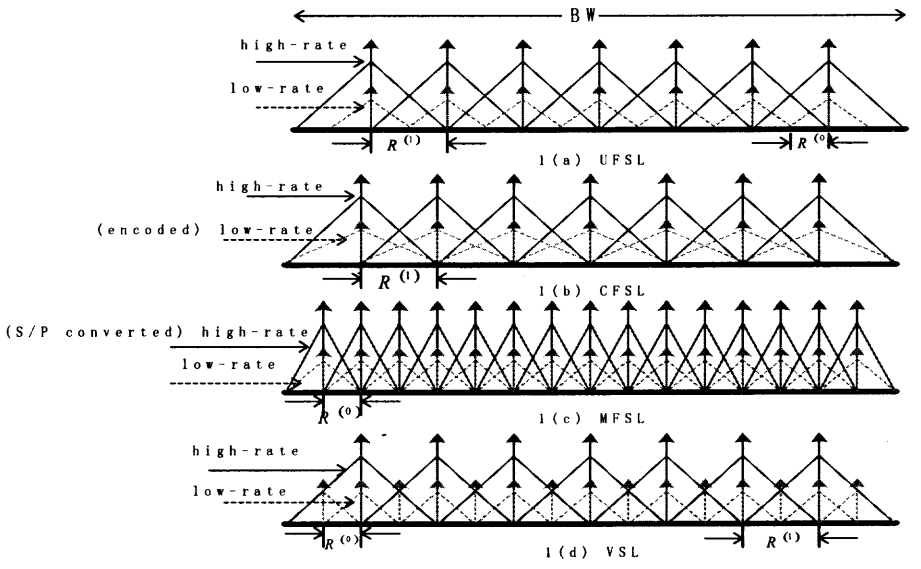

Figure 2.1 Sub-carrier assignment comparison of the dual-rate MC-CDMA schemes with rate ratio 2.

the number of sub-carriers utilized in this scheme is

$$M_U = \frac{BW - R^{(G-1)}}{R^{(G-1)}}. \tag{2.6}$$

The frequency of the m^{th} sub-carrier is, $f_m = mR^{(G-1)}, (m = 1, 2, \cdots, M_U)$. To preserve sub-carrier signals orthogonality for all different rate users, the highest rate should be an integer multiple of any lower rates, i.e., $\frac{R^{(G-1)}}{R^{(g)}}, (g = 0, 1, \cdots, G-2)$ should be an integer. Hence, by satisfying this rate ratio requirement, this sub-carrier assignment protects different rate signals from ICI. An example of a sub-carrier assignment of the dual-rate UFSL MC-CDMA scheme with rate ratio 2 is shown in Figure 2.1(a)[3]. From this figure, it is clear that in the UFSL scheme, the number of sub-carriers M_U is determined by the highest rate supported in the system. With SUE being defined as the ratio between the total used and the total available bandwidth[4], it is obvious that, in this scheme, different rate users have different SUE.

[3]For ease of drawing, the signal spectra are shown triangular and bandlimited.
[4]For simplicity, only the mainlobes of different rate signals are considered.

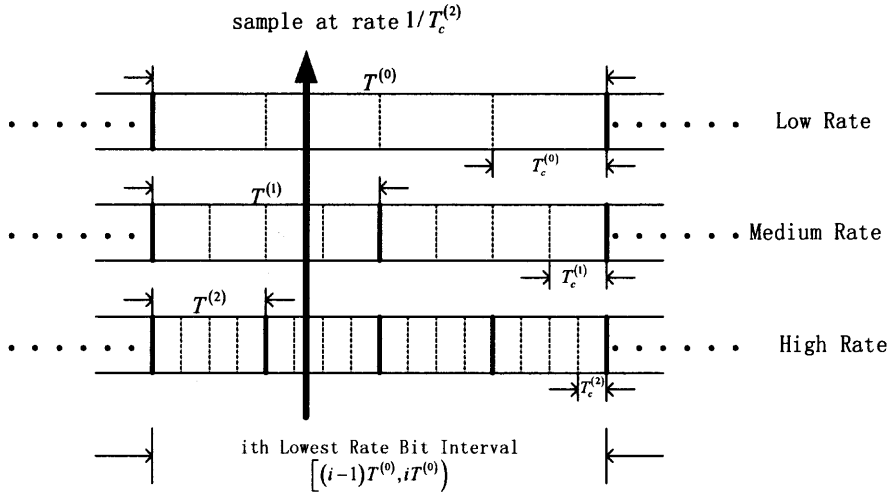

Figure 2.2 An example of the signal structure of the UFSL MC-CDMA scheme (three-rate with rate ratio $\frac{L^{(g)}}{L^{(g-1)}} = 2, (g = 1, 2)$ and $M_U = 4$).

For the group g users, the SUE can be expressed as

$$\begin{aligned} \epsilon_U^{(g)} &= 2R^{(g)}M_U/BW \\ &= 2L^{(g)}\left(BW - R^{(G-1)}\right)/\left(L^{(G-1)}BW\right). \end{aligned} \tag{2.7}$$

Apparently, different rate users have different chip duration $T_c^{(g)} = \frac{T^{(g)}}{M_U}$, hence, the UFSL scheme can be looked upon as a variable chip rate (VCR) scheme. An example of the signal structure of a three-rate UFSL MC-CDMA scheme (with rate ratio $\frac{L^{(g)}}{L^{(g-1)}} = 2, (g = 1, 2)$ and $M_U = 4$) is shown in Figure 2.2 [14]. During each lowest rate bit interval, the multi-rate MC-CDMA signal is composed of different rate signals, each has a different chip duration as shown in this figure. Notice that the time domain symbol is sampled with a duration chosen to be the smallest chip duration, to guarantee no information loss for all different rate signals. Thus, the lower rate user will be oversampled during its chip duration. Each M_U samples are processed by an IDFT for multi-carrier modulation. The block diagram of the transmitter for the UFSL scheme is shown in Figure 2.3(a).

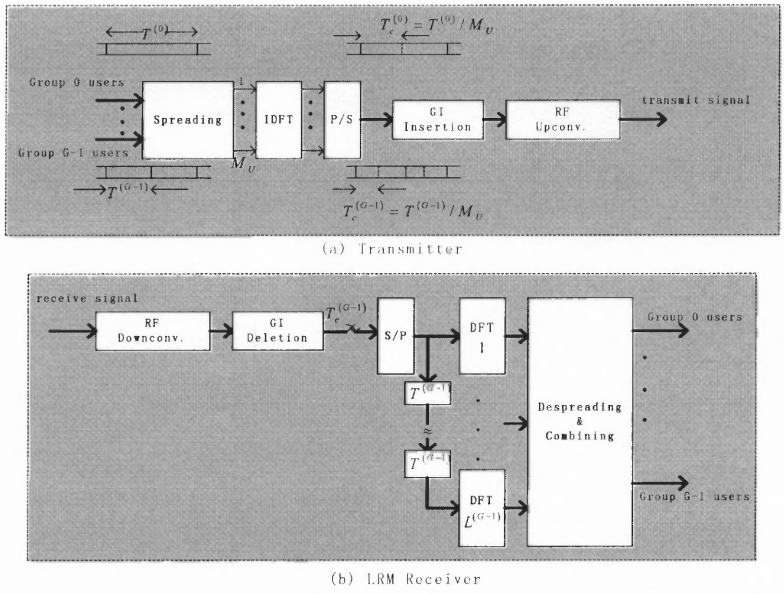

(a) Transmitter

(b) LRM Receiver

Figure 2.3 Block diagram of the transmitter and the LRM receiver of the multi-rate UFSL MC-CDMA scheme.

2.2.2 Receiver Design

The general structure of the receive multi-rate signal in equation (2.3) can be rewritten for the UFSL scheme as

$$r_U(t) = \sum_{i=-\infty}^{+\infty} \left[\sum_{g=0}^{G-1} \sum_{s=(i-1)L^{(g)}+1}^{iL^{(g)}} \sum_{k=1}^{K^{(g)}} \sum_{n=1}^{M_U} a_k^{(g)} b_k^{(g)}(s) \sum_{m=1}^{M_U} h_{k,m}^{(g)} c_{k,m}^{(g)} e^{j2\pi \frac{mn}{M_U}} P^{(g)}\left(t - (sM_U + n) T_c^{(g)}\right) \right] + n(t). \quad (2.8)$$

A low-rate-mode (LRM) receiver and a high-rate-mode (HRM) receiver was proposed for a dual-rate CDMA in [34, 35], which process the receive signal at the low rate bit interval and high rate bit interval, respectively. Obviously, they can be extended to a multi-rate system, by processing the receive signal at the lowest rate bit interval or the highest rate bit interval. To achieve a better performance, the LRM receiver is suggested for the UFSL scheme [36].

Within one lowest rate bit interval, each lowest rate user generates one bit, while each higher rate user in group g generates $L^{(g)}$ successive bits. The l^{th} bit of these

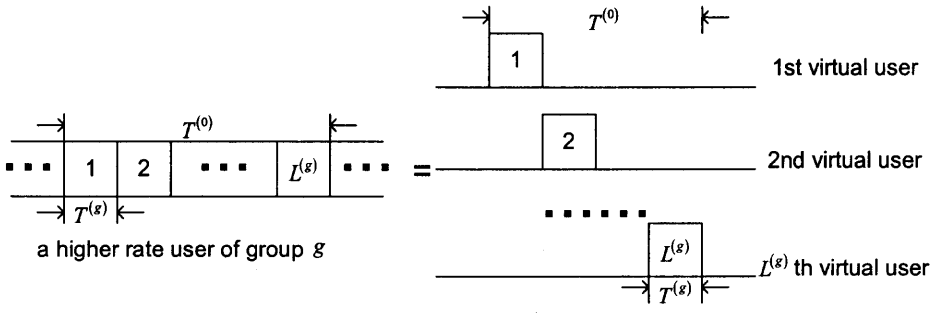

Figure 2.4 Signal equivalence between a higher rate user of group g and its $L^{(g)}$ virtual lowest rate users in the UFSL MC-CDMA scheme.

successive $L^{(g)}$ higher rate bits, where $l = 1, 2, \cdots, L^{(g)}$, can be considered as a virtual lowest rate bit with duration $T^{(0)}$, in which only the l^{th} sub-interval with duration $T^{(g)}$ is non-zero, as depicted in Figure 2.4. From this point of view, the multi-rate system is equivalent to a single lowest rate system with $K_v = \sum_{g=0}^{G-1} L^{(g)} K^{(g)}$ virtual lowest rate users, each generating bits at the rate, $R^{(0)}$.

During the i^{th} lowest rate bit interval $\left[(i-1)\,T^{(0)}, iT^{(0)}\right)$, as at the transmitter, the receive UFSL signal is sampled at the virtual chip rate $\frac{1}{T_c^{(G-1)}}$ and the total $M_U \times L^{(G-1)}$ samples obtained during each $T^{(0)}$ are serial to parallel (S/P) converted and divided into $L^{(G-1)}$ groups in which the l^{th} group contains M_U samples, corresponding to the l^{th} highest rate bit interval $\left[(i-1)\,T^{(0)} + (l-1)\,T^{(G-1)}, (i-1)\,T^{(0)} + lT^{(G-1)}\right)$. Therefore, to perform demodulation, with the LRM receiver, $L^{(G-1)}$ M_U-point DFTs concatenated in serial are needed. That is the M_U samples obtained at the l^{th} highest rate bit interval is processed by the l^{th} M_U-point DFT of the LRM receiver. The block diagram of the LRM receiver for the multi-rate UFSL MC-CDMA system is shown in Figure 2.3(b).

The output of the l^{th} DFT can be described as

$$\mathbf{x}_{U,l}(i) = \left[\frac{1}{\sqrt{\Delta^{(0)}}}\widetilde{\mathbf{C}}^{(0)}, \frac{1}{\sqrt{\Delta^{(1)}}}\widetilde{\mathbf{C}}^{(1)}, \cdots, \frac{1}{\sqrt{\Delta^{(G-1)}}}\widetilde{\mathbf{C}}^{(G-1)}\right] \cdot \begin{bmatrix} \mathbf{A}^{(0)} & & & \\ & \mathbf{A}^{(1)} & & \\ & & \ddots & \\ & & & \mathbf{A}^{(G-1)} \end{bmatrix} \cdot \begin{bmatrix} \mathbf{b}^{(0)}_{\left\lfloor \frac{l-1}{\Delta^{(0)}} \right\rfloor + 1}(i) \\ \mathbf{b}^{(1)}_{\left\lfloor \frac{l-1}{\Delta^{(1)}} \right\rfloor + 1}(i) \\ \vdots \\ \mathbf{b}^{(G-1)}_{\left\lfloor \frac{l-1}{\Delta^{(G-1)}} \right\rfloor + 1}(i) \end{bmatrix} + \boldsymbol{\eta}_l(i), \quad (2.9)$$

where $\Delta^{(g)} = \frac{T^{(g)}}{T^{(G-1)}}$ $(g = 0, 1, \cdots, G-1)$, $\widetilde{\mathbf{C}}^{(g)}$ denotes the channel-modified spreading code matrix of all users in group g, which can be expressed for the uplink as[5]

$$\begin{aligned} \widetilde{\mathbf{C}}^{(g)} &= \left[\widetilde{\mathbf{c}}_1^{(g)}, \widetilde{\mathbf{c}}_2^{(g)}, \cdots, \widetilde{\mathbf{c}}_{K^{(g)}}^{(g)}\right] \\ &= \left[\mathbf{h}_1^{(g)} \odot \mathbf{c}_1^{(g)}, \mathbf{h}_2^{(g)} \odot \mathbf{c}_2^{(g)}, \cdots, \mathbf{h}_{K^{(g)}}^{(g)} \odot \mathbf{c}_{K^{(g)}}^{(g)}\right] \\ &= \begin{bmatrix} h_{1,1}^{(g)} c_{1,1}^{(g)} & h_{2,1}^{(g)} c_{2,1}^{(g)} & \cdots & h_{K^{(g)},1}^{(g)} c_{K^{(g)},1}^{(g)} \\ h_{1,2}^{(g)} c_{1,2}^{(g)} & h_{2,2}^{(g)} c_{2,2}^{(g)} & \cdots & h_{K^{(g)},2}^{(g)} c_{K^{(g)},2}^{(g)} \\ \vdots & \vdots & \vdots & \vdots \\ h_{1,M_U}^{(g)} c_{1,M_U}^{(g)} & h_{2,M_U}^{(g)} c_{2,M_U}^{(g)} & \cdots & h_{K^{(g)},M_U}^{(g)} c_{K^{(g)},M_U}^{(g)} \end{bmatrix}, \end{aligned} \quad (2.10)$$

the matrix $\mathbf{A}^{(g)} = diag(a_1^{(g)}, a_2^{(g)}, \cdots a_{K^{(g)}}^{(g)})$ contains the amplitudes of all users in group g on its diagonal, the vector $\mathbf{b}^{(g)}_{\left\lfloor \frac{l-1}{\Delta^{(g)}} \right\rfloor + 1}(i)$ contains the $\left[(i-1)L^{(g)} + \left\lfloor \frac{l-1}{\Delta^{(g)}} \right\rfloor + 1\right]^{th}$ information bits of all users in group g during the l^{th} sample interval. For example, in

[5]For the downlink MC-CDMA, since different users experience the same fading, $\widetilde{\mathbf{C}}^{(g)}$ can be simplified as

$$\begin{aligned} \widetilde{\mathbf{C}}^{(g)} &= \mathbf{H} \cdot \mathbf{C}^{(g)} \\ &= \begin{bmatrix} h_1 & & & \\ & h_2 & & \\ & & \ddots & \\ & & & h_{M_U} \end{bmatrix} \cdot \begin{bmatrix} c_{1,1}^{(g)} & c_{2,1}^{(g)} & \cdots & c_{K^{(g)},1}^{(g)} \\ c_{1,2}^{(g)} & c_{2,2}^{(g)} & \cdots & c_{K^{(g)},2}^{(g)} \\ \vdots & \vdots & \vdots & \vdots \\ c_{1,M_U}^{(g)} & c_{2,M_U}^{(g)} & & c_{K^{(g)},M_U}^{(g)} \end{bmatrix}. \end{aligned}$$

Figure 2.2, the sample instance ($l = 2$) shown by the arrow denotes the i^{th}, $[2(i-1)+1]^{th}$ and $[4(i-1)+2]^{th}$ information bits of the low rate, medium rate and high rate user, respectively. Also, in equation (2.9), the elements of an $(M_U \times 1)$ white Gaussian noise vector $\boldsymbol{\eta}_l(i)$ have zero mean and variance σ_n^2.

Thus, the output of the LRM receiver at interval $\left[(i-1)T^{(0)}, iT^{(0)}\right)$ can be formed by stacking $L^{(G-1)}$ number of DFT output vectors into an $\left(L^{(G-1)}M_U \times 1\right)$ vector $\mathbf{x}_U(i)$ as

$$\begin{aligned} \mathbf{x}_U(i) &= \left[\begin{array}{cccc} \mathbf{x}_{U,1}(i)^T & \mathbf{x}_{U,2}(i)^T & \cdots & \mathbf{x}_{U,L^{(G-1)}}(i)^T \end{array}\right]^T \\ &= \widetilde{\mathbf{C}}_U \mathbf{A}_U \mathbf{b}_U(i) + \boldsymbol{\eta}_U(i), \end{aligned} \tag{2.11}$$

where

$$\widetilde{\mathbf{C}}_U = \left[\begin{array}{cccc} \underbrace{\frac{1}{\sqrt{\Delta^{(0)}}}\widetilde{\mathbf{C}}^{(0)}}_{\left\lfloor\frac{1-1}{\Delta^{(0)}}\right\rfloor+1} & \underbrace{\frac{1}{\sqrt{\Delta^{(1)}}}\widetilde{\mathbf{C}}^{(1)}}_{\left\lfloor\frac{1-1}{\Delta^{(1)}}\right\rfloor+1} & \cdots & \underbrace{\frac{1}{\sqrt{\Delta^{(G-1)}}}\widetilde{\mathbf{C}}^{(G-1)}}_{\left\lfloor\frac{1-1}{\Delta^{(G-1)}}\right\rfloor+1} \\ \underbrace{\frac{1}{\sqrt{\Delta^{(0)}}}\widetilde{\mathbf{C}}^{(0)}}_{\left\lfloor\frac{2-1}{\Delta^{(0)}}\right\rfloor+1} & \underbrace{\frac{1}{\sqrt{\Delta^{(1)}}}\widetilde{\mathbf{C}}^{(1)}}_{\left\lfloor\frac{2-1}{\Delta^{(1)}}\right\rfloor+1} & \cdots & \underbrace{\frac{1}{\sqrt{\Delta^{(G-1)}}}\widetilde{\mathbf{C}}^{(G-1)}}_{\left\lfloor\frac{2-1}{\Delta^{(G-1)}}\right\rfloor+1} \\ \vdots & \vdots & \vdots & \vdots \\ \underbrace{\frac{1}{\sqrt{\Delta^{(0)}}}\widetilde{\mathbf{C}}^{(0)}}_{\left\lfloor\frac{L^{(G-1)}-1}{\Delta^{(0)}}\right\rfloor+1} & \underbrace{\frac{1}{\sqrt{\Delta^{(1)}}}\widetilde{\mathbf{C}}^{(1)}}_{\left\lfloor\frac{L^{(G-1)}-1}{\Delta^{(1)}}\right\rfloor+1} & \cdots & \underbrace{\frac{1}{\sqrt{\Delta^{(G-1)}}}\widetilde{\mathbf{C}}^{(G-1)}}_{\left\lfloor\frac{L^{(G-1)}-1}{\Delta^{(G-1)}}\right\rfloor+1} \end{array}\right] \tag{2.12}$$

with

$$\underbrace{\frac{1}{\sqrt{\Delta^{(g)}}}\widetilde{\mathbf{C}}^{(g)}}_{\left\lfloor\frac{i-1}{\Delta^{(g)}}\right\rfloor+1} = \overbrace{\left[\mathbf{0}, \cdots, \mathbf{0}, \underbrace{\frac{1}{\sqrt{\Delta^{(g)}}}\widetilde{\mathbf{C}}^{(g)}}_{\text{the } \left[\left\lfloor\frac{i-1}{\Delta^{(g)}}\right\rfloor+1\right]^{th} \text{Block}}, \mathbf{0}, \cdots, \mathbf{0}\right]}^{\text{total } L^{(g)} \text{ Blocks}}. \tag{2.13}$$

The lower label in the above equation denotes the position of block $\frac{1}{\sqrt{\Delta^{(g)}}}\widetilde{\mathbf{C}}^{(g)}$ in the total $L^{(g)}$ blocks, with all the other blocks $\mathbf{0}$. And

$$\mathbf{A}_U = diag\left(\mathbf{A}^{(0)}, \underbrace{\mathbf{A}^{(1)}, \cdots, \mathbf{A}^{(1)}}_{L^{(1)}times}, \cdots, \underbrace{\mathbf{A}^{(G-1)}, \cdots, \mathbf{A}^{(G-1)}}_{L^{(G-1)}times}\right), \tag{2.14}$$

$$\mathbf{b}_U(i) = \left[\mathbf{b}^{(0)}(i)^T, \underline{\mathbf{b}}^{(1)}(i)^T, \cdots, \underline{\mathbf{b}}^{(G-1)}(i)^T\right]^T \tag{2.15}$$

with

$$\underline{\mathbf{b}}^{(g)}(i) = \left[\left(\mathbf{b}_1^{(g)}(i)\right)^T, \left(\mathbf{b}_2^{(g)}(i)\right)^T, \cdots, \left(\mathbf{b}_{L^{(g)}}^{(g)}(i)\right)^T\right]^T. \tag{2.16}$$

$\boldsymbol{\eta}_U(i) = \left[\boldsymbol{\eta}_1(i)^T, \boldsymbol{\eta}_2(i)^T, \cdots, \boldsymbol{\eta}_{L^{(G-1)}}(i)^T\right]^T$ is a vector with zero mean and covariance matrix $\sigma_n^2\mathbf{I}$, where $\mathbf{I}$ is an $\left(L^{(G-1)}M_U \times L^{(G-1)}M_U\right)$ identity matrix.

Equation (2.11) shows that the output vector $\mathbf{x}_U(i)$ contains the information bits of all virtual users during the lowest rate bit interval $\left[(i-1)T^{(0)}, iT^{(0)}\right)$. An MMSEC multiuser detector with an $\left(L^{(G-1)}M_U \times K_v\right)$ matrix $\mathbf{W} = [\mathbf{w}_1, \mathbf{w}_2, \cdots \mathbf{w}_{K_v}]$, is applied to form the sufficient statistic of the transmit bits of all virtual users. The k^{th} column of $\mathbf{W}, \mathbf{w}_k$, can be shown as [37]

$$\begin{aligned}\mathbf{w}_k &= \arg\min_{\mathbf{w}_k} MSE = \frac{a_k}{1 + a_k^2\widetilde{\mathbf{c}}_{U,k}^H\left(\widetilde{\mathbf{C}}_{U,-k}\mathbf{A}_{U,-k}^2\widetilde{\mathbf{C}}_{U,-k}^H + \sigma_n^2\mathbf{I}\right)^{-1}\widetilde{\mathbf{c}}_{U,k}} \times \\ &\left(\widetilde{\mathbf{C}}_{U,-k}\mathbf{A}_{U,-k}^2\widetilde{\mathbf{C}}_{U,-k}^H + \sigma_n^2\mathbf{I}\right)^{-1}\widetilde{\mathbf{c}}_{U,k},\end{aligned} \tag{2.17}$$

where $\widetilde{\mathbf{C}}_{U,-k}$ denotes the matrix $\widetilde{\mathbf{C}}_U$ without the k^{th} column, denoted by $\widetilde{\mathbf{c}}_{U,k}$. $\mathbf{A}_{U,-k}$ denotes the matrix $\mathbf{A}_U$ without the k^{th} element, denoted by a_k. The decision variable is obtained as

$$\mathbf{z}_U(i) = \mathbf{W}^H \cdot \mathbf{x}_U(i). \tag{2.18}$$

2.2.3 Performance Analysis

Without loss of generality, we assume that the first user of each group is the desired user. Then the BER performance of the desired user in group g employing MMSEC detector in the UFSL scheme can be expressed as [37]

$$BER_{U,MMSEC}^{(g)} = E_h\left[Q\left(\sqrt{\left(a_1^{(g)}\right)^2 \widetilde{\mathbf{c}}_{U,k}^H \left(\widetilde{\mathbf{C}}_{U,-k}\mathbf{A}_{U,-k}^2\widetilde{\mathbf{C}}_{U,-k}^H + \sigma_n^2\mathbf{I}\right)^{-1}\widetilde{\mathbf{c}}_{U,k}}\right)\right], \tag{2.19}$$

where $k = \sum_{i=0}^{g-1} L^{(i)}K^{(i)} + 1$[6], $E_h[\cdot]$ denotes expectation over all channel realizations and $Q(\cdot)$ represents the tail of the error function.

When only one lowest rate user presents in the system, the MMSEC receiver achieves a minimum BER, the single user bound (SUB), defined as

$$BER_{U,SUB}^{(0)} = E_h\left[Q\left(\sqrt{\frac{\left(a_1^{(0)}\right)^2}{\sigma_n^2}\frac{1}{M_U}\sum_{m=1}^{M_U}\left|h_{1,m}^{(0)}\right|^2}\right)\right]. \tag{2.20}$$

For each higher rate user of group g, during every time interval $T^{(0)}$, the output of the demodulator contains $L^{(g)}$ successive bits (see Figure 2.4). Notice that these $L^{(g)}$ bits are always orthogonal since they are located at non-overlapped time slots. Thus, there is no SI among these bits of each higher rate user. The SUB achieved by higher rate user of group g ($g = 1, 2, \cdots, G-1$) can be expressed as

$$BER_{U,SUB}^{(g)} = E_h\left[Q\left(\sqrt{\frac{\left(a_1^{(g)}\right)^2}{\sigma_n^2}\frac{1}{M_U}\sum_{m=1}^{M_U}\left|h_{1,m}^{(g)}\right|^2}\right)\right]. \tag{2.21}$$

2.3 Coded Fixed Spreading Length (CFSL) Scheme

2.3.1 Sub-carrier Assignment

In the UFSL scheme, it is clear from equation (2.7) that due to the non-overlapped spectra, lower rate users have lower SUE than the highest rate users. The loss of SUE

[6]Here, the performance of the first lowest rate virtual user is used to represent the performance of its corresponding higher rate user.

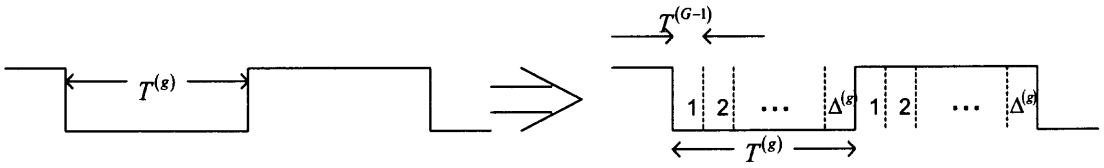

Figure 2.5 Timing structure of the lower rate MC-CDMA signal.

results in a performance loss for all lower rate users. In order to compensate for this performance loss, a channel coding (forward error correction) scheme is added for all lower rate users.

The idea of utilizing channel coding is straightforward: in the time domain, one lower rate bit of a group g user can be seen as equivalent to $\Delta^{(g)}$ times repeated highest rate bit. Thus, a lower rate MC-CDMA signal is equivalent to a repetition encoded highest rate signal, as shown in Figure 2.5. Therefore the performance of these lower rate users can be improved by a coding gain, if more efficient coding schemes other than a repetition coding are used. Furthermore, unlike in other cases where channel coding introduces redundancy into the transmit data bits and hence lowers the transmission data rate, the built-in repetition code structure of the lower rate MC-CDMA signal provides the possibility of adding channel coding without a loss of bandwidth efficiency (in bps/Hz). The CFSL scheme was first implemented by employing a block coding technique in a dual-rate MC-CDMA system [15]. However, the main difficulty of using such codes is that different decoders are needed for different rate encoders, which is quite complex in a multi-rate system. Furthermore, with block codes, it is difficult to perform soft-decision decoding, which is vital for any bandwidth efficient communication system due to the multipath fading channels [38]. Therefore, the block coded FSL scheme might not be suitable for a multi-rate system in the multipath fading environment. Instead, rate compatible punctured convolutional codes (RCPC) and nested codes, derived from the optimum distance spectrum (ODS) parent codes with optimal puncturing matrix, are employed in the CFSL scheme [16].

The ODS criterion ensures that this kind of code can achieve good performance in both AWGN and multipath Rayleigh fading channels. Furthermore, with the same parent code, a large group of rates is produced, providing great flexibility in rate matching and requiring only one decoder [39].

Therefore with the CFSL scheme, the information bits $b_k^{(g)}(i)$ of the k^{th} lower rate user in group g are encoded with code rate $\frac{1}{\Delta^{(g)}}$ before being applied to the multiplexer, to become a highest rate sequence $d_k^{(g)}(j)$. Hence the multi-rate system changes into an equivalent system with the single highest rate. An example of a sub-carrier assignment of the dual-rate CFSL MC-CDMA scheme with rate ratio 2 is shown in Figure 2.1(b). Compared with Figure 2.1(a), the number of sub-carriers M_C is the same as that of the UFSL scheme expressed in equation (2.6), i.e., $M_C = M_U$. Also, the frequency of the m^{th} sub-carrier is the same as that of the UFSL scheme. After encoding, the lower rate users can achieve the same SUE as the highest rate users, which is given by

$$\begin{aligned} \epsilon_C &= 2R^{(G-1)}M_C/BW \\ &= 2\left(BW - R^{(G-1)}\right)/BW. \end{aligned} \tag{2.22}$$

Clearly, with this scheme, different rate users have the same chip duration $T_c = \frac{T^{(G-1)}}{M_C}$. The block diagram of the transmitter of the CFSL scheme is shown in Figure 2.6(a).

2.3.2 Receiver Design

The general structure of the receive multi-rate signal in equation (2.3) can be rewritten for the CFSL scheme as

$$\begin{aligned} r_C(t) = \sum_{i=-\infty}^{+\infty} \Bigg[& \sum_{g=0}^{G-2} \sum_{k=1}^{K^{(g)}} \sum_{n=1}^{M_C} a_k^{(g)} d_k^{(g)}(i) \sum_{m=1}^{M_C} h_{k,m}^{(g)} c_{k,m}^{(g)} e^{j2\pi \frac{mn}{M_C}} p^{(g)}\left(t - (iM_C + n)T_c\right) \\ & + \sum_{k=1}^{K^{(G-1)}} \sum_{n=1}^{M_C} a_k^{(G-1)} b_k^{(G-1)}(i) \sum_{m=1}^{M_C} h_{k,m}^{(G-1)} c_{k,m}^{(G-1)} e^{j2\pi \frac{mn}{M_C}} \cdot \\ & p^{(G-1)}\left(t - (iM_C + n)T_c\right) \Bigg] + n(t), \end{aligned} \tag{2.23}$$

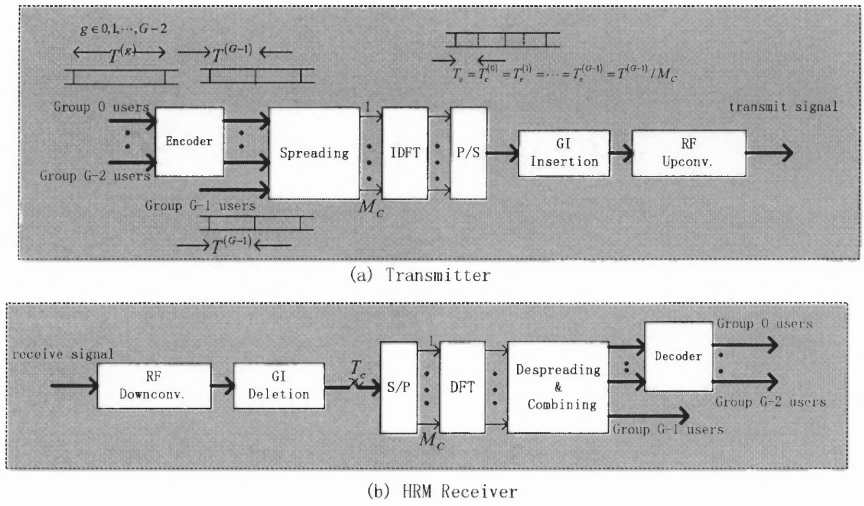

(a) Transmitter

(b) HRM Receiver

Figure 2.6 Block diagram of the transmitter and the HRM receiver of the multi-rate CFSL MC-CDMA scheme.

where i denotes the i^{th} highest rate bit interval $\left[(i-1)\,T^{(G-1)}, iT^{(G-1)}\right)$.

As the transmission rate of lower rate users becomes the same as that of the highest rate users after encoding, a high-rate-mode (HRM) receiver is applied in the CFSL scheme. As opposed to the LRM receiver used in the UFSL scheme, the HRM receiver consists of only one M_C-point DFT and processes the receive signal every $T^{(G-1)}$. The block diagram of the HRM receiver is shown in Figure 2.6(b).

The HRM CFSL receiver samples the receive signal $r_C\,(t)$ at the virtual chip rate $\frac{1}{T_c}$. During every $T^{(G-1)}$ interval, the M_C samples are demodulated by an M_C-point DFT. The output of the demodulator at interval $\left[(i-1)\,T^{(G-1)}, iT^{(G-1)}\right)$ can be

written as

$$\begin{aligned}\mathbf{x}_C(i) &= \left[\frac{1}{\sqrt{\Delta^{(0)}}}\widetilde{\mathbf{C}}^{(0)}, \frac{1}{\sqrt{\Delta^{(1)}}}\widetilde{\mathbf{C}}^{(1)}, \cdots, \frac{1}{\sqrt{\Delta^{(G-2)}}}\widetilde{\mathbf{C}}^{(G-2)}, \frac{1}{\sqrt{\Delta^{(G-1)}}}\widetilde{\mathbf{C}}^{(G-1)}\right] \cdot \\ &\quad \begin{bmatrix} \mathbf{A}^{(0)} & & & & \\ & \mathbf{A}^{(1)} & & & \\ & & \ddots & & \\ & & & \mathbf{A}^{(G-2)} & \\ & & & & \mathbf{A}^{(G-1)} \end{bmatrix} \cdot \begin{bmatrix} \mathbf{d}^{(0)}(i) \\ \mathbf{d}^{(1)}(i) \\ \vdots \\ \mathbf{d}^{(G-2)}(i) \\ \mathbf{b}^{(G-1)}(i) \end{bmatrix} + \boldsymbol{\eta}_C(i) \quad (2.24) \\ &= \widetilde{\mathbf{C}}_C \mathbf{A}_C \mathbf{b}_C(i) + \boldsymbol{\eta}_C(i),\end{aligned}$$

where $\widetilde{\mathbf{C}}^{(g)}$ is given by equation (2.10) with M_U replaced by M_C, $\mathbf{d}^{(g)}(i)$ denotes the i^{th} encoded bits of users in group g ($g = 0, 1, \cdots G-2$), and the $(M_C \times 1)$ white Gaussian noise vector $\boldsymbol{\eta}_C(i)$ has zero mean and covariance matrix $\sigma_n^2\mathbf{I}$, where $\mathbf{I}$ is an $(M_C \times M_C)$ identity matrix. Equation (2.24) shows that $\mathbf{x}_C(i)$ contains only the current transmit bits of the highest rate users and the current transmit coded bits of the lower rates users during the highest rate bit interval $\left[(i-1)T^{(G-1)}, iT^{(G-1)}\right)$, different from the output vector $\mathbf{x}_U(i)$ of the LRM receiver in the UFSL scheme shown in equation (2.11).

As in the UFSL scheme, an MMSEC multiuser detector is utilized after the demodulator to obtain decision variables for all different rate users. An $(M_C \times K)$ coefficient matrix $\mathbf{W} = [\mathbf{w}_1, \mathbf{w}_2, \cdots \mathbf{w}_K]$, where $K = \sum_{i=0}^{G-1} K^{(i)}$ denotes the number of all different rate users, is applied to form the sufficient statistic of all transmit bits. The k^{th} column of $\mathbf{W}, \mathbf{w}_k$ and the decision variable can be obtained from equation (2.17) and equation (2.18) with subscript U replaced by C.

Notice that the decision variables for the lower rate users are encoded, so that a decoder is needed after the MMSEC detector as shown in Figure 2.6(b).

2.3.3 Performance Analysis

Performance of the lower rates users With the assumption that the first lower rate user in group g is the desired user, its decision variable can be obtained as

$$\begin{aligned} z_1^{(g)}(i) &= \mathbf{w}_k^H \cdot \mathbf{x}_C(i) \\ &= \underbrace{\mathbf{w}_k^H \widetilde{\mathbf{c}}_{C,k} a_1^{(g)} d_1^{(g)}(i)}_{signal} + \underbrace{\mathbf{w}_k^H \widetilde{\mathbf{C}}_{C,-k} \mathbf{A}_{C,-k} \overline{\mathbf{d}}_{-1}^{(g)}(i)}_{MAI} + \underbrace{\mathbf{w}_k^H \boldsymbol{\eta}_C(i)}_{noise}, \end{aligned} \tag{2.25}$$

where $k = \sum_{i=0}^{g-1} K^{(i)} + 1$, $\overline{\mathbf{d}}_{-1}^{(g)}(i)$ denotes the vector $\mathbf{b}_C(i)$ without the coded bit of the first user in group g. In equation (2.25), the three items denote the desired signal, the MAI and the noise respectively. If a sufficient number of users are involved, MAI can be approximated by a Gaussian random variable with zero mean. In such a case, the decision variable $z_1^{(g)}(i)$ can be considered as a Gaussian random variable with mean $\widehat{\mu}_1^{(g)}$ and variance $\left(\widehat{\sigma}_1^{(g)}\right)^2$, where

$$\widehat{\mu}_1^{(g)} = \mathbf{w}_k^H \widetilde{\mathbf{c}}_{C,k} a_1^{(g)} d_1^{(g)}(i) \tag{2.26}$$

and

$$\left(\widehat{\sigma}_1^{(g)}\right)^2 = \mathbf{w}_k^H \widetilde{\mathbf{C}}_{C,-k} \mathbf{A}_{C,-k}^2 \widetilde{\mathbf{C}}_{C,-k}^H \mathbf{w}_k + \sigma_n^2 \mathbf{w}_k^H \mathbf{w}_k. \tag{2.27}$$

Therefore, an upper bound (UB) of the BER conditioned on one specific channel for the desired user is given by [39]

$$BER_{1|h}^{(g)} < \frac{1}{p} \sum_{d=d_f}^{\infty} c_d \cdot \left[\mathcal{P}_{1|h}^{(g)}\right], \tag{2.28}$$

where p is the puncturing period, c_d is the information (error) weight, which is the number of bit errors for all error events of weight d; d_f is the free distance of the code; $\mathcal{P}_{1|h}^{(g)}$ is the probability that an error path of weight d is chosen instead of all

zeros path, which can be expressed under the above assumption as

$$\mathcal{P}_{1|h}^{(g)} = Q\left(\sqrt{d\frac{\left|\widehat{\mu}_1^{(g)}\right|^2}{\left(\widehat{\sigma}_1^{(g)}\right)^2}\frac{1}{\Delta^{(g)}}}\right). \tag{2.29}$$

Therefore, an upper bound of the BER performance for the desired user in group g averaged on different channel realizations is given by

$$\begin{aligned} BER_1^{(g)} &= E_h\left[BER_{1|h}^{(g)}\right] < E_h\left[\frac{1}{p}\sum_{d=d_f}^{\infty} c_d \cdot Q\left(\sqrt{d\frac{\left|\widehat{\mu}_1^{(g)}\right|^2}{\left(\widehat{\sigma}_1^{(g)}\right)^2}\frac{1}{\Delta^{(g)}}}\right)\right] \\ &= \frac{1}{p}\sum_{d=d_f}^{\infty} c_d \cdot E_h\left[Q\left(\sqrt{d\frac{\left|\widehat{\mu}_1^{(g)}\right|^2}{\left(\widehat{\sigma}_1^{(g)}\right)^2}\frac{1}{\Delta^{(g)}}}\right)\right]. \end{aligned} \tag{2.30}$$

Performance of the highest rate users As these users' bits are not encoded, the BER performance of the desired user applying an HRM CFSL scheme is similar to equation (2.19), which can be rewritten as

$$BER_{C,MMSEC}^{(G-1)} = E_h\left[Q\left(\sqrt{\left(a_1^{(G-1)}\right)^2 \widetilde{\mathbf{c}}_{C,k}^H\left(\widetilde{\mathbf{C}}_{C,-k}\mathbf{A}_{C,-k}^2\widetilde{\mathbf{C}}_{C,-k}^H + \sigma_n^2\mathbf{I}\right)^{-1}\widetilde{\mathbf{c}}_{C,k}}\right)\right], \tag{2.31}$$

where $k = \sum_{i=0}^{G-2} K^{(i)} + 1$.

When only one highest rate user presents in the system, it achieves the SUB, expressed in equation (2.21), with M_U replaced by M_C.

It has been proved that in a dual-rate DS-CDMA system, the LRM receiver can achieve better performance for both low and high rate users than the HRM receiver [36]. Based on the duality of the DS-CDMA and MC-CDMA systems [40], this conclusion can also be applied and extended to the multi-rate MC-CDMA system.

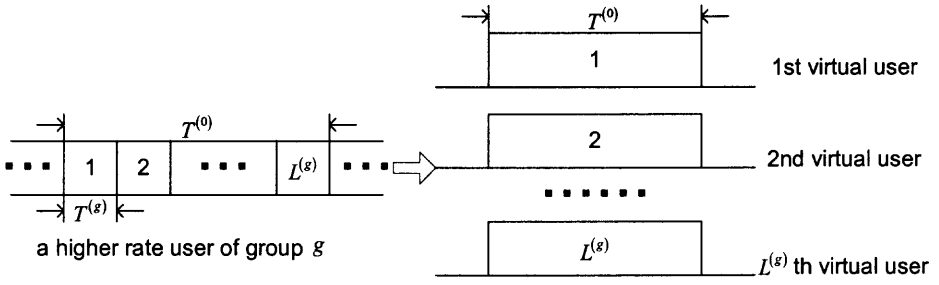

Figure 2.7 Transformation (S/P conversion) from a higher rate user of group g to its $L^{(g)}$ virtual lowest rate users in the MFSL scheme.

2.4 Multi-code Fixed Spreading Length (MFSL) Scheme

2.4.1 Sub-carrier Assignment

In both the UFSL and CFSL schemes, the frequency separation of adjacent sub-carriers equals the bandwidth of the highest rate users, hence the number of sub-carriers might be limited, particularly when a very high rate is supported by the system. In such a case, the short spreading length results in a limited system capacity and reduced interference suppression capability. with the MFSL scheme, during the lowest rate bit interval $\left[(i-1)T^{(0)}, iT^{(0)}\right)$, by S/P conversion, the higher rate stream $b_k^{(g)}(j)$ is split into a plurality of the lowest rate substreams $b_{k,l}^{(g)}(i)$, $\left(l = 1, 2, \cdots, L^{(g)}\right)$, which is shown in Figure 2.7. Each of these lowest rate substreams is then assigned a spreading code $\mathbf{c}_{k,l}^{(g)}$ with the same processing gain. It is obvious that to fulfill this transformation, any higher rate should be an integer multiple of the lowest rate, i.e., $\frac{R^{(g)}}{R^{(0)}}, (g = 1, 2, \cdots, G-1)$ should be an integer. By employing multiple spreading codes for each higher rate user, the multi-rate system is converted into an equivalent single lowest rate system with K_v virtual lowest rate users. Hence, in the MFSL scheme, adjacent sub-carriers can be spaced by the bandwidth of the lowest rate users so that a maximum number of sub-carriers can be utilized, also, a maximum SUE for all different rate users. An example of a sub-carrier assignment of the dual-rate MC-CDMA scheme with rate ratio 2 is shown in Figure 2.1(c). The number of

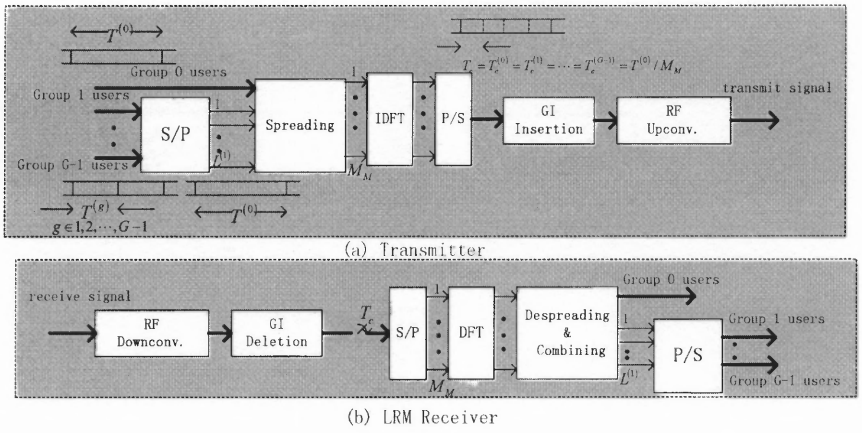

Figure 2.8 Block diagram of the transmitter and the LRM receiver of the multi-rate MFSL MC-CDMA scheme.

sub-carriers utilized in this scheme is

$$M_M = \frac{BW - R^{(0)}}{R^{(0)}}. \tag{2.32}$$

The frequency of the m^{th} sub-carrier is, $f_m = mR^{(0)}, (m = 1, 2, \cdots, M_M)$. The SUE achieved by all different rate users can be expressed as

$$\begin{aligned} \epsilon_M &= 2R^{(0)} M_M / BW \\ &= 2\left(BW - R^{(0)}\right) / BW. \end{aligned} \tag{2.33}$$

As in the CFSL scheme, all different rate users have the same chip duration $T_c = \frac{T^{(0)}}{M_M}$. The block diagram of the transmitter of the MFSL scheme is shown in Figure 2.8(a).

2.4.2 Receiver Design

The general structure of the receive multi-rate signal in equation (2.3) can be rewritten for the MFSL scheme as

$$\begin{aligned} r_M(t) = \sum_{i=-\infty}^{+\infty} \Bigg[& \sum_{g=1}^{G-1} \sum_{k=1}^{K^{(g)}} \sum_{l=1}^{L^{(g)}} \sum_{n=1}^{M_M} a_k^{(g)} b_{k,l}^{(g)}(i) \sum_{m=1}^{M_M} h_{k,m}^{(g)} c_{k,l,m}^{(g)} e^{j2\pi \frac{mn}{M_M}} \cdot \\ & p^{(g)}(t-(iM_M+n)T_c) + \sum_{k=1}^{K^{(0)}} \sum_{n=1}^{M_M} a_k^{(0)} b_k^{(0)}(i) \sum_{m=1}^{M_M} h_{k,m}^{(0)} c_{k,m}^{(0)} e^{j2\pi \frac{mn}{M_M}} \cdot \\ & p^{(0)}(t-(iM_M+n)T_c) \Bigg] + n(t), \end{aligned} \tag{2.34}$$

As the transmission rate of the higher rate users after S/P conversion becomes the same as that of the lowest rate users, an LRM receiver is applied in the MFSL scheme. The LRM receiver consists of only one M_M-point DFT which processes the receive signal every $T^{(0)}$. The block diagram of the LRM receiver for the multi-rate MFSL MC-CDMA is shown in Figure 2.8(b).

The LRM receiver samples the signal $r_M(t)$ at the virtual chip rate $\frac{1}{T_c}$. During every $T^{(0)}$ interval, the M_M samples are demodulated by an M_M-point DFT. The output of the demodulator during the lowest rate bit interval $\left[(i-1)T^{(0)}, iT^{(0)}\right)$ can be written as

$$\mathbf{x}_M(i) = \widetilde{\mathbf{C}}_M \mathbf{A}_M \mathbf{b}_M(i) + \boldsymbol{\eta}_M(i), \tag{2.35}$$

where

$$\widetilde{\mathbf{C}}_M = \left[\widetilde{\mathbf{C}}^{(0)}, \underline{\widetilde{\mathbf{C}}}^{(1)}, \cdots, \underline{\widetilde{\mathbf{C}}}^{(G-1)}\right] \tag{2.36}$$

with $\widetilde{\mathbf{C}}^{(0)}$ given by equation (2.10) and replacing subscript U by M, and

$$\underline{\widetilde{\mathbf{C}}}^{(g)} = \left[\widetilde{\mathbf{C}}_1^{(g)}, \widetilde{\mathbf{C}}_2^{(g)}, \cdots, \widetilde{\mathbf{C}}_{L^{(g)}}^{(g)}\right], \tag{2.37}$$

which contains $L^{(g)}$ different code sets for all users in group g. Each item in equation (2.37) can be expressed as

$$\widetilde{\mathbf{C}}_i^{(g)} = \begin{bmatrix} h_{1,1}^{(g)} c_{1,i,1}^{(g)} & h_{2,1}^{(g)} c_{2,i,1}^{(g)} & \cdots & h_{K^{(g)},1}^{(g)} c_{K^{(g)},i,1}^{(g)} \\ h_{1,2}^{(g)} c_{1,i,2}^{(g)} & h_{2,2}^{(g)} c_{2,i,2}^{(g)} & \cdots & h_{K^{(g)},2}^{(g)} c_{K^{(g)},i,2}^{(g)} \\ \vdots & \vdots & \vdots & \vdots \\ h_{1,M_M}^{(g)} c_{1,i,M_M}^{(g)} & h_{2,M_M}^{(g)} c_{2,i,M_M}^{(g)} & \cdots & h_{K^{(g)},M_M}^{(g)} c_{K^{(g)},i,M_M}^{(g)} \end{bmatrix}. \tag{2.38}$$

$\mathbf{A}_M$ and $\mathbf{b}_M(i)$ are given by equation (2.14) and (2.15), respectively. The $(M_M \times 1)$ white Gaussian noise vector $\boldsymbol{\eta}_M(i)$ has zero mean and covariance matrix $\sigma_n^2\mathbf{I}$, where $\mathbf{I}$ is an $(M_M \times M_M)$ identity matrix.

Equation (2.35) contains all information bits of the K_v virtual users during the lowest bit interval $\left[(i-1)T^{(0)}, iT^{(0)}\right)$. By employing the MMSEC multiuser detector, an $(M_M \times K_v)$ coefficient matrix $\mathbf{W} = [\mathbf{w}_1, \mathbf{w}_2, \cdots \mathbf{w}_{K_v}]$ is applied to form the sufficient statistic for the transmit bits of all virtual users. The k^{th} column of $\mathbf{W}$, $\mathbf{w}_k$ and the decision variable can be obtained from equation (2.17) and (2.18), respectively, with subscript U replaced by M.

Notice that after the MMSEC detector, the decisions of higher rate users should be collected by a parallel-to-serial (P/S) converter to recover the original information bits as shown in Figure 2.8(b).

2.4.3 Performance Analysis

The BER performance of group g users $(g = 0, 1, \cdots, G-1)$ is determined by the average over all its parallel transmit symbols, given by

$$BER_{M,MMSEC}^{(g)} = \frac{1}{L^{(g)}} E_h \left[\sum_{l=k+1}^{k+L^{(g)}} Q\left(\sqrt{\left(a_1^{(g)}\right)^2 \widetilde{\mathbf{c}}_{M,l}^H \left(\widetilde{\mathbf{C}}_{M,-l} \mathbf{A}_{M,-l}^2 \widetilde{\mathbf{C}}_{M,-l}^H + \sigma_n^2 \mathbf{I} \right)^{-1} \widetilde{\mathbf{c}}_{M,l}} \right) \right], \tag{2.39}$$

where $k = \sum_{i=0}^{g-1} L^{(i)} K^{(i)}$.

If only one lowest rate user exists in the system, the lowest rate user can achieve SUB given by equation (2.20), with M_U replaced by M_M.

For each higher rate user, since more than one spreading code are employed, SI may occur so that, in general, higher rate users do not achieve the SUB expressed similarly by equation (2.21). To derive the SUB of higher rate users in the MFSL scheme, with the assumption that only one (the first) higher rate user of group g is present in the system, we can rewrite the DFT output as

$$\mathbf{x}_M^{(g)}(i) = \widetilde{\mathbf{C}}_M^{(g)} \mathbf{A}_M^{(g)} \mathbf{b}_M^{(g)}(i) + \boldsymbol{\eta}_M(i), \tag{2.40}$$

where

$$\begin{aligned} \widetilde{\mathbf{C}}_M^{(g)} &= \left[\widetilde{\mathbf{c}}_{1,1}^{(g)}, \widetilde{\mathbf{c}}_{1,2}^{(g)}, \cdots, \widetilde{\mathbf{c}}_{1,L^{(g)}}^{(g)}\right] \\ &= \mathbf{H} \cdot \begin{bmatrix} c_{1,1,1}^{(g)} & c_{1,2,1}^{(g)} & \cdots & c_{1,L^{(g)},1}^{(g)} \\ c_{1,1,2}^{(g)} & c_{1,2,2}^{(g)} & \cdots & c_{1,L^{(g)},2}^{(g)} \\ \vdots & \vdots & \vdots & \vdots \\ c_{1,1,M_M}^{(g)} & c_{1,2,M_M}^{(g)} & \cdots & c_{1,L^{(g)},M_M}^{(g)} \end{bmatrix} \end{aligned} \tag{2.41}$$

with $\mathbf{H} = diag\left(h_{1,1}^{(g)}, h_{1,2}^{(g)}, \cdots, h_{1,M_M}^{(g)}\right)$ as different virtual users belonging to the same higher rate user experience the same fading, $\mathbf{A}_M^{(g)} = diag\left(a_1^{(g)}, \cdots, a_1^{(g)}\right)$ and $\mathbf{b}_M^{(g)}(i) = \left[b_{1,1}^{(g)}(i), b_{1,2}^{(g)}(i), \cdots, b_{1,L^{(g)}}^{(g)}(i)\right]^T$. Thus the SUB achieved by this higher rate user is expressed as

$$BER_{M,SUB}^{(g)} = \frac{1}{L^{(g)}} E_h \left[\sum_{l=1}^{L^{(g)}} Q\left(\sqrt{\left(a_1^{(g)}\right)^2 \widetilde{\mathbf{c}}_{M,l}^{(g)H} \left[\widetilde{\mathbf{C}}_{M,-l}^{(g)} \left(\mathbf{A}_{M,-l}^{(g)}\right)^2 \widetilde{\mathbf{C}}_{M,-l}^{(g)H} + \sigma_n^2 \mathbf{I}\right]^{-1} \widetilde{\mathbf{c}}_{M,l}^{(g)}}\right)\right]. \tag{2.42}$$

It has been found that in some cases, by properly selecting spreading codes, SI can be reduced significantly [18].

2.5 Variable Spreading Length (VSL) Scheme

2.5.1 Sub-carrier Assignment

In the VSL scheme, instead of assigning different rate users with the same set of sub-carriers as in the UFSL, CFSL and MFSL schemes, they are allocated a different set of sub-carriers. The frequency separation between adjacent sub-carriers for group g users equals $R^{(g)}$, which is the minimum frequency spacing needed to maintain sub-carrier signals orthogonality for this group. Therefore, different rate users employ different number of sub-carriers, which is

$$M_V^{(g)} = \frac{BW - R^{(g)}}{R^{(g)}}. \tag{2.43}$$

The sub-carrier frequencies of group g users is $f_m^{(g)} = mR^{(g)}, \left(m = 1, 2, \cdots, M_V^{(g)}\right)$. An example of a sub-carrier assignment of the dual-rate VSL MC-CDMA scheme with rate ratio 2 is shown in Figure 2.1(d). Due to the overlapped spectra, for each group, this scheme achieves high SUE. The SUE of group g users can be expressed as

$$\begin{aligned} \epsilon_V^{(g)} &= 2R^{(g)}M_V^{(g)}/BW \\ &= 2\left(BW - R^{(g)}\right)/BW. \end{aligned} \tag{2.44}$$

With the assumption that the length of spreading codes equals the number of sub-carriers, different rate users are assigned different length spreading codes. When $BW \gg R^{(g)}$, $\frac{M_V^{(m)}}{M_V^{(n)}} \approx \frac{T^{(m)}}{T^{(n)}}, (m, n = 0, 1, \cdots, G-1)$, $(m \neq n)$, and the chip rate $T_c^{(g)} = \frac{T^{(g)}}{M_V^{(g)}}$ for all different rate users is the same, denoted by T_c. From this point of view, the VSL scheme can be looked upon as a fixed chip rate (FCR) scheme. An example of a signal structure of a three-rate VSL MC-CDMA scheme (with rate ratio $\frac{L^{(g)}}{L^{(g-1)}} = 2, (g = 1, 2)$ and $M_V^{(0)} = 16$) is shown in Figure 2.9. At each lowest rate bit interval, the multi-rate MC-CDMA signal is composed of different rate signals, each of which has the same chip duration. It is obvious that in the VSL scheme, G

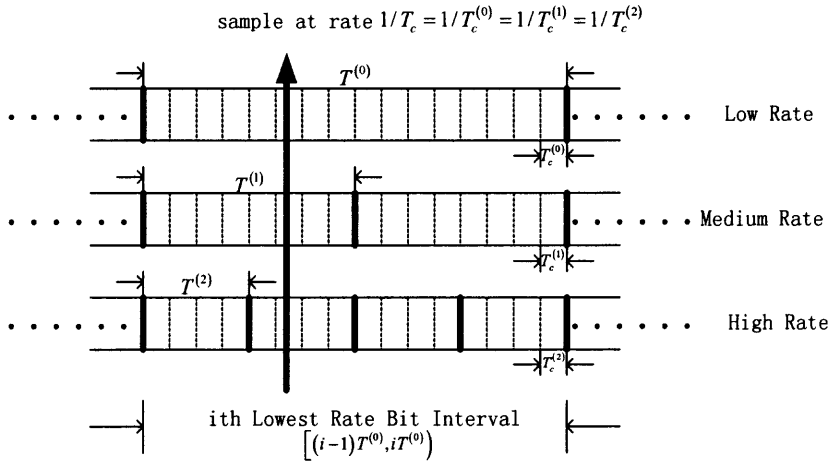

Figure 2.9 An example of the signal structure of the VSL MC-CDMA scheme (three-rate with rate ratio $\frac{L^{(g)}}{L^{(g-1)}} = 2, (g = 1, 2)$ and $M_V^{(0)} = 16$).

number of IDFTs each with $M_V^{(g)}-$point are employed to perform modulation. The block diagram of the transmitter for the VSL scheme is shown in Figure 2.10(a).

2.5.2 Receiver Design

The general structure of the receive multi-rate signal in equation (2.3) can be rewritten for the VSL scheme as

$$\begin{aligned} r_V(t) = \sum_{i=-\infty}^{+\infty} \Bigg[& \sum_{k=1}^{K^{(0)}} \sum_{n=1}^{M_V^{(0)}} a_k^{(0)} b_k^{(0)}(i) \sum_{m=1}^{M_V^{(0)}} h_{k,m}^{(0)} c_{k,m}^{(0)} e^{j2\pi \frac{mn}{M_V^{(0)}}} P^{(0)}\left(t - \left(iM_V^{(0)} + n\right) T_c\right) \\ & + \sum_{g=1}^{G-1} \sum_{s=(i-1)L^{(g)}+1}^{iL^{(g)}} \sum_{k=1}^{K^{(g)}} \sum_{n=1}^{M_V^{(g)}} a_k^{(g)} b_k^{(g)}(s) \sum_{m=1}^{M_V^{(g)}} h_{k,m}^{(g)} c_{k,m}^{(g)} e^{j2\pi \frac{mn}{M_V^{(g)}}} \cdot \\ & P^{(g)}\left(t - \left(sM_V^{(g)} + n\right) T_c\right) \Bigg] + n(t), \end{aligned} \tag{2.45}$$

An LRM receiver is proposed for the VSL scheme. This receiver consists of a single $M_V^{(0)}-$point DFT to perform the multi-carrier demodulation every $T^{(0)}$. The block diagram of the proposed LRM receiver is shown in Figure 2.10(b), wherein the receive signal is sampled at the virtual chip rate $\frac{1}{T_c}$. Note that the sub-carrier sets $\mathbf{f}^{(g)} = \left[f_1^{(g)}, f_2^{(g)}, \cdots, f_{M_V^{(g)}}^{(g)}\right], (g = 1, \cdots, G-1)$ and $\mathbf{f}^{(0)} = \left[f_1^{(0)}, f_2^{(0)}, \cdots, f_{M_V^{(0)}}^{(0)}\right]$ are

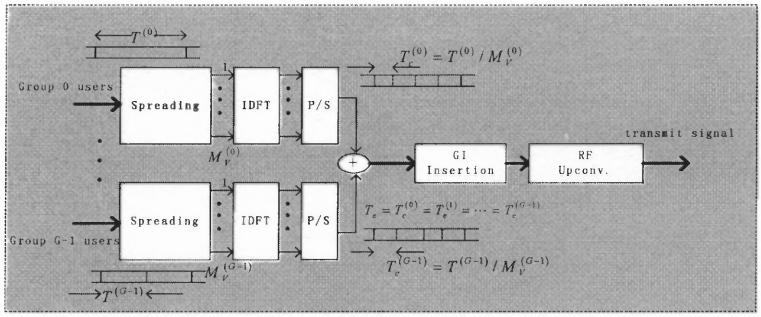

(a) Transmitter

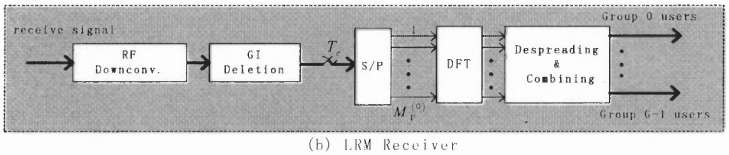

(b) LRM Receiver

Figure 2.10 Block diagram of the transmitter and the LRM receiver of the multi-rate VSL MC-CDMA scheme.

not orthogonal, because,

$$\int_{(i-1)T^{(g)}}^{iT^{(g)}} \cos 2\pi f_m^{(g)} t \cdot \cos 2\pi f_n^{(0)} t \neq \delta\left(f_m^{(g)} - f_n^{(0)}\right). \tag{2.46}$$

Therefore, with the LRM receiver, the VSL scheme introduces ICI.

The sample obtained at the instant $t = (i-1)\,T^{(0)} + sT_c$, for $s = 1, 2, \cdots, M_V^{(0)}$ can be described by

$$\begin{aligned} r_{V,S}(i) &= \frac{1}{\sqrt{M_V^{(0)}}} \sum_{k=1}^{K^{(0)}} a_k^{(0)} b_k^{(0)}(i) \sum_{m=1}^{M_V^{(0)}} h_{k,m}^{(0)} c_{k,m}^{(0)} e^{j2\pi \frac{ms}{M_V^{(0)}}} \\ &+ \frac{1}{\sqrt{M_V^{(g)}}} \sum_{g=1}^{G-1} \sum_{k=1}^{K^{(g)}} a_k^{(g)} b_k^{(g)}\left(i^{(g)}\right) \sum_{m=1}^{M_V^{(g)}} h_{k,m}^{(g)} c_{k,m}^{(g)} e^{j2\pi \frac{ms}{M_V^{(g)}}} + n_S(i), \end{aligned} \tag{2.47}$$

where $i^{(g)} = \left\lfloor \frac{s}{M_V^{(g)}} \right\rfloor + L^{(g)} \cdot (i-1) + 1$ is the index of bits of the higher rate users in group g, which corresponds to the $\left[i^{(g)}\right]^{th}$ higher rate bit interval $\left[\left(i^{(g)} - 1\right) T^{(g)}, i^{(g)} T^{(g)}\right)$. For example, in Figure 2.9, the sample instance ($s = 6$) shown by the arrow denotes the i^{th}, $[2(i-1)+1]^{th}$ and $[4(i-1)+2]^{th}$ information bits of the low rate, medium

rate and high rate user, respectively. The factors $\frac{1}{\sqrt{M_V^{(0)}}}$ and $\frac{1}{\sqrt{M_V^{(g)}}}$ denote the amplitude of the normalized pulse shape functions $P^{(g)}(t)$. Also, $n_S(i)$ denotes a white Gaussian noise sample with zero mean and variance σ_n^2. $M_V^{(0)}$ samples of the receive signal within each interval $\left[(i-1)T^{(0)}, iT^{(0)}\right)$ are processed by the $M_V^{(0)}-$point DFT. The q^{th} output of the DFT can then be shown as

$$\begin{aligned} x_{V,q}(i) &= \frac{1}{M_V^{(0)}} \sum_{s=1}^{M_V^{(0)}} r_{VS}(i)\, e^{-j2\pi \frac{sq}{M_V^{(0)}}} \\ &= \frac{1}{\sqrt{M_V^{(0)}}} \sum_{k=1}^{K^{(0)}} a_k^{(0)} b_k^{(0)}(i)\, h_{k,q}^{(0)} c_{k,q}^{(0)} \\ &\quad + \frac{1}{\sqrt{M_V^{(0)}}} \sum_{g=1}^{G-1} \sum_{k=1}^{K^{(g)}} a_k^{(g)} \sum_{l=1}^{L^{(g)}} b_{k,l}^{(g)} \sum_{m=1}^{M_V^{(g)}} h_{k,m}^{(g)} \frac{c_{k,m}^{(g)}}{\sqrt{L^{(g)}}} \gamma_{q,l,m}^{(g)} + n_q(i), \end{aligned} \tag{2.48}$$

where

$$\gamma_{q,l,m}^{(g)} = \frac{1}{M_V^{(g)}} e^{-j2\pi \frac{q}{L^{(g)}}(l-1)} \sum_{s=1}^{M_V^{(g)}} e^{j2\pi \frac{m-\frac{q}{L^{(g)}}}{M_V^{(g)}} s} \tag{2.49}$$

and

$$n_q(i) = \frac{1}{M_V^{(0)}} \sum_{p=1}^{M_V^{(0)}} n_S(i)\, e^{-j2\pi \frac{sq}{M_V^{(0)}}} \sim N\left(0, \frac{\sigma_n^2}{M_V^{(0)}}\right) \tag{2.50}$$

with $q = 1, 2, \cdots, M_V^{(0)}, m = 1, 2, \cdots, M_V^{(g)}$ and $l = i^{(g)} - (i-1)L^{(g)} \in \left\{1, 2, ..., L^{(g)}\right\}$, which is the index of the subinterval $\left[(i-1)T^{(0)} + (l-1)T^{(g)}, (i-1)T^{(0)} + lT^{(g)}\right)$. The first term of equation (2.48) contains the information of the lowest rate users that is transmitted on the q^{th} sub-carrier. The second term contains the information of the higher rate users that is demodulated by the q^{th} sub-carrier of the lowest rate users. It can be seen that there exists interference between the q^{th} sub-carrier of the lowest rate users and the m^{th} sub-carrier of the higher rate users at the the l^{th} subinterval $T^{(g)}$. This ICI, which is represented by the transformation $\gamma_{q,l,m}^{(g)}$ defined in equation (2.49), is introduced due to the sub-carrier signals non-orthogonality depicted by equation

(2.46) between the higher rate and the lowest rate users. As a result of the presence of ICI, the spreading code of the k^{th} higher rate user in group g at the l^{th} subinterval might be looked upon as being transformed into

$$\widetilde{\theta}_{k,l,q}^{(g)} = \sum_{m=1}^{M_V^{(g)}} h_{k,m}^{(g)} \frac{c_{k,m}^{(g)}}{\sqrt{L^{(g)}}} \gamma_{q,l,m}^{(g)}. \tag{2.51}$$

Therefore, although each higher rate user in group g employs one spreading code with $M_V^{(g)}$ elements, after the $M_V^{(0)}-$point DFT, one can show that, by mathematical manipulation, this code is transformed to become $L^{(g)}$ different complex spreading codes with length $M_V^{(0)}$. Because each higher rate user in group g employs $L^{(g)}$ different spreading codes, one for each higher rate bit, one may consider the VSL scheme as a special kind of multi-code scheme. However, the properties of spreading codes for each higher rate user are different in the MFSL and VSL schemes. It can be proven that in the VSL scheme, the transformed spreading codes of the same higher rate user satisfy the following stated **Properties**.

Property A: In the ideal non-faded AWGN channel, each transformed spreading code of the same higher rate user maintains the same autocorrelation properties of the original codes and those corresponding to different bits are orthogonal:

$$\left[\widetilde{\boldsymbol{\theta}}_{k,i}^{(g)}\right]^H \widetilde{\boldsymbol{\theta}}_{k,i'}^{(g)} = \begin{cases} \left[\mathbf{c}_k^{(g)}\right]^T \mathbf{c}_k^{(g)} & i = i' \\ 0 & i \neq i' \end{cases} \quad i, i' = 1, 2, \cdots, L^{(g)} \ . \tag{2.52}$$

Property B: In the Rayleigh fading channel, the transformed spreading codes corresponding to different bits remain orthogonal.

Hence different from the MFSL scheme, no SI will be produced in the VSL scheme. The detailed proof of these claims is given in Appendix A.

Although no SI will be produced in the VSL scheme, equation (2.51) shows that ICI may cause severe MAI even in the ideal non-faded AWGN channel, i.e., $h_{k,m}^{(g)} = 1 \left(m = 1, 2, \cdots, M_V^{(g)}\right)$. As the correlation properties between the spreading

codes of different users might be impaired by the aforementioned transformation, the performance of both the lowest rate users and higher rate users might be degraded in the VSL scheme. However, it has been found that by employing orthogonal Walsh-Hadamard codes as spreading codes and properly selecting these codes for all users, the MAI caused by ICI can be eliminated in the ideal non-faded AWGN channel, ensuring the feasibility of this scheme[7]. The reason for choosing Walsh-Hadamard codes is their good symmetry properties in the time domain, which imposes good symmetry conditions on their Fourier transform [41]. The procedures of spreading code selection in the VSL scheme is given by Appendix B. Note that this spreading code selection imposes the similar rate ratio requirement as in the UFSL scheme.

By substituting equation (2.51) into equation (2.48) after normalizing by $\frac{1}{\sqrt{M_V^{(0)}}}$, it can be obtained that

$$\begin{aligned} x_{V,q}(i) &= \sum_{k=1}^{K^{(0)}} a_k^{(0)} b_k^{(0)}(i)\, h_{k,q}^{(0)} c_{k,q}^{(0)} \\ &\quad + \sum_{g=1}^{G-1} \sum_{k=1}^{K^{(g)}} a_k^{(g)} \sum_{l=1}^{L^{(g)}} b_{k,l}^{(g)} \widetilde{\theta}_{k,l,q}^{(g)} + n_q(i), \end{aligned} \tag{2.53}$$

where $n_q(i)$ has variance σ_n^2. In order to estimate the desired user's information, the outputs of DFT shown in equation (2.53) are stacked into an $\left(M_V^{(0)} \times 1\right)$ vector $\mathbf{x}_V(i)$

$$\begin{aligned} \mathbf{x}_V(i) &= \left[x_{V,1}(i), x_{V,2}(i), \cdots, x_{V,M_V^{(0)}}(i)\right]^T \\ &= \widetilde{\mathbf{C}}_V \mathbf{A}_V \mathbf{b}_V(i) + \boldsymbol{\eta}_V(i), \end{aligned} \tag{2.54}$$

where

$$\widetilde{\mathbf{C}}_V = \left[\widetilde{\mathbf{C}}^{(0)}, \underline{\widetilde{\boldsymbol{\Theta}}}^{(1)}, \underline{\widetilde{\boldsymbol{\Theta}}}^{(2)}, \cdots, \underline{\widetilde{\boldsymbol{\Theta}}}^{(G-1)}\right]$$

[7]In the Rayleigh fading channel, the MAI caused by ICI can be seen as produced by the impaired orthogonality among spreading codes solely due to the channel fading.

with $\widetilde{\mathbf{C}}^{(0)}$ given by equation (2.10) and replacing subscript U by V, and

$$\underline{\widetilde{\boldsymbol{\Theta}}}^{(g)} = \left[\widetilde{\boldsymbol{\Theta}}_1^{(g)}, \widetilde{\boldsymbol{\Theta}}_2^{(g)}, \cdots, \widetilde{\boldsymbol{\Theta}}_{L^{(g)}}^{(g)}\right], \tag{2.55}$$

which contains $L^{(g)}$ different transformed code sets for all $K^{(g)}$ users in group g. Each item in equation (2.55) can be expressed as

$$\widetilde{\boldsymbol{\Theta}}_l^{(g)} = \begin{bmatrix} \widetilde{\theta}_{1,l,1}^{(g)} & \widetilde{\theta}_{2,l,1}^{(g)} & \cdots & \widetilde{\theta}_{K^{(g)},l,1}^{(g)} \\ \widetilde{\theta}_{1,l,2}^{(g)} & \widetilde{\theta}_{2,l,2}^{(g)} & \cdots & \widetilde{\theta}_{K^{(g)},l,2}^{(g)} \\ \vdots & \vdots & \vdots & \vdots \\ \widetilde{\theta}_{1,l,M_V^{(0)}}^{(g)} & \widetilde{\theta}_{2,l,M_V^{(0)}}^{(g)} & \cdots & \widetilde{\theta}_{K^{(g)},l,M_V^{(0)}}^{(g)} \end{bmatrix}. \tag{2.56}$$

$\mathbf{A}_V$ and $\mathbf{b}_V$ are given by equation (2.14) and (2.15), respectively. The $\left(M_V^{(0)} \times 1\right)$ white Gaussian noise vector $\boldsymbol{\eta}_V(i)$ has zero mean and covariance matrix $\sigma_n^2\mathbf{I}$, where $\mathbf{I}$ is an $\left(M_V^{(0)} \times M_V^{(0)}\right)$ identity matrix.

Since the VSL scheme can be regarded as a special kind of multi-code scheme, we can consider this multi-rate system as a single lowest rate system with K_v virtual users same as the MFSL scheme. The outputs of the demodulator in equation (2.54) are multiplied by the MMSEC coefficients, an $(M_V \times K_v)$ matrix $\mathbf{W} = [\mathbf{w}_1, \mathbf{w}_2, \cdots \mathbf{w}_{K_v}]$, to form the sufficient statistic of the transmitted bits of all virtual users. The k^{th} column of $\mathbf{W}$, $\mathbf{w}_k$ and the decision variable can be obtained from equation (2.17) and (2.18), respectively, with subscript U replaced by V.

2.5.3 Performance Analysis

The performance of different rate users in the VSL scheme is expressed by equation (2.39), with M_U replaced by M_V.

When only one lowest rate user is present in the system, it can achieve the SUB given by equation (2.20), with M_U replaced by M_V.

For each higher rate user, although it can employ more than one transformed spreading codes, as shown in Appendix A, no SI will be produced even in the Rayleigh fading channels. Hence the desired higher rate user in group g can achieve the SUB expressed in equation (2.21), with $M_U^{(g)}$ replaced by $M_V^{(g)}$.

From the above analysis, for ease of comparison, the system features of different multi-rate schemes, the frequency spacing of adjacent sub-carriers Δf, the number of sub-carriers M, the SUE ϵ, the chip duration T_c, the rate ratio (RR) requirement, the receiver mode (RM) and the expressions of BER performance are summarized in the Table **2.1**.

Table 2.1 Comparison of system features of the different multi-rate access schemes

	UFSL	CFSL	MFSL	VSL
Δf	$R^{(G-1)}$	$R^{(G-1)}$	$R^{(0)}$	$R^{(g)}$
M	$\frac{BW-R^{(G-1)}}{R^{(G-1)}}$	$\frac{BW-R^{(G-1)}}{R^{(G-1)}}$	$\frac{BW-R^{(0)}}{R^{(0)}}$	$\frac{BW-R^{(g)}}{R^{(g)}}$
ϵ	$\frac{2L^{(g)}\left(BW-R^{(G-1)}\right)}{L^{(G-1)}.BW}$	$\frac{2\left(BW-R^{(G-1)}\right)}{BW}$	$\frac{2\left(BW-R^{(0)}\right)}{BW}$	$\frac{2\left(BW-R^{(g)}\right)}{BW}$
T_c	$T_c^{(g)}=\frac{T^{(g)}}{M_U}$	$\frac{T^{(G-1)}}{M_C}$	$\frac{T^{(0)}}{M_M}$	$T_c=T_c^{(g)}=\frac{T^{(g)}}{M_V^{(g)}}$
RR	$\frac{R^{(G-1)}}{R^{(g)}}$ be integers	$\frac{R^{(G-1)}}{R^{(g)}}=\triangle^{(g)}$	$\frac{R^{(g)}}{R^{(0)}}$ be integers	$\frac{R^{(G-1)}}{R^{(g)}}$ be integers
RM	LRM/HRM	HRM	LRM	LRM
BER	(19)	(30)&(31)	(39)	(39)

2.6 Simulation Results and Discussions

To evaluate the performance of different schemes, simulation results are presented in this section. Without loss of generality, a three rate system with rate ratio $\frac{L^{(g)}}{L^{(g-1)}}=2$, $(g=1,2)$ is assumed. With the assumption of total available bandwidth $BW=1.06\ MHz$ and the highest rate $R^{(2)}=212kbps$, only 4 sub-carriers can be used in the UFSL and CFSL scheme (see equation (2.6)), while in the MFSL scheme, 16

sub-carriers can be utilized (see equation (2.32)).[8] In the VSL scheme, high rate, medium rate and low rate users can employ 4, 8 and 16 sub-carriers, respectively (see equation (2.43)).

In the UFSL and CFSL schemes, signals over each sub-carrier are considered frequency-flat faded. Therefore, in the MFSL scheme, since $\Delta^{(0)} = \frac{R^{(G-1)}}{R^{(0)}}$ sub-carriers, $f_i, \left(i = (m-1)\Delta^{(0)} + 1, (m-1)\Delta^{(0)} + 2\,, \quad \cdots, m\Delta^{(0)}\right)$ are located inside the same spectrum of the m^{th} sub-carrier of the highest rate signal, they are highly correlated. Without loss of generality, these $\Delta^{(0)}$ sub-carriers are assumed to undergo the same fading. For the same reason, in the VSL scheme, $\Delta^{(g)} = \frac{R^{(G-1)}}{R^{(g)}}$ sub-carriers of lower rate users in group g are assumed to experience the same fading.

To obtain a fair comparison, orthogonal Walsh-Hadamard codes are employed as spreading codes in all schemes. The ICI is eliminated by properly selecting spreading codes for each user in the VSL scheme as described in Appendix B.

In the MFSL scheme, it has been found in [18] that by employing orthogonal Walsh-Hadamard codes which are properly selected for each higher rate user, SI can be reduced significantly. Because several adjacent sub-carriers might experience similar fading (assumed the same in this paper), if properly choosing its spreading codes set for each higher rate user such that the sub-blocks experiencing the similar fading are orthogonal, the SI will be reduced significantly (In fact,in our channel model, the SI can be fully eliminated). Since long orthogonal Walsh-Hadamard codes are composed of short orthogonal Hadamard codes, they have the aforementioned property and hence they are suitable for applying in the MFSL scheme to reduce SI. For example, assume fadings on adjacent two sub-carriers are the same, i.e., $H = [h_1, h_1, h_2, h_2]$. If a higher rate user employs two Hadamard codes, $[1, 1, 1, 1]$ and $[1, -1, 1, -1]$, each of them is composed of two short orthogonal Hadamard codes, $[1, 1]$ and $[1, -1]$, and after being modified by the channel, they become $[h_1, h_1, h_2, h_2]$ and

[8]It is assumed that the number of sub-carriers is a power of 2 in all schemes.

$[h_1, -h_1, h_2, -h_2]$. It is not difficult to find that they can still preserve orthogonality due to the orthogonality of sub-blocks $[1, 1]$ and $[1, -1]$.

In the CFSL scheme, we use RCPC codes with code rate 8/32, 8/16, derived from the same parent code with code rate $\frac{1}{4}$, puncturing period 8 and constraint length 7. After the MMSEC, soft-decision Viterbi decoding is employed.

Simulations are carried out under 200 i.i.d. frequency selective Rayleigh channels. The sub-carrier frequency correlation is expressed by equation (2.5) with $\tau_d = 0.5us$. With the assumption that the length of the spreading codes equals the number of sub-carriers, only 4 users can be contained in the UFSL and CFSL schemes. For a fair comparison, 2 high rate users, 1 medium rate user and 1 low rate user are assumed in all multi-rate access schemes.

For the downlink MC-CDMA, all users are assumed to undergo the same fading. The BER versus ISR[9] performance of three different rate users, with the SNR[10] of the desired user $15dB$, is shown in Figure 2.11, 2.12 and 2.13, respectively. From these simulation results, it is clear that all different rate users in the UFSL, MFSL and VSL schemes can achieve the same SUB. This result proves that no SI is produced in the VSL scheme and the SI in the MFSL scheme has been fully eliminated by the aforementioned spreading code selection. In the low interference region, the performance of these three schemes is quite similar. However, with different sub-carrier assignment, they present different performance in the high interference region. For the low rate and medium rate user, MFSL and VSL schemes show a much stronger interference suppression capability than the UFSL scheme, which is caused by the better cross-correlation property of the longer spreading codes. For the high rate user, these three schemes perform similarly. It is interesting to note that the performance of the MFSL and VSL schemes are quite similar due to the similar structure of their

[9]The ISR is defined as the power ratio between each undesired user and the desired user.

[10]The SNR of the k^{th} in group g is defined as $10\log_{10}\left(\frac{\left(a_k^{(g)}\right)^2}{\sigma_n^2}\right)(dB)$.

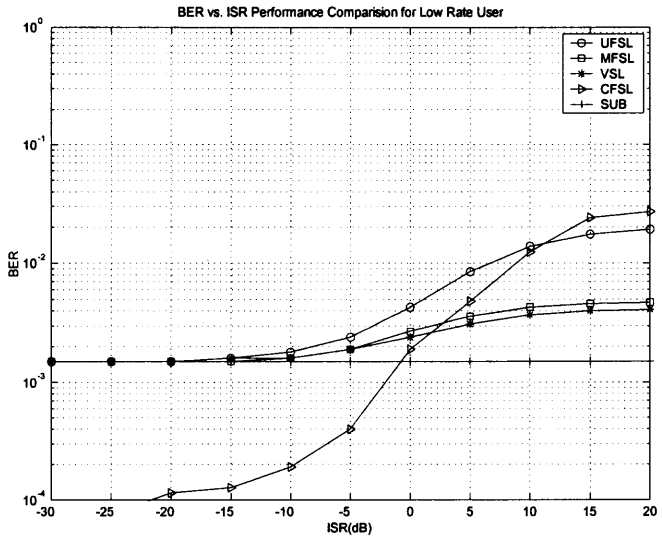

Figure 2.11 BER versus ISR performance of the low rate user in the downlink MC-CDMA.

spreading code matrix. With the CFSL scheme, because of the coding gain, the BER of the low rate and medium rate users is improved significantly in the low interference region. However, due to the error propagation it increases more rapidly than the other schemes in the high interference region. For the high rate user, the performance of the CFSL scheme in the high interference region is worse than the other three schemes, because of using the HRM receiver in the former and the LRM receiver in the latter [36].

The BER versus SNR performance of three different rate users, with ISR= $15dB$ (solid line) and ISR= $-15dB$ (dot line) are presented in Figures 2.14, 2.15 and 2.16, respectively. Similar conclusions can be drawn from these figures. It can be seen clearly that when SNR= $15dB$, for the low rate and medium rate users, the MFSL and the VSL schemes are nearly $5dB$ and $2.5dB$ better than the UFSL scheme in the high interference region (ISR = $15dB$), while the CFSL scheme is nearly $5dB$ and $3dB$ better than the other three schemes in the low interference region (ISR = $-15dB$).

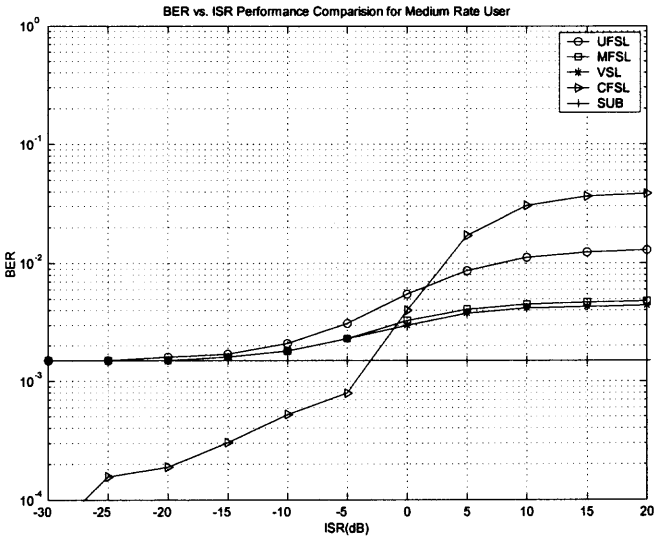

Figure 2.12 BER versus ISR performance of the medium rate user in the downlink MC-CDMA.

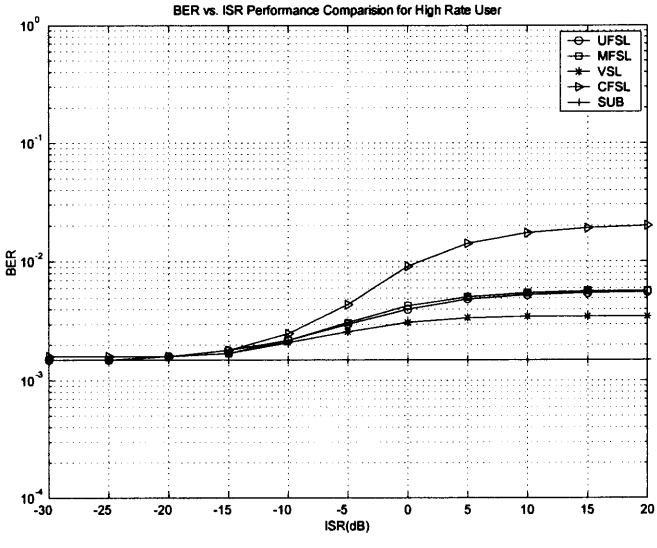

Figure 2.13 BER versus ISR performance of the high rate user in the downlink MC-CDMA.

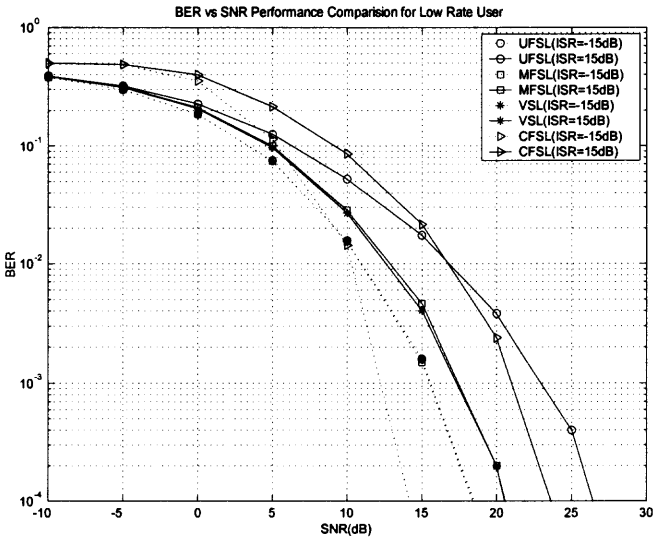

Figure 2.14 BER versus SNR performance of the low rate user in the downlink MC-CDMA.

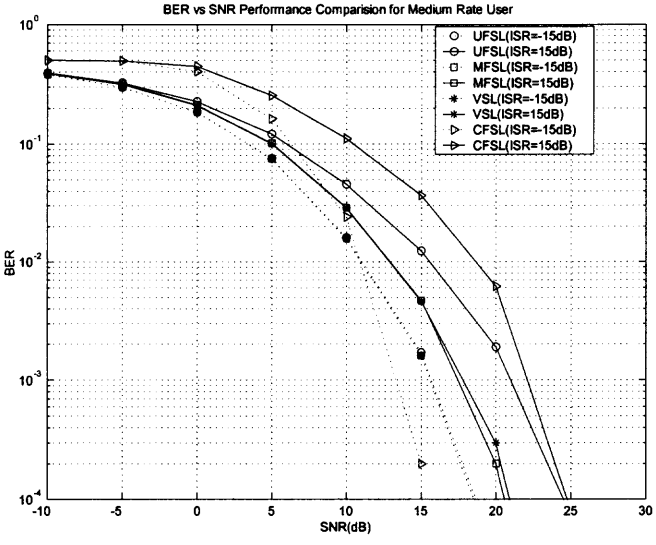

Figure 2.15 BER versus SNR performance of the medium rate user in the downlink MC-CDMA.

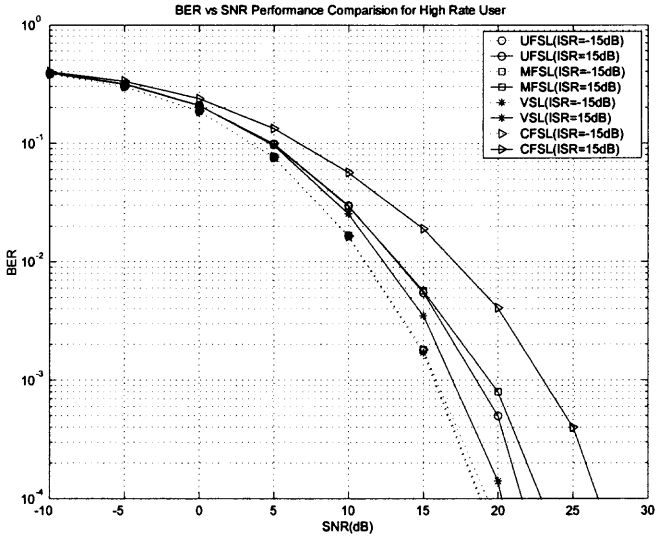

Figure 2.16 BER versus SNR performance of the high rate user in the downlink MC-CDMA.

For comparison, the BER versus ISR performance in the quasi-synchronous uplink for three different rate users is given in Figures 2.17, 2.18 and 2.19, respectively. Different from the downlink, the channels of different users are randomly selected from 200 i.i.d. Rayleigh fading channels. It can be easily found that for the different multi-rate access schemes, all the conclusions for the downlink MC-CDMA still apply for the uplink MC-CDMA.

2.7 Conclusions

In this chapter, four multi-rate access schemes for an MC-CDMA system termed UFSL, CFSL, MFSL and VSL are presented. For each scheme, the performance of all different rate users (low, medium and high rate) was derived by theoretical analysis and simulation results under correlated frequency-selective Rayleigh fading channels for both synchronous downlink and quasi-synchronous uplink MC-CDMA. Due to the different sub-carrier assignment strategies, these schemes present different properties. From the SUE point of view, the MFSL and VSL schemes are the best among all schemes due to their densely spaced spectra. From the rate ratio requirement point of

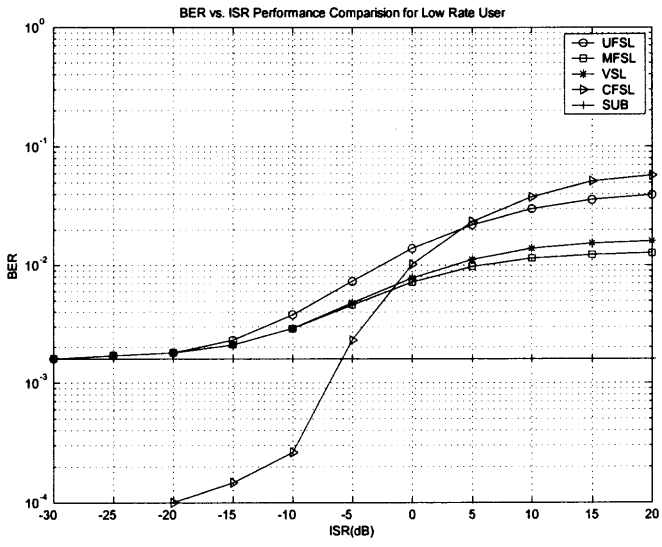

Figure 2.17 BER versus ISR performance of the low rate user in the uplink MC-CDMA.

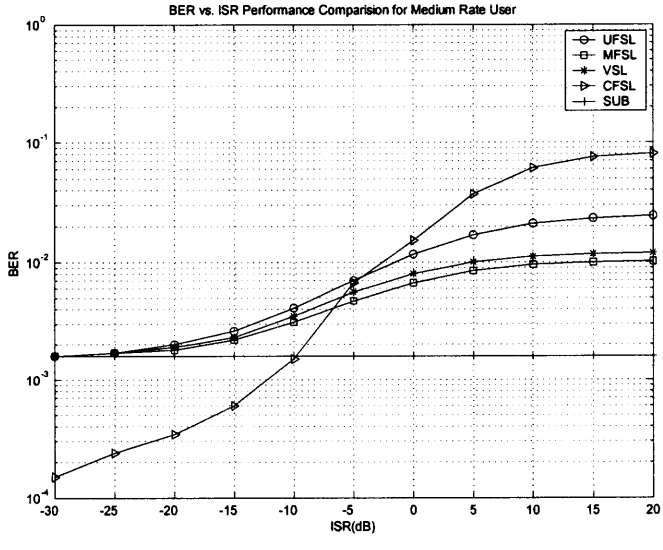

Figure 2.18 BER versus ISR performance of the medium rate user in the uplink MC-CDMA.

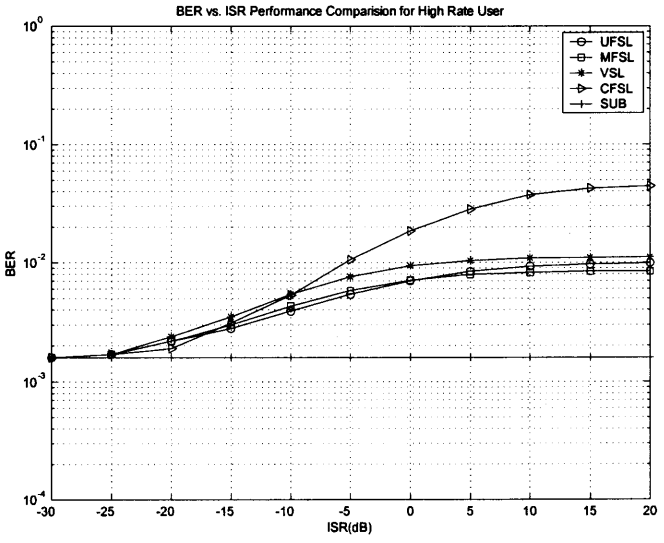

Figure 2.19 BER versus ISR performance of the high rate user in the uplink MC-CDMA.

view, the CFSL has the best capability in rate matching by employing RCPC codes. From the user capacity point of view, the MFSL and VSL schemes can usually support more users than the other two schemes due to their longer spreading codes. From the complexity point of view, the CFSL and MFSL schemes have lower complexity due to their simple modulation and demodulation structure. From the BER performance point of view, the MFSL and VSL schemes are the best in the high interference region, while the CFSL scheme is the best for all lower rate users in the low interference region. Therefore, based on those comparisons, among all these schemes, the MFSL and CFSL schemes are two promising candidates for practical applications, as they present better performance, greater flexibility in rate matching and lower complexity.

CHAPTER 3

SUCCESSIVE INTERFERENCE CANCELLATION FOR MULTI-RATE MC-CDMA

3.1 System Model

In this chapter, a quasi-synchronous uplink multi-rate MC-CDMA system employing the MFSL scheme is considered for SIC. K active users are considered in the system and the k^{th} $(k = 1, 2, \cdots, K)$ user is assigned with l_k spreading codes, which are linearly independent. With a total number of sub-carriers M, the total number of utilized spreading codes $L = \sum_{k=1}^{K} l_k \leq M$. The block diagram of the transmitter for the k^{th} user is shown in Figure 3.1.

As depicted by this figure, the information data, assume BPSK modulated with bit duration T, is 1 to l_k S/P converted, then, each one of the parallel symbols is replicated into M copies and each multiplied by a chip of a preassigned spreading code of length M (frequency domain spreading). After combining corresponding chips of l_k symbols, a discrete-time multi-carrier modulation is performed by an M-point IDFT. Then, after P/S conversion to form an OFDM symbol (time domain), a cyclic prefix of proper length is inserted between successive symbols to avoid ISI. Finally, following RF upconversion, the signal $s_k(t)$ is transmitted through the fading channel.

A correlated Rayleigh fading channel model described in Chapter 2 is considered. Similarly, for the k^{th} user, with the assumption that different users experience the same path loss which equals 1, the channel is represented by an $(M \times 1)$ vector $\mathbf{h}_k$, given by

$$\mathbf{h}_k = [h_{k,1}, h_{k,2}, \cdots, h_{k,M}]^T, \tag{3.1}$$

where $h_{k,m}$ $(m = 1, 2, \cdots, M)$ represents the fading over the m^{th} sub-carrier which is a complex Gaussian random variable with unit variance.

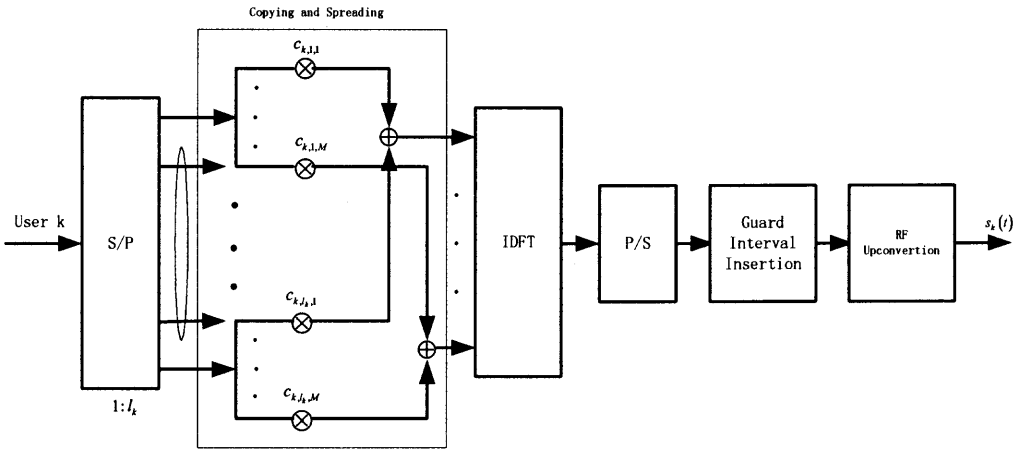

Figure 3.1 Block diagram of the transmitter for the k^{th} user in the MFSL MC-CDMA system.

At the receiver, after RF downconversion and discarding the guard intervals, the receive signal $r(t)$ can be expressed as

$$r(t) = \sum_{i=-\infty}^{+\infty} \left[\sum_{k=1}^{K} \sum_{l=1}^{l_k} \sum_{n=1}^{M} a_{k,l} b_{k,l}(i) \sum_{m=1}^{M} h_{k,m} c_{k,l,m} \cdot e^{j2\pi \frac{mn}{M}} p\left(t - (iM+n)T_c\right) \right] + n(t), \tag{3.2}$$

where the chip duration $T_c = \frac{T}{M}$. The additive white Gaussian noise process $n(t)$ has zero mean and variance σ_n^2.

After demodulation (DFT), the output during the i^{th} OFDM symbol interval $[(i-1)T, iT)$ can be expressed in a compact matrix form as

$$\mathbf{x}(i) = \widetilde{\mathbf{C}}\mathbf{A}\mathbf{b}(i) + \boldsymbol{\eta}(i). \tag{3.3}$$

Similarly, as in equation (2.35), $\widetilde{\mathbf{C}}$ is the channel-modified spreading code matrix, expressed as

$$\widetilde{\mathbf{C}} = \left[\widetilde{\mathbf{C}}_1, \widetilde{\mathbf{C}}_2, \cdots, \widetilde{\mathbf{C}}_K\right], \tag{3.4}$$

where $\widetilde{\mathbf{C}}_k$ $(k = 1, 2, \cdots, K)$ is given by

$$\widetilde{\mathbf{C}}_k = \left[\widetilde{\mathbf{c}}_{k,1}, \widetilde{\mathbf{c}}_{k,2}, \cdots, \widetilde{\mathbf{c}}_{k,l_k}\right], \tag{3.5}$$

which contains l_k different code vectors of the k^{th} user. Each item in equation (3.5) can be expressed as

$$\begin{aligned} \widetilde{\mathbf{c}}_{k,l} &= \mathbf{h}_k \odot \mathbf{c}_{k,l} \\ &= \left[h_{k,1}c_{k,l,1}, h_{k,2}c_{k,l,2}, \cdots, h_{k,N}c_{k,l,N}\right]^T. \end{aligned} \tag{3.6}$$

$\mathbf{A}$ is an $(L \times L)$ diagonal matrix containing the transmit amplitudes of all symbols, given by

$$\mathbf{A} = \mathbf{diag}\left(\left[\mathbf{a}_1^T, \mathbf{a}_2^T, \cdots, \mathbf{a}_K^T\right]^T\right), \tag{3.7}$$

where $\mathbf{a}_k = \left[a_{k,1}, a_{k,2}, \cdots, a_{k,l_k}\right]^T$, $(k = 1, 2, \cdots, K)$. $\mathbf{b}(i)$ is an $(L \times 1)$ vector containing the parallel transmit symbols of all users with normalized power, given by

$$\mathbf{b}(i) = \left[\mathbf{b}_1^T(i), \mathbf{b}_2^T(i), \cdots, \mathbf{b}_K^T(i)\right]^T \tag{3.8}$$

where $\mathbf{b}_k(i) = \left[b_{k,1}(i), b_{k,2}(i), \cdots, b_{k,l_k}(i)\right]^T$, $(k = 1, 2, \cdots, K)$. The $(L \times 1)$ white Gaussian noise vector $\boldsymbol{\eta}(i)$ has zero mean and covariance matrix $\sigma^2\mathbf{I}$, where $\mathbf{I}$ is an $(M \times M)$ identity matrix.

After matched-filtering, the following expression can be obtained

$$\begin{aligned} \mathbf{y}(i) &= \widetilde{\mathbf{C}}^H \cdot \mathbf{x}(i) \\ &= \mathbf{R}_c\mathbf{A}\mathbf{b}(i) + \widetilde{\boldsymbol{\eta}}(i), \end{aligned} \tag{3.9}$$

where $\mathbf{R}_c = \widetilde{\mathbf{C}}^H\widetilde{\mathbf{C}}$ is the channel-modified cross-correlation matrix.

With a nonlinear SIC receiver, the symbols transmitted in parallel on different spreading codes are detected successively. The interference caused by earlier detected

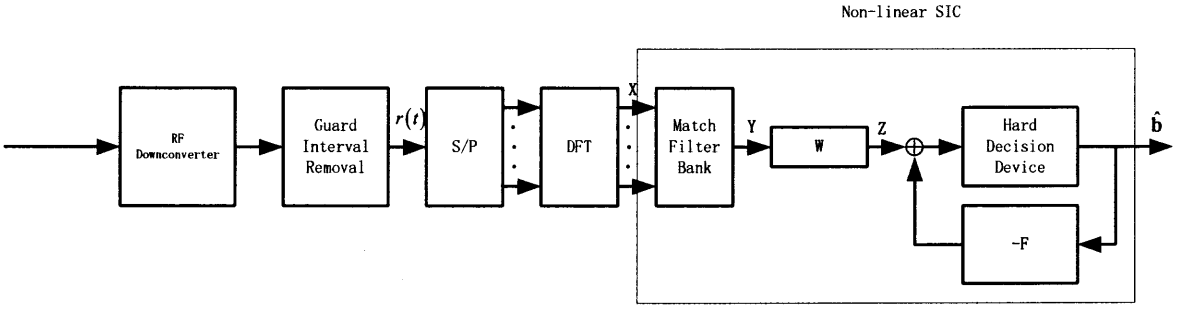

Figure 3.2 Block diagram of a general nonlinear SIC receiver for the MFSL MC-CDMA system.

symbols are regenerated using the hard decisions and then cancelled from the composite signal to assist in detecting other symbols that have not been detected yet. The SIC receiver can be parameterized by the pair of matrices $(\mathbf{W}, \mathbf{F})$. Both the feedforward matrix $\mathbf{W}$ and the feedback matrix $\mathbf{F}$ are of dimension $L \times L$, while the latter is also constrained to be strictly upper triangular (i.e., it is nonzero only above the main diagonal). The j^{th} symbol is detected by slicing

$$z_j(i) = \left[\left[\mathbf{W}^H\right]_j\right]^H \mathbf{y}(i) - \sum_{l=j+1}^{L} [\mathbf{F}]_{j,l} \left[\widehat{\mathbf{b}}(i)\right]_l, \tag{3.10}$$

where $[\mathbf{x}]_j$, $[\mathbf{X}]_j$ and $[\mathbf{X}]_{i,j}$ denote the j^{th} element of a vector $\mathbf{x}$, the j^{th} column and the $(i,j)^{th}$ element of a matrix $\mathbf{X}$, respectively; $\left[\widehat{\mathbf{b}}(i)\right]_l$ denotes the hard decision of the l^{th} symbol. The block diagram of a general nonlinear SIC receiver is shown in Figure 3.2.

The ZF-SIC and MMSE-SIC receiver, originally proposed for single-rate CDMA systems [21] are applied in the MFSL MC-CDMA system, which will be discussed in the following two sections.

3.2 Zero-forcing Successive Interference Cancellation (ZF-SIC)

With the ZF-SIC receiver, $\mathbf{W}$ and $\mathbf{F}$ are chosen to eliminate all MAI provided that all feedback is correct. Thus, the first detected symbol does not involve feedback, and

is equivalent to the decorrelator. On the other hand, the last detected symbol utilizes decisions of all other symbols and ideally (i.e., when feedback symbols are correct) achieves the performance of the single-user system.

3.2.1 SIC Algorithm

The cross-correlation matrix $\mathbf{R}_c$ is assumed positive definite, which is reasonable in practice. Hence, by performing CF, it can be uniquely decomposed as $\mathbf{R}_c = \mathbf{\Gamma}^H \mathbf{D}^2 \mathbf{\Gamma}$, where $\mathbf{\Gamma}$ is upper triangular and monic (having all 1s along the diagonal), $\mathbf{D} = \mathbf{diag}\left(\left[\mathbf{d}_1^T, \mathbf{d}_2^T, \cdots, \mathbf{d}_K^T\right]^T\right)$ is a real diagonal matrix, where $\mathbf{d}_k = [d_{k,1}, d_{k,2}, \cdots, d_{k,l_k}]^T$, $(k = 1, 2, \cdots, K)$. By multiplying on both sides of equation (3.9) $\mathbf{D}^{-2}\mathbf{\Gamma}^{-H}$, the following equation can be obtained

$$\begin{aligned} \mathbf{z}(i) &= \mathbf{D}^{-2}\mathbf{\Gamma}^{-H} \cdot \mathbf{y}(i) \\ &= \mathbf{\Gamma}\mathbf{A}\mathbf{b}(i) + \widehat{\boldsymbol{\eta}}(i), \end{aligned} \tag{3.11}$$

where $\widehat{\boldsymbol{\eta}}(i)$ is an $(L \times 1)$ Gaussian vector with uncorrelated components, whose covariance matrix equals $\sigma_n^2 \mathbf{D}^{-2}$, shown in Appendix C.

From (3.11), since $\mathbf{\Gamma}$ is upper triangular and $\widehat{\boldsymbol{\eta}}(i)$ has uncorrelated components, the receive symbols $\widehat{\mathbf{b}}(i) = \left[\widehat{\mathbf{b}}_1^T(i), \widehat{\mathbf{b}}_2^T(i), \cdots, \widehat{\mathbf{b}}_K^T(i)\right]^T$ can be recovered by back-substitution combined with symbol-by-symbol detection. The SIC algorithm is described as follows;

$$\begin{aligned} \text{for } l &= 0 \text{ to } L-1 \\ \left[\widehat{\mathbf{b}}(i)\right]_{L-l} &= \text{hard decision}\Big([\mathbf{z}(i)]_{L-l} \\ &\qquad - \sum_{m=1}^{l} [\mathbf{A}]_{L-l+m,L-l+m} \cdot [\mathbf{\Gamma}]_{L-l,L-l+m} \left[\widehat{\mathbf{b}}(i)\right]_{L-l+m} \Big) \\ &\qquad \text{end}, \end{aligned} \tag{3.12}$$

Apparently, for the ZF-SIC receiver, $\mathbf{W} = \mathbf{D}^{-2}\mathbf{\Gamma}^{-H}$ and $\mathbf{F} = \mathbf{A}\mathbf{\Gamma}$.

With the assumption of perfect cancellation, the sufficient statistic of the l^{th} $(l = 1, 2, \cdots, L)$ symbol $\left[\widehat{\mathbf{b}}(i)\right]_{L-l+1}$ can be expressed as

$$[\mathbf{z}(i)]_{L-l+1} = [\mathbf{A}]_{L-l+1,L-l+1} [\mathbf{b}(i)]_{L-l+1} + [\widehat{\boldsymbol{\eta}}(i)]_{L-l+1}. \tag{3.13}$$

The SIR γ_{L-l+1} can be expressed as

$$\gamma_{L-l+1} = \frac{[\mathbf{A}^2]_{L-l+1,L-l+1}}{\sigma_n^2 [\mathbf{D}^{-2}]_{L-l+1,L-l+1}}. \tag{3.14}$$

As aforementioned, the SIR of the first detected symbol $\left[\widehat{\mathbf{b}}(i)\right]_L$ is the same as that of the ZF detector, whereas other symbols are detected by substracting a linear combination of previous hard decisions from $\mathbf{z}(i)$. Since decision errors are ignored, the SIR expressed in equation (3.14) will be higher than actually achieved in the real system. Hence, the following equation leads to a LB of the BER performance for the k^{th} user with the ZF-SIC receiver,

$$BER_{LB,ZF-SIC}^{(k)} = \frac{1}{l_k} E_h \left[\sum_{l=1}^{l_k} Q\left(\sqrt{\frac{a_{k,l}^2}{\sigma_n^2 \cdot d_{k,l}^{-2}}} \right) \right]. \tag{3.15}$$

3.2.2 Simulation Results and Discussions

An indoor Rayleigh fading channel model is employed in the simulations. The total available bandwidth is assumed to be $100MHz$ with $\tau_d = 25ns$. The number of sub-carriers is chosen as 16. Orthogonal Walsh Hadamard codes are employed for spreading. For simplicity, two users are assumed, each employing 8 codes in the fully loaded system. BPSK modulation is used and all simulation results are obtained over 1000 channel realizations.

Without power distribution control (PDC), in the multi-code system, it is customary to distribute the transmit power evenly among all symbols transmitted in parallel on different spreading codes. This situation is considered for all simulations.

In Figure 3.3, *the average BER performance over two users* versus the E_b/N_0 in the fully loaded system is shown. From this figure, it is clear that the performances of

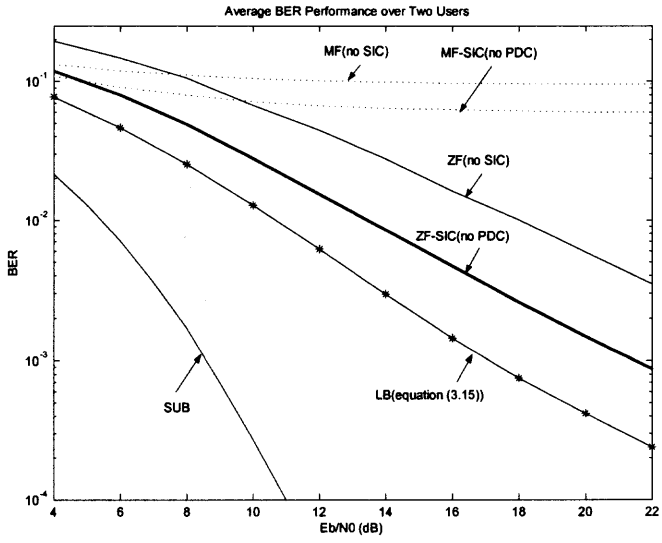

Figure 3.3 BER performance (averaged over two users) in the fully loaded system.

the MF (no SIC) and the MF-SIC without PDC are heavily limited by interference. Compared with the MF, the ZF can suppress interference much better when the E_b/N_0 is above a certain level. By employing SIC, even with equal distributed transmit power, significant performance improvement can be obtained. The LB expressed in equation (3.15) and the SUB are also plotted for comparison. The performance difference between the LB and the simulation result implies that the decision error propagation significantly degrades the BER performance.

The BER performances of *the two sequentially detected users* are compared in Figure 3.4. It can be easily found that with the equal transmit power (no PDC), for both the MF-SIC and the ZF-SIC receivers, the performance difference between two users is very large. The second detected user achieves much better performance than the first one, since more interference has been cancelled.

In Figure 3.5, the required E_b/N_0 versus the number of spreading codes, at a target BER of 10^{-4}, is shown. In this figures, for simplicity, a single user with a variable number of spreading codes is assumed. When 1 code is employed, the system can be looked upon as a single user system; when 16 codes are employed, it is

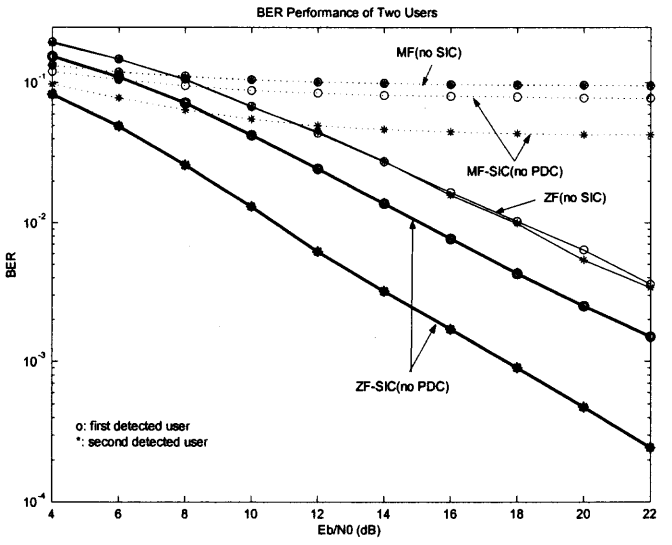

Figure 3.4 BER performance of two sequentially detected users in the fully loaded system.

equivalent to a fully loaded system. It can be seen clearly that under different system load, ZF-SIC always needs less power than the ZF receiver, particularly when the system is highly loaded.

3.3 Minimum Mean Square Error Successive Interference Cancellation (MMSE-SIC)

With the MMSE-SIC receiver, $\mathbf{W}$ and $\mathbf{F}$ are chosen to simultaneously maximize all symbols' SIR (i.e., minimize the MSE), for a given decision order [42]. Although the ZF can eliminate all interference, it usually produces higher error rates than the MMSE due to the noise enhancement. Therefore, the MMSE-SIC receiver outperforms the ZF-SIC receiver [43]. Similarly, the first detected symbol does not involve feedback, and is equivalent to the MMSE detector, while the last detected symbol utilizes decisions of all other symbols and ideally, it can achieve the performance of the single-user system, provided that all feedback is correct.

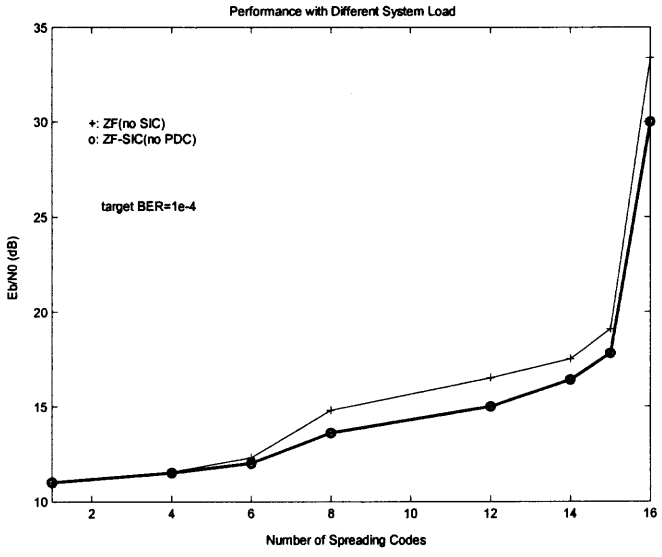

Figure 3.5 Required E_b/N_0 for achieving a target BER of 10^{-4} versus different system load.

3.3.1 SIC Algorithm

Unlike the ZF-SIC, the MMSE-SIC receiver is implemented using the CF of the positive definite matrix $\mathbf{R}_m = \mathbf{R}_c + \sigma^2\mathbf{A}^{-2}$, which can be uniquely decomposed as $\mathbf{R}_m = \overline{\mathbf{\Gamma}}^H \overline{\mathbf{D}}^2 \overline{\mathbf{\Gamma}}$. Similarly, $\overline{\mathbf{\Gamma}}$ is upper triangular and monic (having all 1s along the diagonal) and $\overline{\mathbf{D}} = \mathbf{diag}\left(\left[\overline{\mathbf{d}}_1^T, \overline{\mathbf{d}}_2^T, \cdots, \overline{\mathbf{d}}_K^T\right]^T\right)$ is a real diagonal matrix with $\overline{\mathbf{d}}_k = \left[\overline{d}_{k,1}, \overline{d}_{k,2}, \cdots, \overline{d}_{k,l_k}\right]^T$. By multiplying on both sides of equation (3.9) $\overline{\mathbf{D}}^{-2}\overline{\mathbf{\Gamma}}^{-H}$, the following expression can be obtained

$$\begin{aligned} \overline{\mathbf{z}}(i) &= \overline{\mathbf{D}}^{-2}\overline{\mathbf{\Gamma}}^{-H} \cdot \mathbf{y}(i) \\ &= \overline{\mathbf{\Gamma}}\mathbf{A}\mathbf{b}(i) + \overline{\boldsymbol{\eta}}(i), \end{aligned} \tag{3.16}$$

where $\overline{\boldsymbol{\eta}}(i)$ is an $(L \times 1)$ Gaussian vector with uncorrelated components, whose covariance matrix equals $\sigma_n^2\overline{\mathbf{D}}^{-2}$. The detailed proof is shown in Appendix C.

Similarly, the SIC algorithm can be expressed as follows:

$$\begin{aligned} \text{for } l &= 0 \text{ to } L-1 \\ \left[\widehat{\mathbf{b}}(i)\right]_{L-l} &= \text{hard decision}\Big(\left[\overline{\mathbf{z}}(i)\right]_{L-l} \\ &\quad - \sum_{m=1}^{l} [\mathbf{A}]_{L-l+m,L-l+m} \cdot \left[\overline{\mathbf{\Gamma}}\right]_{L-l,L-l+m} \left[\widehat{\mathbf{b}}(i)\right]_{L-l+m} \Big) \\ &\quad \text{end,} \end{aligned} \tag{3.17}$$

Apparently, for the MMSE-SIC receiver, $\mathbf{W} = \overline{\mathbf{D}}^{-2}\overline{\mathbf{\Gamma}}^{-H}$ and $\mathbf{F} = \mathbf{A}\overline{\mathbf{\Gamma}}$.

With the assumption of perfect cancellation, the sufficient statistic of the l^{th} $(l = 1, 2, \cdots, L)$ symbol $\left[\widehat{\mathbf{b}}(i)\right]_{L-l+1}$ can be expressed as

$$\left[\overline{\mathbf{z}}(i)\right]_{L-l+1} = [\mathbf{A}]_{L-l+1,L-l+1} \left[\mathbf{b}(i)\right]_{L-l+1} + \left[\overline{\boldsymbol{\eta}}(i)\right]_{L-l+1}. \tag{3.18}$$

By applying the orthogonal principle in [44], the SIR of $\left[\widehat{\mathbf{b}}(i)\right]_{L-l+1}$ can be expressed as

$$\begin{aligned} \gamma_{L-l+1} &= \frac{E\left[\left|[\mathbf{A}]_{L-l+1,L-l+1}\left[\widehat{\mathbf{b}}(i)\right]_{L-l+1}\right|^2\right]}{mmse} - 1 \\ &= \frac{[\mathbf{A}]^2_{L-l+1,L-l+1}}{\sigma_n^2 \left[\overline{\mathbf{D}}\right]^{-2}_{L-l+1,L-l+1}} - 1. \end{aligned} \tag{3.19}$$

Similarly, the following equation leads to a LB of the BER performance for the k^{th} user with the MMSE-SIC receiver,

$$BER^{(k)}_{LB,MMSE-SIC} = \frac{1}{l_k} E_h \left[\sum_{l=1}^{l_k} Q\left(\sqrt{\frac{a^2_{k,l}}{\sigma_n^2 \cdot \overline{d}^{-2}_{k,l}} - 1} \right) \right]. \tag{3.20}$$

3.3.2 Simulation Results and Discussions

The same simulation conditions described in the previous section are used for the MMSE-SIC receiver.

In Figure 3.6, *the average BER performance over two users* versus the E_b/N_0 in the fully loaded system is shown. It is clear from this figure that the MMSE receiver

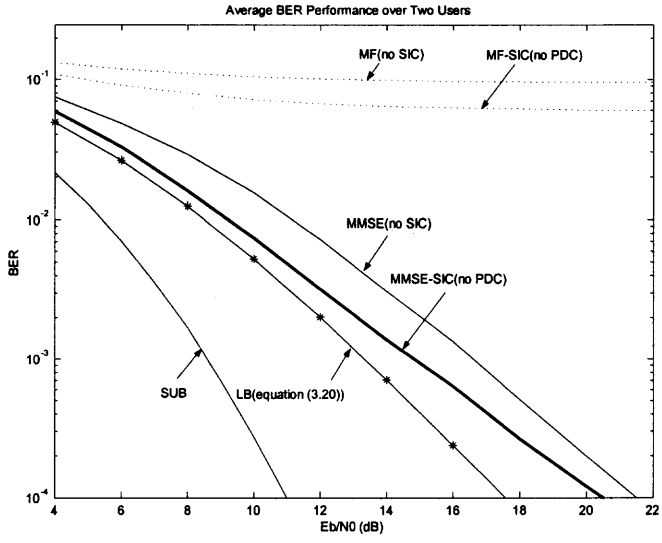

Figure 3.6 BER performance (averaged over two users) in the fully loaded system.

can suppress interference more effectively that the MF and MF-SIC receivers. By employing SIC, the performance can be further improved. At a BER of 10^{-4}, about 1dB performance improvement can be obtained. The performance difference between the LB (equation (3.20)) and the simulation result is smaller than that of the ZF receiver shown in Figure 3.3, which implies that the cancellation errors might have a smaller effect on the MMSE-SIC receiver than on the ZF-SIC receiver. However, at a BER of 10^{-4}, it can be found that the MMSE-SIC with evenly distributed transmit power is still more than 10dB worse than the SUB.

The BER performances of *the two sequentially detected users* are compared in Figure 3.7. Similar conclusions can be obtained as in Figure 3.4.

In Figure 3.8, the required E_b/N_0 versus the number of spreading codes, at a target BER of 10^{-4}, is shown. Similarly, under different system load, the MMSE-SIC always requires less E_b/N_0 than the MMSE receiver. However, the performance improvement is not very significant even in the fully loaded system.

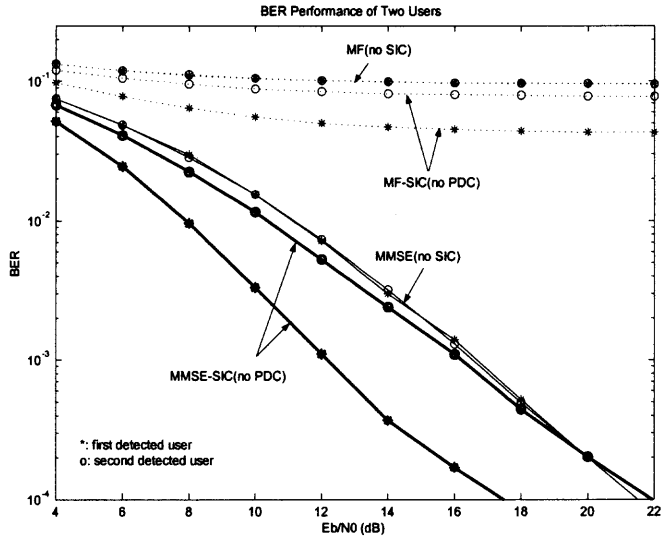

Figure 3.7 BER performance of two sequentially detected users in the fully loaded system.

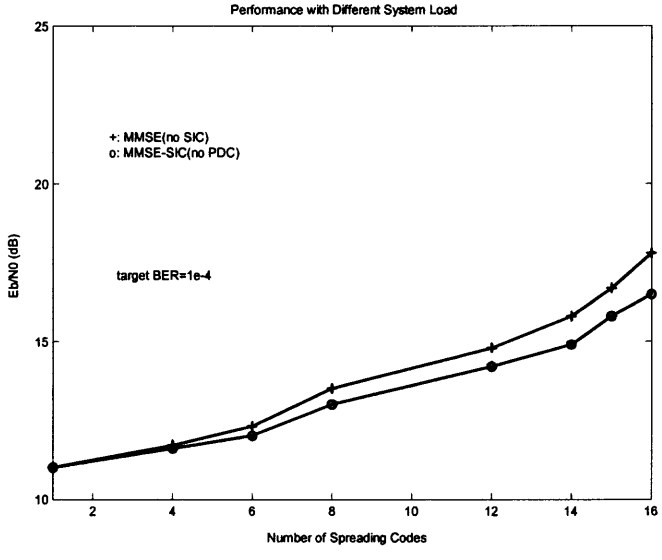

Figure 3.8 Required E_b/N_0 for achieving a target BER of 10^{-4} versus different system load.

3.4 Conclusions

In this chapter, the nonlinear ZF-SIC and MMSE-SIC receivers are applied in the MFSL MC-CDMA systems. Without PDC, the transmit power is considered to be evenly distributed among all symbols transmitted in parallel on difference spreading codes. Simulation results in correlated Rayleigh fading channels show that both the nonlinear ZF-SIC and MMSE-SIC receivers outperform the linear counterparts without SIC. Moreover, they are remarkably better that the MF-SIC receiver, whose performance is heavily limited by MAI in the fully loaded system. It is also found that without PDC, particularly for the MMSE-SIC receiver, the performance improvement with SIC is not very significantly. Therefore, this motivates an investigation of PDC algorithms, which can increase the efficiency of SIC.

CHAPTER 4

POWER DISTRIBUTION CONTROL FOR ZF-SIC

As stated in the introduction, for a multi-code system, the equal BER criterion is also suitable to derive the power distribution, which ensures each virtual lowest rate user the same BER after SIC. With the equal BER PDC, the earlier detected symbols will be allocated more power since they are exposed to higher interference than the later detected ones. Hence, compared with the power distribution that ensures equal receive power (which could happen in a multi-code system), such an approach suppresses interference more effectively by improving the reliability of earlier detected symbols. However, a multi-code system is different from a single-code system in that each user's BER is decided by the average over all its parallel transmit symbols. Hence, the equal BER PDC does not minimize each user's BER. For the ZF-SIC receiver, both the equal BER PDC and the optimal PDC algorithms, which minimize each user's BER, will be investigated, under both a STPC and a LTPC, in the following sections.

In the sequel, perfect cancellation is assumed for deriving the PDC algorithms. Although no firm analysis of feedback errors in SIC receivers in general scenarios, it is known that in uncoded systems, the effects of error propagation can for the most part be mitigated, at least asymptotically in the received signal-to-interference ratios (SIRs), when users are detected in decreasing order of SIR [43].

4.1 Equal BER PDC Algorithm

To achieve equal BER, it is clear that

$$\gamma_L = \gamma_{L-1} = \cdots = \gamma_1 \tag{4.1}$$

from (3.14), the following relationship should be satisfied

$$\frac{[\mathbf{A}^2]_{L,L}}{[\mathbf{D}^{-2}]_{L,L}} = \frac{[\mathbf{A}^2]_{L-1,L-1}}{[\mathbf{D}^{-2}]_{L-1,L-1}} = \cdots = \frac{[\mathbf{A}^2]_{1,1}}{[\mathbf{D}^{-2}]_{1,1}}. \tag{4.2}$$

4.1.1 PDC Algorithm under STPC

Under each channel realization, the STPC $\overline{\mathcal{P}}$, is defined as

$$\overline{\mathcal{P}} = \frac{1}{L} tr\left(\mathbf{A}^2\right), \tag{4.3}$$

where $tr\left(\mathbf{X}\right)$ denotes the trace of a matrix $\mathbf{X}$. For a given a channel realization, from equation (3.14) and (4.2), $\mathbf{A}$ must satisfy

$$\left[\mathbf{A}^2\right]_{L-l,L-l} = \gamma_{|h} \cdot \sigma_n^2 \left[\mathbf{D}^{-2}\right]_{L-l,L-l} \quad (l = 0, 1, \cdots, L-1), \tag{4.4}$$

where $\gamma_{|h}$ denotes the achievable SIR, which depends on the channel realization. Applying (4.3), it can be shown that

$$\begin{aligned} \overline{\mathcal{P}} &= \frac{1}{L}\gamma_{|h}\sigma_n^2 \cdot \sum_{l=0}^{L-1} \left[\mathbf{D}^{-2}\right]_{L-l,L-l} \\ &= \frac{1}{L}\gamma_{|h}\sigma_n^2 tr\left(\mathbf{D}^{-2}\right). \end{aligned} \tag{4.5}$$

Therefore, the achievable SIR $\gamma_{|h}$ can be expressed as

$$\gamma_{|h} = \frac{L\overline{\mathcal{P}}}{\sigma_n^2 tr\left(\mathbf{D}^{-2}\right)}, \tag{4.6}$$

and the power distribution is given by

$$\left[\mathbf{A}^2\right]_{L-l,L-l} = \frac{L\left[\mathbf{D}^{-2}\right]_{L-l,L-l}\overline{\mathcal{P}}}{tr\left(\mathbf{D}^{-2}\right)} \quad (l = 0, 1, \cdots, L-1). \tag{4.7}$$

Note that $\mathbf{A}$ and $\mathbf{D}$ also depend on the channel realization. The notations are omitted for simplicity. Since decision errors are ignored, $\gamma_{|h}$ is higher than actually can be achieved in the real system. Therefore, with the equal BER PDC, under the STPC,

the average BER performance obtained with $\gamma_{|h}$ in (4.6) leads to a lower bound LB of the BER of the ZF-SIC receiver, which can be expressed as

$$\begin{aligned} BER_{LB-ST} &= E_h\left[Q\left(\sqrt{\gamma}\right)\right] \\ &= E_h\left[Q\left(\sqrt{\frac{L\overline{\mathcal{P}}}{\sigma_n^2 tr\left(\mathbf{D}^{-2}\right)}}\right)\right]. \end{aligned} \tag{4.8}$$

4.1.2 PDC Algorithm under LTPC

Under the LTPC, the transmit power is adapted with channel variations for achieving a target SIR γ (which is kept the same for all channel realizations). The LTPC $\overline{\mathcal{P}}$ is determined by the average of power over all channel realizations, which is

$$\overline{\mathcal{P}} = \frac{1}{L} E_h\left[tr\left(\mathbf{A}^2\right)\right]. \tag{4.9}$$

Therefore, for a certain channel realization, $\overline{\mathcal{P}}_{|h}$ is defined as the required power for achieving γ, and from (4.5),

$$\overline{\mathcal{P}}_{|h} = \frac{1}{L}\gamma\sigma_n^2 tr\left(\mathbf{D}^{-2}\right). \tag{4.10}$$

Substituting it into the power constraint expressed by (4.9), it can be shown that

$$\begin{aligned} \overline{\mathcal{P}} &= E_h\left[\overline{\mathcal{P}}_{|h}\right] \\ &= \frac{1}{L}\gamma\sigma_n^2 \cdot E_h\left[tr\left(\mathbf{D}^{-2}\right)\right]. \end{aligned} \tag{4.11}$$

The SIR γ for a LTPC $\overline{\mathcal{P}}$ can be expressed as

$$\gamma = \frac{L\overline{\mathcal{P}}}{\sigma_n^2 E_h\left[tr\left(\mathbf{D}^{-2}\right)\right]}, \tag{4.12}$$

and the power distribution under each channel realization is given by

$$\left[\mathbf{A}^2\right]_{L-l,L-l} = \frac{L\left[\mathbf{D}^{-2}\right]_{L-l,L-l}}{E_h\left[tr\left(\mathbf{D}^{-2}\right)\right]}\overline{\mathcal{P}} \quad (l = 0, 1, \cdots, L-1). \tag{4.13}$$

Similarly, under the LTPC, the LB for the equal BER PDC can be expressed as

$$BER_{LB-LT} = Q\left(\sqrt{\gamma}\right) = Q\left(\sqrt{\frac{L\overline{\mathcal{P}}}{\sigma_n^2 E_h \left[tr\left(\mathbf{D}^{-2}\right)\right]}}\right). \tag{4.14}$$

4.2 Optimal PDC Algorithm

In a multi-code system, for the k^{th} user, its BER performance is the average over all the l_k parallel transmit symbols, which can be expressed as

$$\overline{p}_{e,k}\left(\mathbf{a}_k^2\right) = \frac{1}{l_k}\sum_{l=1}^{l_k} p_{e,k,l}\left(a_{k,l}^2\right). \tag{4.15}$$

The optimal PDC aims to minimize $\overline{p}_{e,k}\left(\mathbf{a}_k^2\right)$, under both a STPC and a LTPC.

4.2.1 PDC Algorithm under STPC

With the STPC $\overline{\mathcal{P}}$, under each channel realization, the optimization problem can be stated as follows,

$$\begin{aligned} &\textit{For the } k^{th}\textit{user, find the optimal power distribution } \mathbf{a}_k^{2\dagger}, \\ &\textit{which satisfies: } \mathbf{a}_k^{2\dagger} = \arg\min_{\mathbf{a}_k^2}\left(\overline{p}_{e,k}\left(\mathbf{a}_k^2\right)\right) \\ &\textit{subject to: } \begin{cases} a_{k,l}^{2\dagger} \geq 0 \quad (l = 1, 2, \cdots, l_K) \\ \frac{1}{l_k}\sum_{l=1}^{l_k} a_{k,l}^{2\dagger} = \overline{\mathcal{P}}_k \end{cases}, \end{aligned} \tag{4.16}$$

where $\overline{\mathcal{P}}_k$ is the average transmit power allocated to the k^{th} user, which satisfies

$$\frac{1}{L}\sum_{k=1}^{K} l_k \overline{\mathcal{P}}_k = \overline{\mathcal{P}}. \tag{4.17}$$

Without loss of generality and for ease of comparison with the equal BER PDC, different users are assumed to have the same BER requirement, i.e., $\overline{p}_{e,k}\left(\mathbf{a}_k^{2\dagger}\right) = \overline{p}_{e,l}\left(\mathbf{a}_l^{2\dagger}\right)$ $(k, l = 1, 2, \cdots, K \text{ and } k \neq l)$. This determines the average transmit power $\overline{\mathcal{P}}_k$ allocated to the k^{th} $(k = 1, 2, \cdots, K)$ user, which will be explained later.

By ignoring cancellation errors, equation (4.15) can be rewritten as

$$\overline{p}_{e,k}\left(\mathbf{a}_k^2\right) = \frac{1}{l_k}\sum_{l=1}^{l_k} Q\left(\sqrt{\frac{a_{k,l}^2}{\sigma_n^2 \cdot d_{k,l}^{-2}}}\right), \tag{4.18}$$

It is clear that (4.16) is a convex optimization problem with differentiable objects and constraint functions, for which exists a unique and global optimal solution. Here, the Karush-Kuhn-Tucker (KKT) optimality conditions [45] are used to solve this problem, as shown in Appendix D. For the k^{th} user, the optimal power distribution is found to be

$$a_{k,l}^{2\dagger} = \begin{cases} -2d_{k,l}^{-2}\sigma_n^2 \ln\left(4\vartheta_k^{\dagger} d_{k,l}^{-2}\sigma_n^2\right) & 0 < \vartheta_k^{\dagger} < \frac{1}{4\sigma_n^2 d_{k,l}^{-2}} \\ 0 & \vartheta_k^{\dagger} \geq \frac{1}{4\sigma_n^2 d_{k,l}^{-2}} \end{cases} \tag{4.19}$$

or equivalently

$$a_{k,l}^{2\dagger} = \max\left[0, -2d_{k,l}^{-2}\sigma_n^2 \ln\left(4\vartheta_k^{\dagger} d_{k,l}^{-2}\sigma_n^2\right)\right], \tag{4.20}$$

where $\vartheta_k^{\dagger}$ is the Lagrange multiplier, which can be found from the average power constraint, expressed as

$$\frac{1}{l_k}\sum_{l=1}^{l_k} \max\left[0, -2d_{k,l}^{-2}\sigma_n^2 \ln\left(4\vartheta_k^{\dagger} d_{k,l}^{-2}\sigma_n^2\right)\right] = \overline{\mathcal{P}}_k. \tag{4.21}$$

As stated in Appendix D, for $\vartheta_k^{\dagger} \in \left(0, \frac{1}{4\sigma_n^2 d_{k,l}^{-2}}\right]$, $a_{k,l}^{2\dagger} \in [0, +\infty)$ and it is monotonically decreasing with $\vartheta_k^{\dagger}$. Hence, for $\vartheta_k^{\dagger} \in \left(0, \max_{l=1,2,\cdots,l_k}\left(\frac{1}{4\sigma_n^2 d_{k,l}^{-2}}\right)\right]$, $\overline{\mathcal{P}}_k \in [0, +\infty)$ and also, it is monotonically decreasing with $\vartheta_k^{\dagger}$. Based on these conclusions and with (4.18), it is not difficult to find that $\overline{p}_{e,k}\left(\mathbf{a}_k^2\right)$ is monotonically decreasing with $\overline{\mathcal{P}}_k$.

For simplicity, considering only two users, under each channel realization, the algorithm can be concluded as follows: 1) let $\overline{\mathcal{P}}_1 = \overline{\mathcal{P}}$ and $\overline{\mathcal{P}}_2 = 0$. 2) apply (4.21), $\vartheta_1^{\dagger}$ and $\vartheta_2^{\dagger}$ can be found. Then with (4.19), the power allocation $\mathbf{a}_1^{2\dagger}$ and $\mathbf{a}_2^{2\dagger}$ can

be obtained. 3) substitute $\mathbf{a}_1^{2\dagger}$ and $\mathbf{a}_2^{2\dagger}$ into equation (2.28), $\overline{p}_{e,1}\left(\mathbf{a}_1^{2\dagger}\right)$ and $\overline{p}_{e,2}\left(\mathbf{a}_2^{2\dagger}\right)$ can be obtained. 4) compare $\overline{p}_{e,1}\left(\mathbf{a}_1^{2\dagger}\right)$ and $\overline{p}_{e,2}\left(\mathbf{a}_2^{2\dagger}\right)$, if $\overline{p}_{e,1}\left(\mathbf{a}_1^{2\dagger}\right)<\overline{p}_{e,2}\left(\mathbf{a}_2^{2\dagger}\right)$, let $\overline{\mathcal{P}}_1 = \overline{\mathcal{P}}_1 - \Delta\overline{\mathcal{P}}$ and $\overline{\mathcal{P}}_2 = \overline{\mathcal{P}}_2 + \Delta\overline{\mathcal{P}}$, and go back to 2) until finally, $\overline{p}_{e,1}\left(\mathbf{a}_1^{2\dagger}\right)=\overline{p}_{e,2}\left(\mathbf{a}_2^{2\dagger}\right)$ with predefined accuracy. This algorithm can be extended to the scenario where the number of users is greater than two[1]. Similarly, since decision errors are ignored, for the k^{th} $(k = 1, 2, \cdots, K)$ user, the LB of the proposed optimal PDC, under the STPC can be expressed as

$$BER_{LB-ST}^{(k)} = \frac{1}{l_k} E_h \left[\sum_{l=1}^{l_k} Q\left(\sqrt{\frac{a_{k,l}^{2\dagger}}{\sigma_n^2 \cdot d_{k,l}^{-2}}} \right) \right]. \tag{4.22}$$

4.2.2 PDC Algorithm under LTPC

With the LTPC, two possible optimization problems are considered. One is the optimization over each channel realization, in which the same target BER is required under different channel realizations. The other is the optimization over all channel realizations.

Optimization over Each Channel Realization As aforementioned, for the k^{th} user, $\overline{p}_{e,k}\left(\mathbf{a}_k^{2\dagger}\right)$ is monotonically decreasing with $\overline{\mathcal{P}}_k$. Hence, under each channel realization, for achieving a target BER $\overline{p}$, the required transmit power $\overline{\mathcal{P}}_{k|h}$ can easily be found from the following algorithm: 1) let $\vartheta_k^{\dagger}$ be a value slightly greater than 0. 2) apply (4.19), the corresponding power allocation $\mathbf{a}_k^{2\dagger}$ can be found. 3) with (4.18), the approximate BER performance $\overline{p}_{e,k}\left(\mathbf{a}_k^{2\dagger}\right)$ can be obtained. 4) compare $\overline{p}_{e,k}\left(\mathbf{a}_k^{2\dagger}\right)$ with $\overline{p}$, if $\overline{p}_{e,k}\left(\mathbf{a}_k^{2\dagger}\right) < \overline{p}$, then $\vartheta_k^{\dagger} = \vartheta_k^{\dagger} + \Delta\vartheta_k^{\dagger}$ and go back to 2) until finally, $\overline{p}_{e,k}\left(\mathbf{a}_k^{2\dagger}\right) = \overline{p}$ with predefined accuracy. Hence, the transmit power $\overline{\mathcal{P}}_{k|h} = \frac{1}{l_k}\sum_{l=1}^{l_k} a_{k,l}^{2\dagger}$.

[1]With a larger number of users, the complexity of the search algorithms might become very high. However, in practise, the power constraint on all users can be relaxed to a separated power constraint on each user, under which the optimal PDC can be easily derived.

The LTPC is determined by the average over all channel realizations, which can be expressed as

$$\begin{aligned} \overline{\mathcal{P}}_k &= E_h\left[\mathcal{P}_{k|h}\right] \\ &= \frac{1}{l_k} E_h\left[\sum_{l=1}^{l_k} a_{k,l}^{2\dagger}\right]. \end{aligned} \tag{4.23}$$

Similarly, for the k^{th} $(k = 1, 2, \cdots, K)$ user, the LB of the BER performance, under the LTPC, is given by

$$BER_{LB-LT1}^{(k)} = \frac{1}{l_k} \sum_{l=1}^{l_k} Q\left(\sqrt{\frac{a_{k,l}^{2\dagger}}{\sigma_n^2 \cdot d_{k,l}^{-2}}}\right) \tag{4.24}$$

Optimization over All Channel Realizations With the LTPC $\overline{\mathcal{P}}$, the optimization problem can be stated as follows,

$$\begin{aligned} &\textit{For the } k^{th}\textit{user, find the optimal power distribution } \mathbf{a}_k^{2\dagger} \\ &\textit{which satisfies: } \mathbf{a}_k^{2\dagger} = \arg\min_{\mathbf{a}_k^2} \left(E_h\left[\overline{p}_{e,k}\left(\mathbf{a}_k^2\right)\right]\right) \\ &\textit{subject to: } \begin{cases} a_{k,l}^{2*} \geq 0 \quad (l = 1, 2, \cdots, l_K) \\ E_h\left[\frac{1}{l_k}\sum_{l=1}^{l_k} a_{k,l}^{2\dagger}\right] = \overline{\mathcal{P}}_k \end{cases}, \end{aligned} \tag{4.25}$$

where $E_h\left[\overline{p}_{e,k}\left(\mathbf{a}_k^2\right)\right]$ denotes the BER of the k^{th} user, averaged over all channel realizations, given by

$$E_h\left[\overline{p}_{e,k}\left(\mathbf{a}_k^2\right)\right] = E_h\left[\frac{1}{l_k}\sum_{l=1}^{l_k} p_{e,k,l}\left(a_{k,l}^2\right)\right]. \tag{4.26}$$

Similarly, $\overline{\mathcal{P}}_k$ satisfies

$$\frac{1}{L}\sum_{k=1}^{K} l_k \overline{\mathcal{P}}_k = \overline{\mathcal{P}}. \tag{4.27}$$

After solving the KKT optimality conditions, shown in Appendix E, the optimal power distribution for the k^{th} user can be obtained, expressed exactly the same as

equation (4.19) or (4.20), while $\vartheta_k^\dagger$ is obtained from the following power constraint,

$$\frac{1}{l_k} E_h \left[\sum_{l=1}^{l_k} \max \left[0, -2d_{k,l}^{-2}\sigma_n^2 \ln \left(4\vartheta_k^\dagger d_{k,l}^{-2}\sigma_n^2 \right) \right] \right] = \overline{\mathcal{P}}_k, \tag{4.28}$$

instead of (4.21). Similar algorithm as stated in the previous subsection can be applied here. Note in this case, $\vartheta_k^\dagger$ is found over all channel realizations. Also, under the LTPC, for the k^{th} user, the LB of the optimal PDC over all channel realizations is given by

$$BER_{LB-LT}^{(k)} = \frac{1}{l_k} E_h \left[\sum_{l=1}^{l_k} Q \left(\sqrt{\frac{a_{k,l}^{2\dagger}}{\sigma_n^2 \cdot d_{k,l}^{-2}}} \right) \right]. \tag{4.29}$$

From the above analyses, it can be found that with the optimal PDC, when $d_{k,l}^{-2} \geq 1/4\sigma_n^2\vartheta_k^\dagger$ ($\vartheta_k^\dagger$ has to be determined), no power will be allocated to the l^{th} symbol of the k^{th} user. It implies that unlike the equal BER PDC, which always consumes more power to compensate for higher noise power[2] for achieving the same SIR, the optimal PDC allocates no power to those symbols whose noise power is equal to or higher than a certain level ($1/4\sigma_n^2\vartheta_k^\dagger$), while allocating more power for other "better" symbols, to ensure more reliable transmissions. Also, for those symbols whose noise power is less than a certain level ($1/4\sigma_n^2\vartheta_k^\dagger$), then from (4.19), under a chosen $\vartheta_k^\dagger$, since $a_{k,l}^{2\dagger}$ is monotonically increasing with $d_{k,l}^{-2}$, more power will be allocated to the symbols with higher noise power to ensure the reliability of earlier detected symbols. These two different PDC strategies, the equal BER PDC and the optimal PDC, will result in different BER performances, which will be presented in the next section.

4.3 Simulation Results and Discussions

The same simulation conditions described in Chapter 3 are used. Furthermore, for comparison, the performance of the nonlinear MF-SIC with the equal BER PDC proposed in the literature will also be presented.

[2]From equation (3.14), $d_{k,l}^{-2}$ can be looked upon as the noise power with $\sigma_n^2 = 1$.

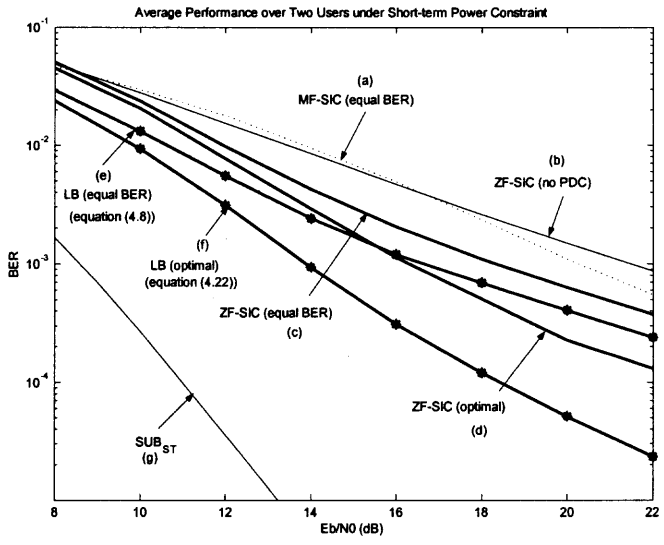

Figure 4.1 BER performance (averaged over two users) in the fully loaded system under the STPC, ((a) MF-SIC (equal BER), (b) ZF-SIC (no PDC), (c) ZF-SIC (equal BER), (d) ZF-SIC (optimal), (e) LB (equal BER, equation (4.8)), (f) LB (optimal, equation (4.22)), (g) SUB_{ST}).

Under the STPC, the BER performance *averaged over two users* versus E_b/N_0 ($10\log_{10}\frac{\overline{\mathcal{P}}}{2\sigma_n^2}$ (dB)) in the fully loaded system is shown in Figure 4.1. From this figure, it is clear that integrated with PDC, the performance of ZF-SIC can be improved significantly. With the equal BER PDC ((c)), at a BER of 10^{-3}, 3.5dB performance improvement over the ZF-SIC without PDC ((b)) can be obtained. Not surprisingly, the optimal PDC ((d)) significantly outperforms the equal BER PDC ((c)); at a BER of 10^{-3}, an extra 2 dB performance improvement can be obtained. The ZF-SIC with both PDC strategies is superior to the MF-SIC with the equal BER PDC ((a)). For comparison, the LBs based on equation (4.8) ((e)) and (4.22) ((f)) and the SUB, under the STPC, are plotted in this figure. From these LBs, it can be concluded that if cancellation errors can properly be taken into consideration, the performance might be further improved, particularly for the ZF-SIC with the optimal PDC.

The BER performances of *the two sequentially detected users* with SIC are compared in Figure 4.2. It can be seen from this figure that with the equal BER

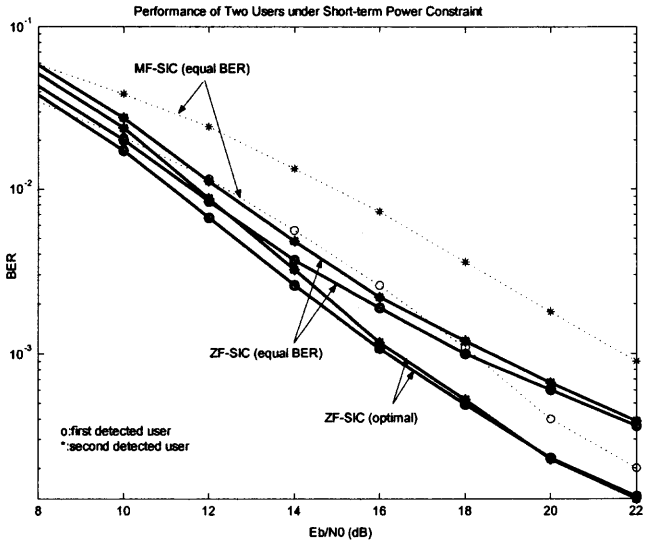

Figure 4.2 BER performance of two sequentially detected users in the fully loaded system under the STPC.

PDC, the performance of two users becomes close with the increase of E_b/N_0, because the decision errors have nearly the same effects on both. With the optimal PDC, two users achieve very similar performance, which is superior to that with the equal BER PDC. It is also interesting to note that with both the equal BER PDC and optimal PDC, the first detected user can achieve slightly better performance than the second detected, because the PDC ignoring decision errors results in a lower power for the later detected user than it actually needs [23], which is different from the SIC with equal receive power. For the MF-SIC, even with the equal BER PDC, the performance difference between the two users is still large, which means cancellation errors might have a larger effect on it than on the ZF-SIC.

Under the LTPC, the BER performance *averaged over two users* in the fully loaded system is shown in Figure 4.3. Different from the performance shown in Figure 4.1, in this case, adapting transmit power with channel variations can compensate channel fading more effectively at high E_b/N_0. It is clear that for the ZF-SIC, both optimal PDC strategies outperform the equal BER PDC. Moreover, the optimization

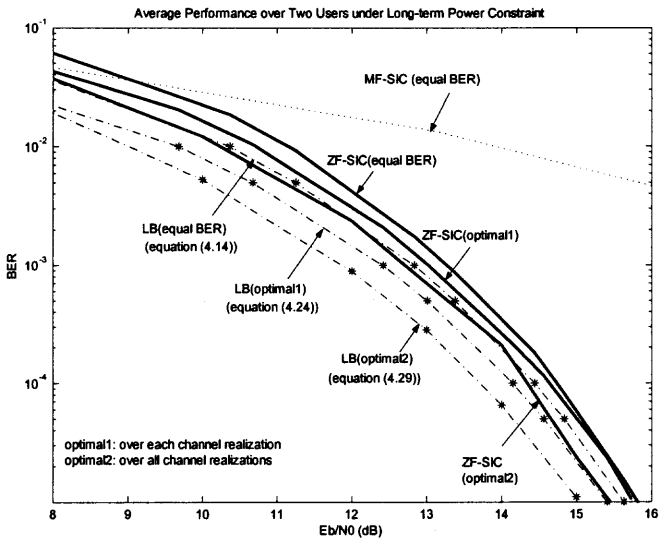

Figure 4.3 BER performance (averaged over two users) in the fully loaded system under the LTPC.

over all channel realizations achieves the best performance. Also, the ZF-SIC with the proposed PDC presents dramatic performance advantage over the MF-SIC with equal BER PDC. The LBs based on equation (4.14), equation (4.24) and (4.29) are also shown for comparison, from which, it can be noted that in this case, the performance loss caused by ignoring cancellation errors is negligible. The BER performances of *the two sequentially detected users* with SIC is compared in Figure 4.4, from which similar conclusions as in Figure 4.2 can be obtained.

In Figure 4.5 and 4.6, the normalized transmit power (divided by σ_n^2) distribution, among the 16 symbols transmitted in parallel on different spreading codes is shown for the STPC and LTPC, with E_b/N_0 12dB and 15dB, respectively. In these two figures, larger index denotes earlier detected symbols. For all schemes, under the chosen E_b/N_0, it was found that the earlier detected symbols are allocated more power than the later detected ones. However, it is interesting to note that compared with the equal BER PDC, the optimal PDC allocated less power to earlier detected symbols, while more for later detected ones. This compensates for a certain performance loss

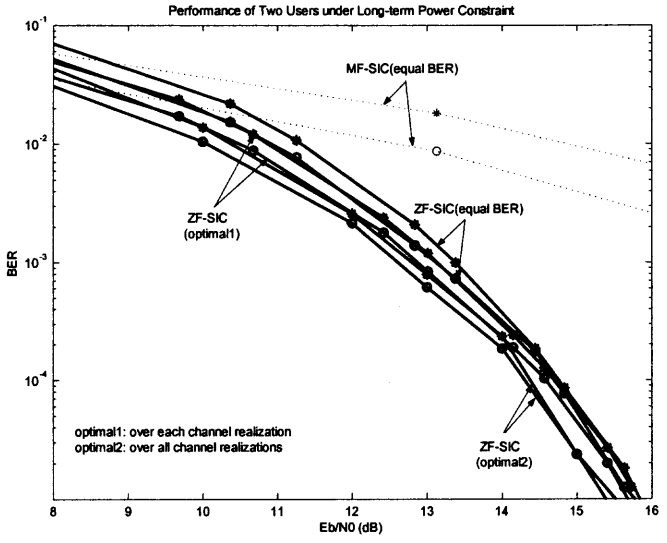

Figure 4.4 BER performance of two sequentially detected users in the fully loaded system under the LTPC.

caused by underestimating the required power of later detected symbols with the equal BER PDC, resulting in a better performance.

In the previous figures, the performance of the fully loaded system was studied. In Figure 4.7 and 4.8, the required E_b/N_0 versus the number of spreading codes, at a target BER of 10^{-4}, is shown for the STPC and LTPC, respectively. In these two figures, similarly, a single user is assumed with a variable number of spreading codes. From these two figures, it can be found that with the increase of the system load, the performance of the MF-SIC with the equal BER PDC degrades very quickly. Integrated with the optimal PDC, the ZF-SIC receiver needs the smallest power, particularly under the STPC and when the system is highly loaded.

4.4 Conclusions

In this chapter, to increase the efficiency of SIC, PDC algorithms are investigated for the nonlinear ZF-SIC receiver, under both a STPC and a LTPC. Under the assumption of perfect CSI at the receiver and reliable feedback from the receiver

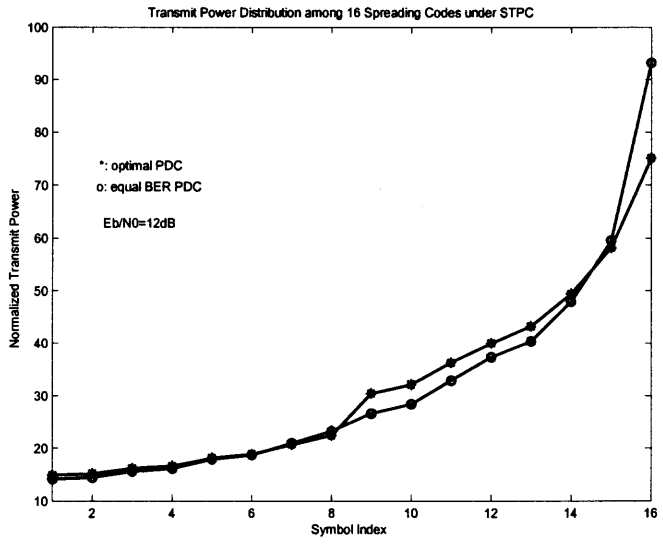

Figure 4.5 Normalized transmit power distribution (averaged over 1000 channel realizations) on 16 parallel transmit symbols under the STPC.

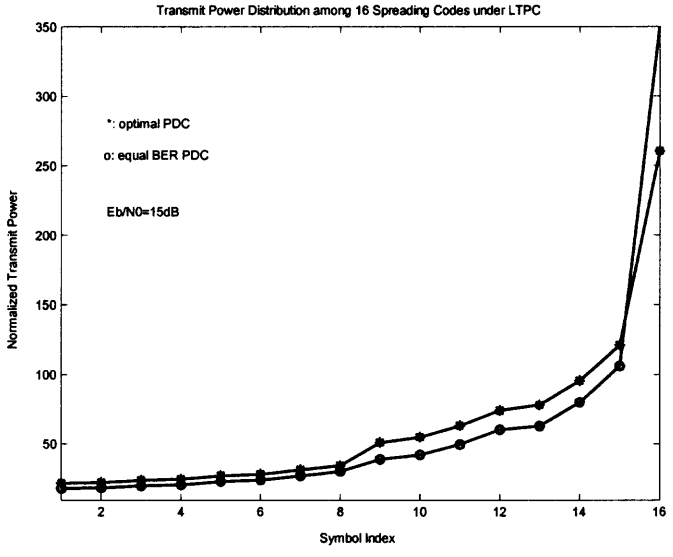

Figure 4.6 Normalized transmit power distribution (averaged over 1000 channel realizations) on 16 parallel transmit symbols under the LTPC.

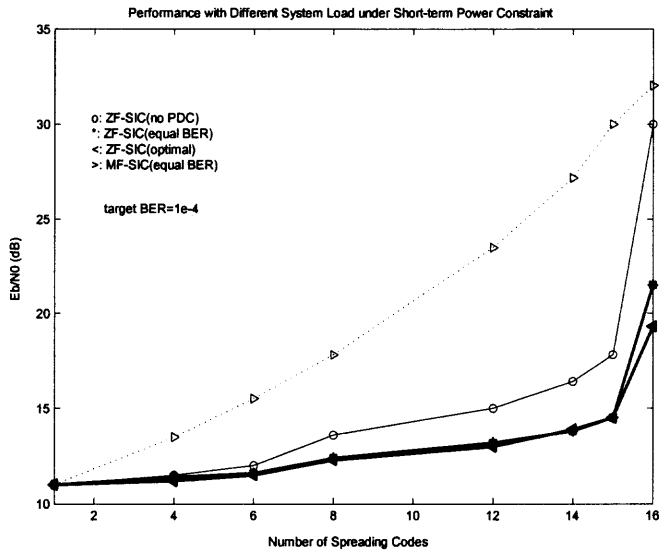

Figure 4.7 Required E_b/N_0 for achieving a target BER of 10^{-4} versus different system load under the STPC.

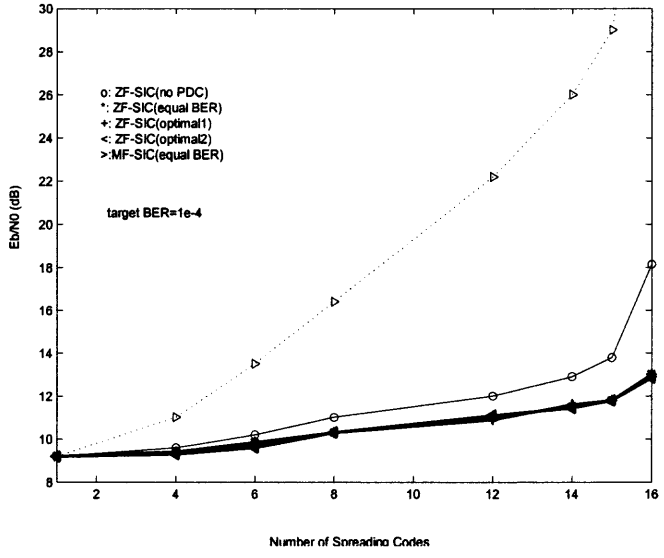

Figure 4.8 Required E_b/N_0 for achieving a target BER of 10^{-4} versus different system load under the LTPC.

to the transmitter, it is found that integrate ZF-SIC with the equal BER PDC can improve the performance significantly. However, it is not surprising that the optimal PDC significantly outperforms the equal BER PDC, particularly under the STPC and highly loaded system. Moreover, the optimal PDC combined with ZF-SIC significantly outperforms the MF-SIC with the equal BER PDC proposed in the literature. To further improve the performance with SIC, the MMSE-SIC [46] integrated with PDC seems a promising solution, which will be investigated in the next chapter.

CHAPTER 5

POWER DISTRIBUTION CONTROL FOR MMSE-SIC

For the MMSE-SIC receiver, the equal BER PDC algorithms are investigated under both a STPC and a LTPC.

5.1 Equal BER PDC Algorithm

From (3.19), it is clear that to achieve the same BER for all parallel transmit symbols, a similar relationship as equation (4.2) should be satisfied, which is given by

$$\frac{[\mathbf{A}]_{L,L}^2}{[\overline{\mathbf{D}}]_{L,L}^{-2}} = \frac{[\mathbf{A}]_{L-1,L-1}^2}{[\overline{\mathbf{D}}]_{L-1,L-1}^{-2}} = \cdots = \frac{[\mathbf{A}]_{1,1}^2}{[\overline{\mathbf{D}}]_{1,1}^{-2}}. \tag{5.1}$$

Expressing $\mathbf{R}_m = \mathbf{R}_c + \sigma_n^2 \mathbf{A}^{-2}$ and its CF, $\mathbf{R}_m = \overline{\mathbf{\Gamma}}^H \overline{\mathbf{D}}^2 \overline{\mathbf{\Gamma}}$ in details, the following two equal matrices can be obtained,

$$\begin{bmatrix} [\mathbf{R}_c]_{1,1} + \frac{\sigma^2}{[\mathbf{A}]_{1,1}^2} & [\mathbf{R}_c]_{1,2} & \cdots & [\mathbf{R}_c]_{1,L} \\ [\mathbf{R}_c]_{2,1} & [\mathbf{R}_c]_{2,2} + \frac{\sigma^2}{[\mathbf{A}]_{2,2}^2} & \cdots & [\mathbf{R}_c]_{2,L} \\ \vdots & \vdots & \ddots & \vdots \\ [\mathbf{R}_c]_{L,1} & [\mathbf{R}_c]_{L,2} & \cdots & [\mathbf{R}_c]_{L,L} + \frac{\sigma^2}{[\mathbf{A}]_{L,L}^2} \end{bmatrix} \tag{5.2}$$

and

$$\begin{bmatrix} [\overline{\mathbf{D}}]_{1,1}^2 & [\overline{\mathbf{\Gamma}}]_{1,2} [\overline{\mathbf{D}}]_{1,1}^2 & \cdots & [\overline{\mathbf{\Gamma}}]_{1,L} [\overline{\mathbf{D}}]_{1,1}^2 \\ [\overline{\mathbf{\Gamma}}]_{1,2}^* [\overline{\mathbf{D}}]_{1,1}^2 & \sum_{l=1}^{2} \left| [\overline{\mathbf{\Gamma}}]_{l,2} \right|^2 [\overline{\mathbf{D}}]_{l,l}^2 & \cdots & \sum_{l=1}^{2} [\overline{\mathbf{\Gamma}}]_{l,L} [\overline{\mathbf{\Gamma}}]_{l,2} [\overline{\mathbf{D}}]_{l,l}^2 \\ \vdots & \vdots & \ddots & \vdots \\ [\overline{\mathbf{\Gamma}}]_{1,L}^* [\overline{\mathbf{D}}]_{1,1}^2 & \sum_{l=1}^{2} [\overline{\mathbf{\Gamma}}]_{l,L}^* [\overline{\mathbf{\Gamma}}]_{l,2} [\overline{\mathbf{D}}]_{l,l}^2 & \cdots & \sum_{l=1}^{L} \left| [\overline{\mathbf{\Gamma}}]_{l,L} \right|^2 [\overline{\mathbf{D}}]_{l,l}^2 \end{bmatrix}. \tag{5.3}$$

Notice $[\overline{\mathbf{\Gamma}}]_{i,j} = 1$, when $i = j$. From the above two equal matrices, the relationship between $\mathbf{A}^2$ and $\overline{\mathbf{D}}^2$ can be constructed. Since $\mathbf{R}_m$ is Hermitian symmetric, only the

lower (or upper) triangle should be considered. Letting $[\mathbf{A}]_{l,l}^2 \left[\overline{\mathbf{D}}\right]_{l,l}^2 \triangleq \lambda \ (l = 1, 2, \cdots, L)$ and $\lambda \geq \sigma_n^2$, then all symbols have the same SIR, which equals $\frac{\lambda}{\sigma_n^2} - 1 \geq 0$. By equating the first column of (5.2) and (5.3), the following L equations can be obtained

$$\begin{cases} [\mathbf{R}_c]_{1,1} + \sigma_n^2 [\mathbf{A}]_{1,1}^{-2} = \left[\overline{\mathbf{D}}\right]_{1,1}^2 \\ [\mathbf{R}_c]_{2,1} = \left[\overline{\mathbf{\Gamma}}\right]_{1,2}^* \left[\overline{\mathbf{D}}\right]_{1,1}^2 \\ \vdots \\ [\mathbf{R}_c]_{L,1} = \left[\overline{\mathbf{\Gamma}}\right]_{1,L}^* \left[\overline{\mathbf{D}}\right]_{1,1}^2 \end{cases} . \tag{5.4}$$

By substituting $\left[\overline{\mathbf{D}}\right]_{1,1}^2 = \frac{\lambda}{[\mathbf{A}]_{1,1}^2}$ into the first equation of (5.4), it can be shown that $[\mathbf{A}]_{1,1}^2 = \frac{\lambda - \sigma_n^2}{[\mathbf{R}_c]_{1,1}}$ and $\left[\overline{\mathbf{D}}\right]_{1,1}^2 = \frac{\lambda [\mathbf{R}_c]_{1,1}}{\lambda - \sigma_n^2}$. Applying $\left[\overline{\mathbf{D}}\right]_{1,1}^2$ in the rest equations, we obtain $\left[\overline{\mathbf{\Gamma}}\right]_{1,l} = \frac{[\mathbf{R}_c]_{l,1}^*}{\left[\overline{\mathbf{D}}\right]_{1,1}^2}$ $(l = 2, 3, \cdots, L)$. Similarly, from the $L - 1$ equations of the second column,

$$\begin{cases} [\mathbf{R}_c]_{2,2} + \sigma_n^2 [\mathbf{A}]_{2,2}^{-2} = \sum_{l=1}^{2} \left| \left[\overline{\mathbf{\Gamma}}\right]_{l,2} \right|^2 \left[\overline{\mathbf{D}}\right]_{l,l}^2 \\ [\mathbf{R}_c]_{3,2} = \sum_{l=1}^{2} \left[\overline{\mathbf{\Gamma}}\right]_{l,3}^* \left[\overline{\mathbf{\Gamma}}\right]_{l,2} \left[\overline{\mathbf{D}}\right]_{l,l}^2 \\ \vdots \\ [\mathbf{R}_c]_{L,2} = \sum_{l=1}^{2} \left[\overline{\mathbf{\Gamma}}\right]_{l,L}^* \left[\overline{\mathbf{\Gamma}}\right]_{l,2} \left[\overline{\mathbf{D}}\right]_{l,l}^2 \end{cases} \tag{5.5}$$

we get $[\mathbf{A}]_{2,2}^2 = \frac{\lambda - \sigma^2}{[\mathbf{R}_c]_{2,2} - \left|\left[\overline{\mathbf{\Gamma}}\right]_{1,2}\right|^2 \left[\overline{\mathbf{D}}\right]_{1,1}^2}$. With $\left[\overline{\mathbf{D}}\right]_{2,2}^2 = \frac{\lambda}{[\mathbf{A}]_{2,2}^2}$ and the results obtained from the first column, $\left[\overline{\mathbf{\Gamma}}\right]_{2,l}$ $(l = 3, 4, \cdots, L)$ can be deduced. Applying the same method successively for the rest columns, $[\mathbf{A}]_{l,l}^2$ $(l > 3)$ can be derived. Finally, the obtained power distribution can be expressed in the general recursive form as

$$\begin{cases} [\mathbf{A}]_{1,1}^2 = \frac{\lambda - \sigma_n^2}{[\mathbf{R}_c]_{1,1}} \\ [\mathbf{A}]_{l,l}^2 = \frac{\lambda - \sigma_n^2}{[\mathbf{R}_c]_{l,l} - \sum_{j=1}^{l-1} \left|\left[\overline{\mathbf{\Gamma}}\right]_{j,l}\right|^2 [\mathbf{A}]_{j,j}^{-2} \lambda} \ (l = 2, 3, \cdots, L) \end{cases} . \tag{5.6}$$

From (5.6), it is clear that $[\mathbf{A}]_{l,l}^2$ $(l = 1, 2, \cdots, L)$ is a function of λ, which can be proved to satisfy the following property: $[\mathbf{A}]_{l,l}^2 \in [0, +\infty)$ $(l = 1, 2, \cdots, L)$ *are*

monotonically increasing with $\lambda \in [\sigma^2, +\infty)$. The detailed proof is shown in Appendix E.

5.1.1 Equal BER PDC Algorithm under STPC

With the above conclusions, under the STPC $\overline{\mathcal{P}} \in [0, +\infty)$, it is clear that there uniquely exists a $\lambda^{\dagger}$, and with (5.6), a unique power distribution $[\mathbf{A}]_{l,l}^{2\dagger}$, which satisfies

$$\overline{\mathcal{P}} = \frac{1}{L} \sum_{l=1}^{L} [\mathbf{A}]_{l,l}^{2\dagger} . \tag{5.7}$$

In conclusion, the equal BER PDC algorithm can be described as follows: 1) let $\lambda = \sigma_n^2$. 2) with (5.6), calculate $[\mathbf{A}]_{l,l}^2$ $(l = 1, 2, \cdots, L)$. 3) compare $\frac{1}{L}\sum_{l=1}^{L} [\mathbf{A}]_{l,l}^2$ with $\overline{\mathcal{P}}$, if smaller, increase λ and go back to step 2) until finally $\overline{\mathcal{P}} = \frac{1}{L}\sum_{l=1}^{L} [\mathbf{A}]_{l,l}^2$ with predefined accuracy.

Since decision errors are ignored, the actually achieved SIR will be lower than the expected, which equals $\frac{(\lambda)^{\dagger}}{\sigma_n^2} - 1$. Therefore, the following expression leads to a BER LB for the MMSE-SIC receiver with the proposed equal BER PDC

$$BER_{LB-ST} = E_h \left[Q\left(\sqrt{\frac{(\lambda)^{\dagger}}{\sigma_n^2} - 1} \right) \right] . \tag{5.8}$$

5.1.2 Equal BER PDC Algorithm under LTPC

Under the LTPC, similar as for the ZF-SIC receiver, the transmit power is adapted with channel variations for achieving a target SIR γ (which is kept the same for all channel realizations). Therefore, under each channel realization, by applying (5.6) and noting $\gamma = \frac{\lambda}{\sigma_n^2} - 1$, $[\mathbf{A}]_{l,l}^2$ $(l = 1, 2, \cdots, L)$ can be obtained, hence, the required transmit power $\overline{\mathcal{P}}_{|h}$ is decided as

$$\overline{\mathcal{P}}_{|h} = \frac{1}{L} \sum_{l=1}^{L} [\mathbf{A}]_{l,l}^2 . \tag{5.9}$$

Therefore, the LTPC $\overline{\mathcal{P}}$ is determined by the average of power over all channel realizations, which is

$$\overline{\mathcal{P}} = \frac{1}{L} E_h \left[\sum_{l=1}^{L} [\mathbf{A}]_{l,l}^2 \right]. \tag{5.10}$$

Similarly, under the LTPC, the LB for the proposed equal BER PDC can be expressed as

$$BER_{LB-LT} = Q\left(\sqrt{\gamma}\right), \tag{5.11}$$

where γ is a function of $\overline{\mathcal{P}}$.

5.2 Simulation Results and Discussions

With the same simulation conditions as stated before, in Figure 5.1, *the average BER performance over two users* versus the E_b/N_0 $\left(10\log_{10}\frac{\overline{\mathcal{P}}}{2\sigma_n^2}(dB)\right)$ in the fully loaded system under STPC is shown. From this figure, by integrating the MMSE-SIC with the equal BER PDC ((d)), at a BER of 10^{-4}, a 7dB performance improvement over the MMSE-SIC with equal receive power ((c)) can be achieved, which is only 2dB away from the SUB ((f)). And it is significantly better than that of the MF-SIC receiver with the equal BER PDC ((a)). Moreover, it is interesting to note that the performance difference between the actual simulation result of the MMSE-SIC with equal BER PDC ((d)) and the LB ((e), equation (5.8)) is very small, which justifies the assumption of ignoring cancellation errors.

The *BER performances of the two sequentially detected users* with SIC in the fully loaded system are compared in Figure 5.2. From this figure, similarly, it can be found that with the equal BER PDC, the first detected user achieves better performance than the second detected, because the PDC ignoring decision errors results in lower power for later detected user than it actually needs [23]. For the MMSE-SIC receiver, the performance difference between the two users is quite small, while for the MF-SIC, even with the equal BER PDC, the performance difference is

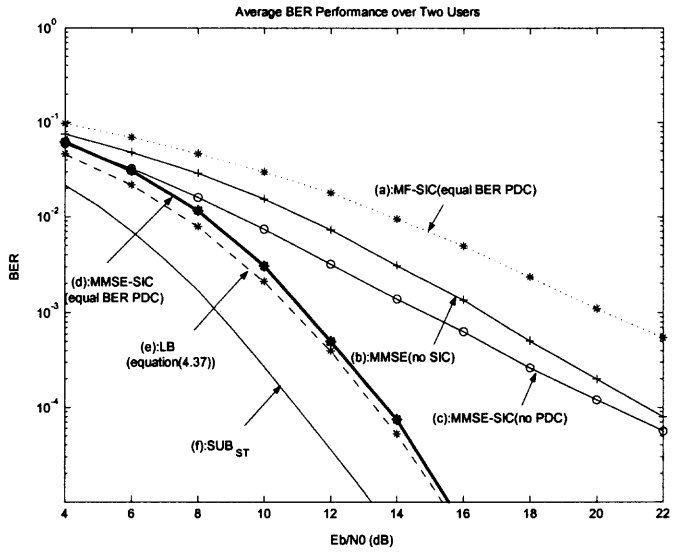

Figure 5.1 Average BER performance over two users versus E_b/N_0 in the fully loaded system under the STPC ((a) MF-SIC (equal BER), (b) MMSE (no SIC), (c) MMSE-SIC (no PDC), (d) MMSE-SIC (equal BER), (e) LB (equation (5.8)), (f) SUB_{ST}).

still large, which implies that cancellation errors might have a larger effect on it than on the MMSE-SIC receiver.

In Figure 5.3, *the average BER performance over two users* versus the E_b/N_0 in the fully loaded system under LTPC is shown. Clearly, by adjusting the transmit power with channel variations, the MMSE-SIC with the equal BER PDC can suppress interference more effectively. At a BER of 10^{-5}, it is 2dB better than that under the STPC, which is only 3dB away from the SUB, under the LTPC. The *BER performances of the two sequentially detected users* with SIC in the fully loaded system under the LTPC are compared in Figure 5.4, from which, similar conclusions can be made as in the Figure 5.2.

Figure 5.5 and Figure 5.6 show the normalized transmit power distribution on 16 successive detected symbols, under the STPC and LTPC, respectively. Not surprisingly, under different E_b/N_0, earlier detected symbols (larger index) are always allocated more power than the later detected ones (smaller index). Therefore, as

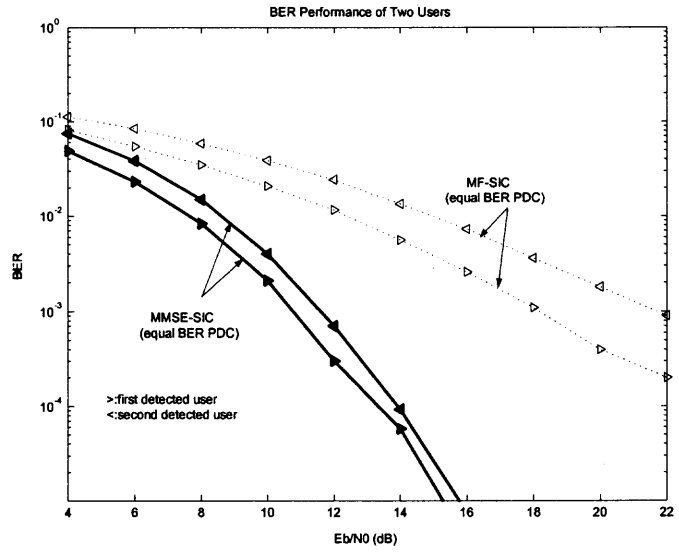

Figure 5.2 BER performance of two users versus E_b/N_0 in the fully loaded system under the STPC.

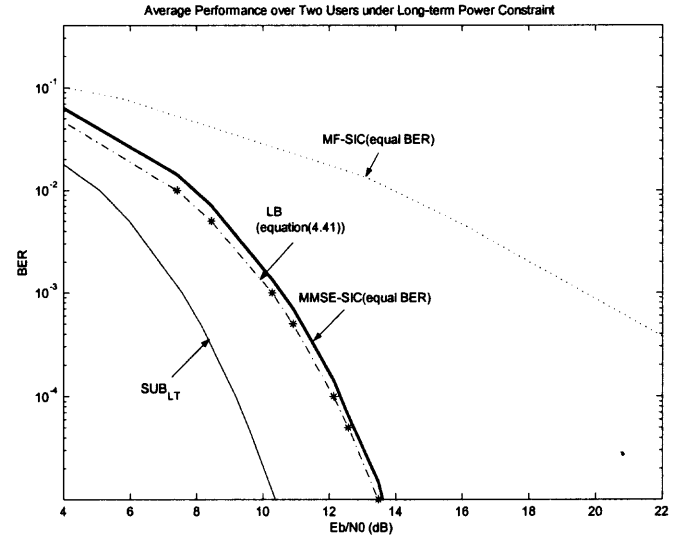

Figure 5.3 Averaged BER performance over two users versus E_b/N_0 in the fully loaded system under the LTPC.

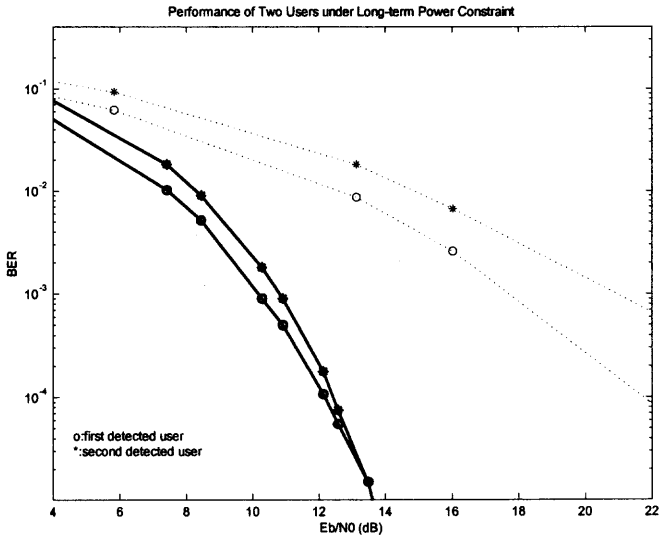

Figure 5.4 BER performance of two users versus E_b/N_0 in the fully loaded system under the LTPC.

aforementioned, the equal BER PDC improves the system performance by increasing the reliability of earlier detected symbols.

In Figure 5.7 and Figure 5.8, the required E_b/N_0 (averaged over 1000 channels) versus the number of spreading codes, at a target BER of 10^{-4}, under the STPC and the LTPC is shown, respectively. Similarly, a single user with a variable number of spreading codes is assumed. From these figures, it can be seen clearly that the MMSE-SIC receiver integrated with the equal BER PDC can suppress interference very effectively, resulting in a very robust performance with the increase of the system load.

5.3 Conclusions

In this chapter, a simple PDC algorithm, under the equal BER criterion, is derived for the MMSE-SIC receiver. With the assumption of the perfect CSI at the receiver and reliable feedback of power distribution from the receiver to the transmitter, the performance of the MMSE-SIC receiver integrated with the proposed PDC for multi-code MC-CDMA is investigated and compared with other receivers, under both STPC

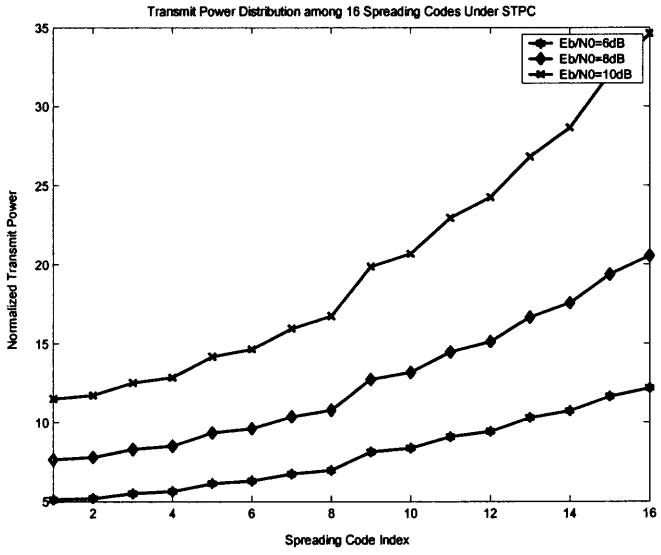

Figure 5.5 Normalized transmit power distribution (averaged over 1000 channels) over 16 successively detected symbols under the STPC.

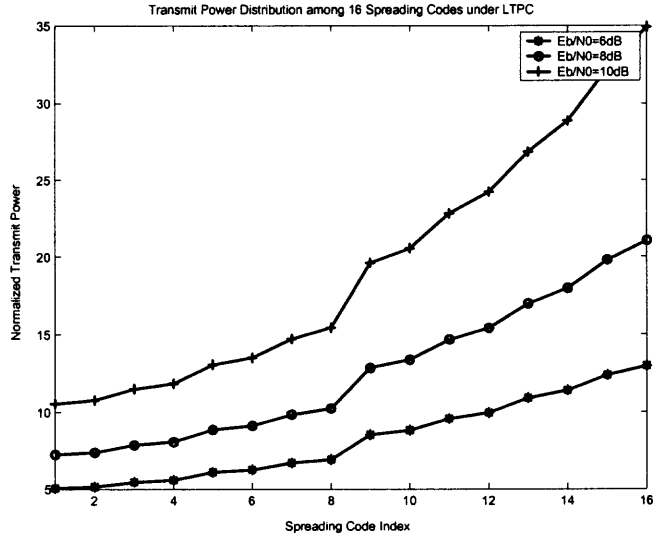

Figure 5.6 Normalized transmit power distribution (averaged over 1000 channels) over 16 successively detected symbols under the LTPC.

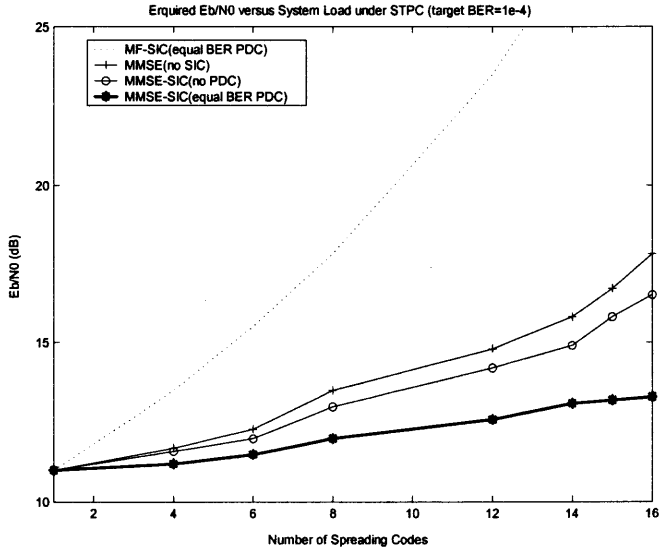

Figure 5.7 Required E_b/N_0 (averaged over 1000 channels) versus the number of spreading codes at a target BER of 10^{-4} under the STPC.

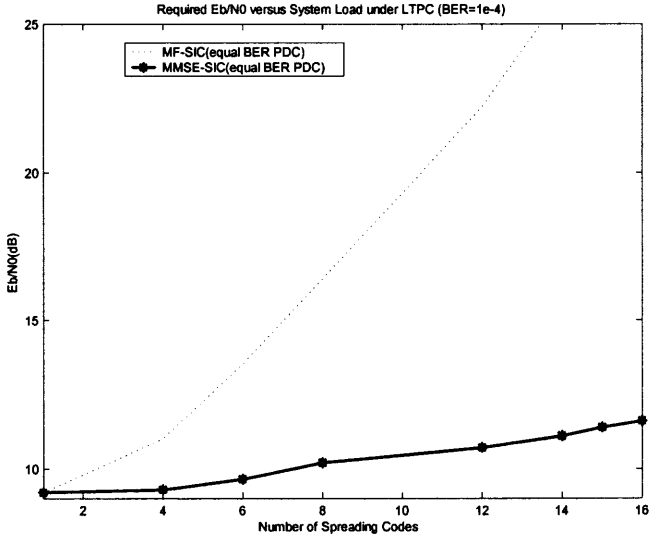

Figure 5.8 Required E_b/N_0 (averaged over 1000 channels) versus the number of spreading codes at a target BER of 10^{-4} under the LTPC.

and LTPC. The simulation results in correlated Rayleigh fading channels confirm the effectiveness of the proposed PDC, from which, it can be concluded that the MMSE-SIC receiver integrated with the equal BER PDC provides a powerful solution for MAI suppression.

CHAPTER 6

EFFECT OF CHANNEL ESTIMATION ERRORS ON THE PERFORMANCE OF THE MMSE-SIC WITH THE EQUAL BER PDC

In the previous two chapters, the PDC algorithms for the ZF-SIC and MMSE-SIC receivers were derived under the assumption of perfect CSI at the receiver. From the simulation results, it is clear that the proposed PDC algorithms can improve the efficiency of SIC significantly. However, in practise, CSI can only be obtained from estimation, thus, channel estimation errors (CEE) are inevitable. The CEE will result in a "non-perfect" power distribution, also, cause a mismatched ZF or MMSE detection. Therefore, the analysis of the robustness of the SIC receivers with the proposed PDC to CEE is of great interest and importance.

In this chapter, the performance of the MMSE-SIC with the equal BER PDC will be investigated under CEE. A method of second-order approximation, which was proposed in [31] for analysis of CEE effects with respect to the MMSE decision feedback equalizer (DFE) for ISI suppression, is applied to estimate the mean excess MSE (MEMSE) of the parallel transmit symbols, under a given decision order and power distribution. A simple approximation can be derived for the MEMSE, whose accuracy is confirmed by simulation results. Furthermore, it is interesting to find that although the PDC becomes "non-perfect" under CEE, it can still significantly improve the efficiency of SIC, which makes the MMSE-SIC more robust to CEE.

6.1 MMSE under Perfect CSI

As described in Chapter 3, the MMSE-SIC can simultaneously maximize all symbol's SIR, (i.e., minimize the MSE), provided all feedback is correct. With the assumption of perfect CSI, the MMSE of the l^{th} symbol can be obtained from CF, which is $[\overline{\mathbf{D}}]_l^{-2}$. Although CF provides an efficient way of performing SIC, it does not reveal very

informative relationship of the MMSE with the feedforward and feedback matrices. To analyze the MEMSE under CEE, in the section, an alternative MMSE expression will be first introduced under perfect CSI .

For simplicity, the output of the DFT, expressed by equation (3.3), can be rewritten as

$$\mathbf{x}(i) = \mathcal{H}\mathbf{b}(i) + \boldsymbol{\eta}(i), \tag{6.1}$$

where $\mathcal{H} = \widetilde{\mathbf{C}} \cdot \mathbf{A}$. *With perfect cancellation*, under SIC, the decision error of the l^{th} symbol is given by[1]

$$\begin{aligned} e_l &= b_l - \left(\mathbf{w}_l^H \mathbf{x} - \sum_{i=1}^{L-l} f_{L-i+1} b_{L-i+1} \right) \\ &= \widetilde{\mathbf{f}}_l^H \mathbf{b} - \mathbf{w}_l^H \mathbf{x}. \end{aligned} \tag{6.2}$$

In the above equation, $\mathbf{w}_l \triangleq [w_{l,1}, w_{l,2}, \cdots, w_{l,M}]^H$ and $\widetilde{\mathbf{f}}_l \triangleq \left[\mathbf{0}_{(l-1)\times 1}^T, \mathbf{f}_l^H\right]^H$ represent the feedforward and feedback vectors of the l^{th} symbol, with $\mathbf{f}_l = [1, f_{l+1}, \cdots, f_L]^H$ and $\mathbf{0}_{m\times n}$ denoting an $(m \times n)$ zero matrix[2]. The MSE of the l^{th} symbol can be expressed as

$$\begin{aligned} \mathbf{MSE}_l &\triangleq E[e_l \cdot e_l^*] \\ &= \widetilde{\mathbf{f}}_l^H \mathbf{R}_{\mathbf{bb}} \widetilde{\mathbf{f}}_l - \widetilde{\mathbf{f}}_l^H \mathbf{R}_{\mathbf{bx}} \mathbf{w}_l - \mathbf{w}_l^H \mathbf{R}_{\mathbf{xb}} \widetilde{\mathbf{f}}_l + \mathbf{w}_l^H \mathbf{R}_{\mathbf{xx}} \mathbf{w}_l, \end{aligned} \tag{6.3}$$

where $\mathbf{R}_{\mathbf{bb}} = E\left[\mathbf{b} \cdot \mathbf{b}^H\right] = \mathbf{I}_L$, $\mathbf{R}_{\mathbf{bx}} = E\left[\mathbf{b} \cdot \mathbf{x}^H\right] = \mathcal{H}^H$, $\mathbf{R}_{\mathbf{xb}} = E\left[\mathbf{x} \cdot \mathbf{b}^H\right] = \mathbf{R}_{\mathbf{bx}}^H$ and $\mathbf{R}_{\mathbf{xx}} = E\left[\mathbf{x} \cdot \mathbf{x}^H\right] = \mathcal{H}\mathcal{H}^H + \sigma_n^2 \mathbf{I}_L$, where $\mathbf{I}_L$ denotes an $(L \times L)$ identity matrix.

To minimize the $\mathbf{MSE}_l$, it can be shown that the optimal forward and feedback vectors are [47]

$$\mathbf{w}_{l,o} = \mathbf{R}_{\mathbf{xx}}^{-1} \mathbf{R}_{\mathbf{xb}} \widetilde{\mathbf{f}}_{l,o} \tag{6.4}$$

---

[1]Notice that the symbol with larger index will be detected earlier. Also, for simplicity, the time index i is omitted.

[2]Notice that the operation of matched-filtering has been incorperated into the feedforward and feedback vectors.

and

$$\mathbf{f}_{l,o} = \frac{\mathbf{R}_{\Delta,l}^{-1}\mathbf{u}_l}{\mathbf{u}_l^T\mathbf{R}_{\Delta,l}^{-1}\mathbf{u}_l}, \tag{6.5}$$

where $\mathbf{R}_{\Delta,l} = \left[\mathbf{0}_{(L-l+1)\times(l-1)}, \mathbf{I}_{L-l+1}\right]\mathbf{R}\begin{bmatrix}\mathbf{0}_{(L-l+1)\times(l-1)}\\ \mathbf{I}_{L-l+1}\end{bmatrix}$ with $\mathbf{R} = \mathbf{R_{bb}} - \mathbf{R_{bx}}\mathbf{R_{xx}^{-1}}\mathbf{R_{xb}}$ and $\mathbf{u}_l = \left[1, \mathbf{0}_{(L-l)\times 1}^T\right]^T$. The resulting MMSE of the l^{th} symbol can be expressed as

$$\mathbf{MMSE}_l = \widetilde{\mathbf{f}}_{l,o}^H\mathbf{R}\widetilde{\mathbf{f}}_{l,o} = \mathbf{f}_{l,o}^H\mathbf{R}_{\Delta,l}\mathbf{f}_{l,o} = \frac{1}{\mathbf{u}_l^T\mathbf{R}_{\Delta,l}^{-1}\mathbf{u}_l} \tag{6.6}$$

with $\widetilde{\mathbf{f}}_{l,o} \triangleq \left[\mathbf{0}_{(l-1)\times 1}^T, \mathbf{f}_{l,o}^H\right]^H$.

6.2 Mean Excess MSE (MEMSE) under CEE

6.2.1 Excess MSE (EMSE) under a given CEE

After a certain channel estimation procedure, estimates $\widehat{\mathbf{h}}_l$ can be obtained for the l^{th} symbol. Then, the CEE of the l^{th} symbol is denoted as $\Delta\mathbf{h}_l \triangleq \widehat{\mathbf{h}}_l - \mathbf{h}_l$ with the assumption of $\|\Delta\mathbf{h}_l\|_2 \ll \|\mathbf{h}_l\|_2$ $(l = 1, 2, \cdots, L)$. Under CEE, the "equal BER" power distribution results in a different distribution $\widetilde{\mathbf{A}}^\dagger$ from that under the perfect CSI, denoted as $\mathbf{A}^\dagger$. Thus, $\widehat{\mathcal{H}} \triangleq \widehat{\mathbf{C}} \cdot \widetilde{\mathbf{A}}^\dagger$, where $\widehat{\mathbf{C}} = \left[\widehat{\mathbf{h}}_1 \odot \mathbf{c}_1, \widehat{\mathbf{h}}_2 \odot \mathbf{c}_2, \cdots, \widehat{\mathbf{h}}_L \odot \mathbf{c}_L\right]$ and $\widetilde{\mathbf{A}}^\dagger = \mathbf{diag}\left(\widetilde{a}_1^\dagger, \widetilde{a}_2^\dagger, \cdots, \widetilde{a}_L^\dagger\right)$ with $\widetilde{a}_l^\dagger = a_l^\dagger + \Delta a_l$ (Δa_l denotes the amplitude difference for the l^{th} symbol.) By defining $\Delta\mathcal{H} \triangleq \widehat{\mathcal{H}} - \mathcal{H}$, it is clear that $\Delta\mathcal{H}_{i,j} = \widetilde{a}_i^\dagger c_{j,i}\Delta h_{j,i} + \Delta a_i c_{j,i} h_{j,i}$.

In this case, the resulting "optimal" feedforward and feedback vectors can be expressed as

$$\widehat{\mathbf{w}}_{l,o} = \widehat{\mathbf{R}}_{\mathbf{xx}}^{-1}\widehat{\mathbf{R}}_{\mathbf{xb}}\widehat{\widetilde{\mathbf{f}}}_{l,o} \tag{6.7}$$

and

$$\widehat{\mathbf{f}}_{l,o} = \frac{\widehat{\mathbf{R}}_{\Delta,l}^{-1}\mathbf{u}_l}{\mathbf{u}_l^T\widehat{\mathbf{R}}_{\Delta,l}^{-1}\mathbf{u}_l} \tag{6.8}$$

where

$$\begin{aligned}\widehat{\mathbf{R}}_{\mathbf{xx}} &= \widehat{\mathcal{H}}\widehat{\mathcal{H}}^H + \boldsymbol{\sigma}_n^2\mathbf{I}_L \\ &\approx \underbrace{\mathcal{H}\mathcal{H}^H + \boldsymbol{\sigma}_n^2\mathbf{I}_L}_{\mathbf{R}_{\mathbf{xx}}} + \underbrace{\mathcal{H}\Delta\mathcal{H}^H + \Delta\mathcal{H}\mathcal{H}^H}_{\Delta\mathbf{R}_{\mathbf{xx}}},\end{aligned} \tag{6.9}$$

$$\begin{aligned}\widehat{\mathbf{R}}_{\mathbf{bx}} &= \widehat{\mathcal{H}}^H \\ &= \underbrace{\mathcal{H}^H}_{\mathbf{R}_{\mathbf{bx}}} + \underbrace{\Delta\mathcal{H}^H}_{\Delta\mathbf{R}_{\mathbf{bx}}},\end{aligned} \tag{6.10}$$

$$\widehat{\mathbf{R}}_{\mathbf{xb}} = \widehat{\mathbf{R}}_{\mathbf{bx}}^H \tag{6.11}$$

and

$$\widehat{\mathbf{R}}_{\Delta,l} = \left[\mathbf{0}_{(L-l+1)\times(l-1)}, \mathbf{I}_{L-l+1}\right]\widehat{\mathbf{R}}\begin{bmatrix}\mathbf{0}_{(l-1)\times(L-l+1)} \\ \mathbf{I}_{L-l+1}\end{bmatrix} \tag{6.12}$$

with $\widehat{\mathbf{R}}$=$\widehat{\mathbf{R}}_{\mathbf{bb}} - \widehat{\mathbf{R}}_{\mathbf{bx}}\widehat{\mathbf{R}}_{\mathbf{xx}}^{-1}\widehat{\mathbf{R}}_{\mathbf{xb}}$. Similarly, by defining $\widehat{\mathbf{R}}_{\Delta,l} = \mathbf{R}_{\Delta,l} + \Delta\mathbf{R}_{\Delta,l}$ and $\widehat{\mathbf{R}} = \mathbf{R} + \Delta\mathbf{R}$ and using the well-known first-order expansion

$$(\mathbf{X} + \Delta\mathbf{X})^{-1} \approx \mathbf{X}^{-1} - \mathbf{X}^{-1}\Delta\mathbf{X}\mathbf{X}^{-1}, \tag{6.13}$$

it is not difficult to show that

$$\Delta\mathbf{R}_{\Delta,l} = \left[\mathbf{0}_{(L-l+1)\times(l-1)}, \mathbf{I}_{L-l+1}\right]\Delta\mathbf{R}\begin{bmatrix}\mathbf{0}_{(l-1)\times(L-l+1)} \\ \mathbf{I}_{L-l+1}\end{bmatrix} \tag{6.14}$$

with

$$\begin{aligned}\Delta\mathbf{R} &= -\mathbf{R}_{\mathbf{bx}}\mathbf{R}_{\mathbf{xx}}^{-1}\Delta\mathbf{R}_{\mathbf{xb}} - \Delta\mathbf{R}_{\mathbf{bx}}\mathbf{R}_{\mathbf{xx}}^{-1}\mathbf{R}_{\mathbf{xb}} + \mathbf{R}_{\mathbf{bx}}\mathbf{R}_{\mathbf{xx}}^{-1}\Delta\mathbf{R}_{\mathbf{xx}}\mathbf{R}_{\mathbf{xx}}^{-1}\mathbf{R}_{\mathbf{xb}} \\ &= -\mathbf{R}_{\mathbf{bx}}\mathbf{R}_{\mathbf{xx}}^{-1}\Delta\mathcal{H}\mathbf{R} - \mathbf{R}\Delta\mathcal{H}^H\mathbf{R}_{\mathbf{xx}}^{-1}\mathbf{R}_{\mathbf{xb}}.\end{aligned} \tag{6.15}$$

Ignoring cancellation errors, under CEE, the MSE of the l^{th} symbol can be expressed as

$$\widehat{\mathbf{MSE}}_l = \widehat{\widetilde{\mathbf{f}}}_{l,o}^H \mathbf{R}_{\mathbf{bb}} \widehat{\widetilde{\mathbf{f}}}_{l,o} - \widehat{\widetilde{\mathbf{f}}}_{l,o}^H \mathbf{R}_{\mathbf{bx}} \widehat{\mathbf{w}}_{l,o} - \widehat{\mathbf{w}}_{l,o}^H \mathbf{R}_{\mathbf{xb}} \widehat{\widetilde{\mathbf{f}}}_{l,o} + \widehat{\mathbf{w}}_{l,o}^H \mathbf{R}_{\mathbf{xx}} \widehat{\mathbf{w}}_{l,o}. \tag{6.16}$$

Comparing equation (6.3) and (6.16), it can be deduced that $\widehat{\mathbf{MSE}}_l$ is the value of the constrained quadratic function MSE at the point $\left(\widehat{\mathbf{w}}_{l,o}^H, \widehat{\widetilde{\mathbf{f}}}_{l,o}^H\right)$, which is close to the optimal point $\left(\mathbf{w}_{l,o}^H, \widetilde{\mathbf{f}}_{l,o}^H\right)$ under small CEE. By defining the first-order perturbations as $\Delta\mathbf{w}_{l,o} = \widehat{\mathbf{w}}_{l,o} - \mathbf{w}_{l,o}$ and $\Delta\widetilde{\mathbf{f}}_{l,o} = \widehat{\widetilde{\mathbf{f}}}_{l,o} - \widetilde{\mathbf{f}}_{l,o}$, the $\widehat{\mathbf{MSE}}_l$ can be approximated as

$$\begin{aligned} \widehat{\mathbf{MSE}}_l \approx\ & \mathbf{MMSE}_l + \textit{first-order error terms} \\ & + \underbrace{\begin{bmatrix} \Delta\widetilde{\mathbf{f}}_{l,o}^H & \Delta\mathbf{w}_{l,o}^H \end{bmatrix} \begin{bmatrix} \mathbf{R}_{\mathbf{bb}} & -\mathbf{R}_{\mathbf{bx}} \\ -\mathbf{R}_{\mathbf{xb}} & \mathbf{R}_{\mathbf{xx}} \end{bmatrix} \begin{bmatrix} \Delta\widetilde{\mathbf{f}}_{l,o} \\ \Delta\mathbf{w}_{l,o} \end{bmatrix}}_{\textit{second-order error terms}}. \end{aligned} \tag{6.17}$$

In the above equation, the "first-order error terms" is identically zero due to the optimality of the point $\left(\mathbf{w}_{l,o}^H, \widetilde{\mathbf{f}}_{l,o}^H\right)$. Therefore, the excess MSE (EMSE) under CEE can be estimated by the second-order error term (SOT), which is termed as a second-order approximation [31]. With mathematical manipulations, shown in Appendix G, SOT of the l^{th} symbol, can be expressed as

$$\begin{aligned} \mathbf{SOT}_l =\ & \left(\widetilde{\mathbf{f}}_{l,o}^H \Delta\mathbf{R}_{\mathbf{bx}} - \mathbf{w}_{l,o}^H \Delta\mathbf{R}_{\mathbf{xx}}\right) \mathbf{R}_{\mathbf{xx}}^{-1} \left(\Delta\mathbf{R}_{\mathbf{xb}} \widetilde{\mathbf{f}}_{l,o}^H - \Delta\mathbf{R}_{\mathbf{xx}} \mathbf{w}_{l,o}\right) \\ & + \mathbf{f}_{l,o}^H \Delta\mathbf{R}_{\Delta,l} \mathbf{R}_{\Delta,l}^{-1} \Delta\mathbf{R}_{\Delta,l} \mathbf{f}_{l,o} - \frac{\mathbf{f}_{l,o}^H \Delta\mathbf{R}_{\Delta,l} \mathbf{f}_{l,o}}{\mathbf{MMSE}_l}. \end{aligned} \tag{6.18}$$

With the above equation, the EMSE of the l^{th} user under a given CEE can be approximated by $\mathbf{SOT}_l$.

6.2.2 MEMSE under a given channel realization

To derive a close form of the MEMSE (i.e., averaged over all CEE) under a given channel realization, a relationship between the MEMSE and the CEE covariance matrix should be constructed.

By defining $\Delta\mathfrak{h} \triangleq \left[[\Delta\mathcal{H}]_1^H, [\Delta\mathcal{H}]_2^H, \cdots, [\Delta\mathcal{H}]_L^H\right]^H$, where $[\Delta\mathcal{H}]_j$ denotes the j^{th} column of $\Delta\mathcal{H}$, the covariance matrix of $\Delta\mathfrak{h}$ can be expressed as

$$\mathbf{R}_{\Delta\mathfrak{h}} = E\left[\Delta\mathfrak{h}\Delta\mathfrak{h}^H\right]. \tag{6.19}$$

If a matrix $\mathcal{S}_l$ could be found, which satisfies the following equation

$$\mathbf{SOT}_l = \Delta\mathfrak{h}^H\mathcal{S}_l\Delta\mathfrak{h} = tr\left(\Delta\mathfrak{h}^H\mathcal{S}_l\Delta\mathfrak{h}\right), \tag{6.20}$$

then, using the well-known property $Tr\left(\mathbf{AB}\right) = Tr(\mathbf{BA})$, the following relationship between the MEMSE and $\mathbf{R}_{\Delta\mathfrak{h}}$ can be constructed, which is given by

$$E\left[\mathbf{SOT}_l\right] = E_{\Delta\mathfrak{h}}\left[tr\left(\Delta\mathfrak{h}^H\mathcal{S}_l\Delta\mathfrak{h}\right)\right] = Tr\left(\mathcal{S}_l\mathbf{R}_{\Delta\mathfrak{h}}\right). \tag{6.21}$$

To solve $\mathcal{S}_l$, a new matrix $\mathcal{W}_{l,o}$ is introduced, which satisfies

$$\mathbf{w}_{l,o}^H\Delta\mathcal{H} = \Delta\mathfrak{h}^H\mathcal{W}_{l,o}. \tag{6.22}$$

It can be shown that $\mathcal{W}_{l,o}$ is an $(LM \times L)$ matrix, which can be expressed as

$$\mathcal{W}_{l,o} = \begin{bmatrix} \mathbf{w}_{l,o}^* & \mathbf{0}_{N\times 1} & \cdots & \mathbf{0}_{M\times 1} \\ \mathbf{0}_{M\times 1} & \mathbf{w}_{l,o}^* & \cdots & \mathbf{0}_{M\times 1} \\ \vdots & \vdots & \ddots & \vdots \\ \mathbf{0}_{M\times 1} & \mathbf{0}_{M\times 1} & \cdots & \mathbf{w}_{l,o}^* \end{bmatrix}. \tag{6.23}$$

Also, by defining

$$\begin{aligned}\mathbf{g}_{l,o} &\triangleq [g_{l,o,1}, g_{l,o,2}, \cdots, g_{l,o,L}]^H \\ &\triangleq \widetilde{\mathbf{f}}_{l,o} - \mathcal{H}^H \mathbf{w}_{l,o}, \\ &= \mathbf{R}\widetilde{\mathbf{f}}_{l,o}, \end{aligned} \tag{6.24}$$

similarly, another new $(LM \times L)$ dimensional matrix $\mathcal{G}_{l,o}$ can be constructed, which satisfies the following relationship

$$\mathbf{g}_{l,o}^H \Delta\mathcal{H} = \Delta\mathfrak{h}^H \mathcal{G}_{l,o}, \tag{6.25}$$

with the j^{th} column $[\mathcal{G}_{l,o}]_j = \left[\mathbf{0}_{(j-1)\times 1}^T, g_{l,o,1}, \mathbf{0}_{(M-1)\times 1}^T, g_{l,o,2}, \mathbf{0}_{(M-1)\times 1}^T, \cdots, g_{l,o,L}, \mathbf{0}_{(M-j)\times 1}^T\right]^H$.

By using $\mathcal{W}_{l,o}$ and $\mathcal{G}_{l,o}$ and previous obtained results, with mathematical manipulations, the MEMSE, under a given channel realization, can be expressed as:

$$\mathbf{MEMSE}_{l|\mathcal{H}} = Tr\left(\mathcal{S}_l \cdot \mathbf{R}_{\Delta\mathfrak{h}}\right). \tag{6.26}$$

In the above equation, $\mathcal{S}_l \triangleq \Psi_1 \mathbf{R}_{\mathbf{xx}}^{-1} \Psi_1^H + \Psi_2 \Xi \Psi_2^H - \frac{\Psi_3}{\mathbf{MMSE}_l}$, in which $\Psi_1 = \mathcal{G}_{l,o} - \mathcal{W}_{l,o}\mathcal{H}^H$, $\Psi_2 = \mathcal{W}_{l,o}\mathbf{R} - \mathcal{G}_{l,o}\mathbf{R}_{\mathbf{xx}}^{-1}\mathbf{R}_{\mathbf{xb}}$, $\Xi = \begin{bmatrix} \mathbf{0}_{(l-1)\times(L-l+1)} \\ \mathbf{I}_{L-l+1} \end{bmatrix} \mathbf{R}_{\Delta,l}^{-1} \left[\mathbf{0}_{(L-l+1)\times(l-1)}, \mathbf{I}_{L-l+1}\right]$ and $\Psi_3 = 4\mathcal{W}_{l,o}\mathbf{g}_{l,o}\mathbf{g}_{l,o}^H\mathcal{W}_{l,o}^H$. The detailed derivation is shown in Appendix H.

6.2.3 MEMSE under all channel realizations

With equation (6.26), the MEMSE under all channel realizations can be expressed as

$$\mathbf{MEMSE}_l = E_{\mathcal{H}}\left[Tr\left(\mathcal{S}_l \cdot \mathbf{R}_{\Delta\mathfrak{h}}\right)\right]. \tag{6.27}$$

In equation (6.27), $\mathbf{R}_{\Delta\mathfrak{h}}$ is difficult to know in advance, since the statistic property of Δa_l $(l = 1, 2, \cdots, L)$ is hard to estimate due to the nonlinear calculation. However, it can be deduced that under small CEE, Δa_l could be negligible, which can be shown later from the simulation results a valid assumption.

Therefore, $\mathbf{R}_{\Delta\mathfrak{h}}$ depends mainly on CEE and the power distribution $\mathbf{A}^{2\dagger}$, derived under the perfect CSI. For example, by considering i.i.d CEE among different users and sub-carriers, and an extreme case of each user employing one spreading code, $\mathbf{R}_{\Delta\mathfrak{h}}$ can be expressed as

$$\mathbf{R}_{\Delta\mathfrak{h}} \approx \frac{1}{M}\sigma_e^2 \left(\mathbf{I}_M \otimes \mathbf{A}^{2\dagger}\right), \tag{6.28}$$

where σ_e^2 denotes the variance of CEE. Therefore, the MEMSE, for the l^{th} user, averaged over all channel realizations, can be simplified as

$$\mathbf{MEMSE}_l \approx \frac{1}{M}\sigma_e^2 E_{\mathcal{H}}\left[Tr\left(\mathcal{S}_l \cdot \left(\mathbf{I}_M \otimes \mathbf{A}^{2\dagger}\right)\right)\right]. \tag{6.29}$$

6.3 Simulation Results and Discussions

A CEE model described in [48] is employed for simulations, by which, the CEE among different users and sub-carriers are i.i.d.. The variance of the CEE on each sub-carrier depends on the SNR of the pilot symbols and the ICI caused by frequency offset. In all the following simulation results, without loss of generality, the case of each user employing one spreading code is considered, in which, each transmit symbol experiences i.i.d. channel realizations and CEE. The STPC is considered for all simulations.

In Figure 6.1, the MEMSE (averaged over 100 channel realizations) versus E_b/N_0 for the 8^{th} user is shown. Under each channel realization, 100 random CEE are produced and the results are averaged over all CEE. From this figure, it is clear that the theoretical derivation (equation (6.29)) matches the simulation result ignoring cancellation errors very well[3], particularly in higher E_b/N_0. Therefore, the amplitude difference Δa_l caused by CEE does not arouse significant MEMSE, which confirms the assumption of ignoring it. The actual simulation result considering cancellation errors is also plotted for comparison, from which, it is clear that for the 8^{th} user,

[3]Since cancellation errors are ignored in the derivation of MEMSE, to examine its accuracy, in the simulations, the cancellation errors are intentionally ignored.

under the equal BER PDC, cancellation errors cause only slight extra MEMSE at low E_b/N_0.

In Figure 6.2, the MEMSE of different users is shown under $E_b/N_0 = 10dB$. From this figure, the accuracy of the second-order approximation is confirmed again. Also, it is very interesting to find that under the "equal BER" PDC, earlier detected user (larger index) have smaller MEMSE then later detected ones (smaller index), therefore, the earlier detected users have a higher reliability than the later detected ones, which can still benefit SIC. The cancellation error propagation among different users can also be seen very clearly from this figure. For the later detected users, more cancellation errors result in higher additional MEMSE.

In Figure 6.3, the average BER performance over 16 users under CEE is compared with that under the perfect CSI by actual simulations. From this figure, it is clear that under CEE, the performances of the MMSE-SIC with the equal BER PDC and equal received power will both be degraded. However, it is interesting to find that under CEE, the MMSE-SIC with the equal BER PDC still retains a significant performance advantage over the MMSE-SIC with the equal received power. For example, at a BER of 10^{-3}, the performance advantage is around 4dB, which is even slightly larger than the 3.5dB, obtained under the perfect CSI. Therefore, from these observations, it can be concluded that the equal BER PDC makes the MMSE-SIC more robust to CEE.

6.4 Conclusions

In this chapter, the effects of CEE on the performance of the MMSE-SIC with the equal BER PDC is investigated. By applying a method of second-order approximation, the MEMSE can be derived for different transmit symbols, under a given decision order and power distribution. Under the assumption of ignoring cancellation errors, the accuracy of the approximation is confirmed by simulation results. Furthermore, it is very interesting to find that under small CEE, the equal BER PDC can still benefit

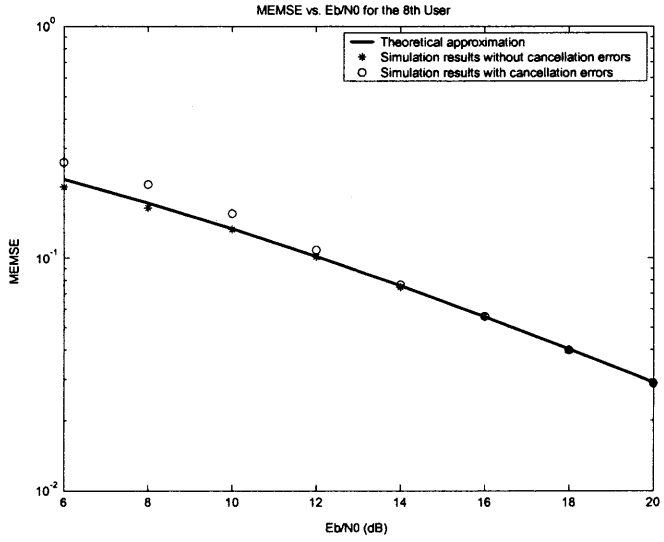

Figure 6.1 MEMSE versus E_b/N_0 of the 8^{th} user.

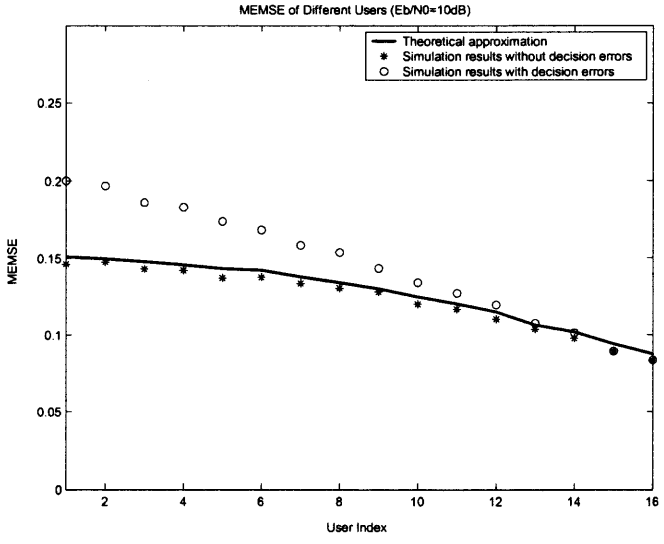

Figure 6.2 MEMSE of different users ($E_b/N_0 = 10dB$).

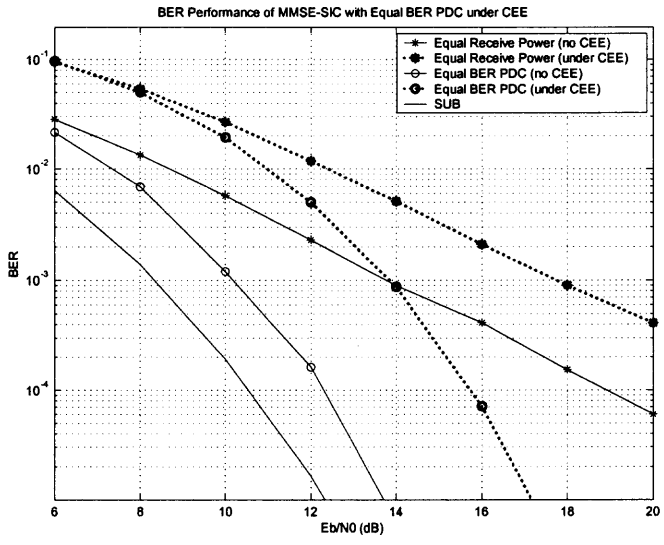

Figure 6.3 Average BER performance over 16 users of the MMSE-SIC under CEE.

MMSE-SIC, making it more robust to CEE than the equal receive power. Therefore, the MMSE-SIC with the equal BER PDC provides a very powerful solution for MAI suppression in a practical MC-CDMA system.

CHAPTER 7

SUMMARY

Characterized by the robustness to frequency-selective fading and flexibility of handling multiple data rates, MC-CDMA has become a promising candidate for supporting multimedia services in future wireless communications. To ensure seamless multi-rate transmission, in this dissertation, different multi-rate access schemes were developed for MC-CDMA. Furthermore, to ensure high QoS requirements, PDC algorithms for the ZF-SIC and MMSE-SIC receivers were investigated, which provides very powerful solutions for MAI suppression. In conclusion, the original contributions of this dissertation are:

- Design of multi-rate access schemes by different sub-carrier assignment strategies.
- Performance comparison of different multi-rate access schemes from various points of view, such as SUE, rate matching capability, receiver structure and BER performance.
- Derivation of the equal BER PDC for the ZF-SIC receiver under both the STPC and LTPC for the MFSL MC-CDMA.
- Derivation of the optimal PDC for the ZF-SIC receiver under both the STPC and LTPC for the MFSL MC-CDMA.
- Derivation of the equal BER PDC for the MMSE-SIC under both the STPC and LTPC for the MFSL MC-CDMA.
- Performance analysis of the MMSE-SIC with the equal BER PDC under CEE.

APPENDIX A

CORRELATION BETWEEN TRANSFORMED SPREADING CODES OF THE SAME HIGHER RATE USER

Property A: In the ideal non-faded AWGN channel, each transformed spreading code of the same higher rate user maintains the same autocorrelation properties of the original codes and those corresponding to different bits are orthogonal:

$$\left[\widetilde{\boldsymbol{\theta}}_{k,i}^{(g)}\right]^H \widetilde{\boldsymbol{\theta}}_{k,i'}^{(g)} = \begin{cases} \left[\mathbf{c}_k^{(g)}\right]^T \mathbf{c}_k^{(g)} & i = i' \\ 0 & i \neq i' \end{cases} \quad i, i' = 1, 2, \cdots, L^{(g)} \tag{A.1}$$

Proof: In an ideal non-fading AWGN channel, $\widetilde{\boldsymbol{\theta}}_{k,i}^{(g)}$ can be rewritten as,

$$\widetilde{\boldsymbol{\theta}}_{k,i}^{(g)} = \frac{1}{\sqrt{L^{(g)}}} \boldsymbol{\Gamma}_i^{(g)} \mathbf{c}_k^{(g)}, \tag{A.2}$$

where

$$\boldsymbol{\Gamma}_i^{(g)} = \left[\boldsymbol{\gamma}_{i,1}^{(g)}, \boldsymbol{\gamma}_{i,2}^{(g)}, \cdots, \boldsymbol{\gamma}_{i,M_V^{(g)}}^{(g)}\right] \tag{A.3}$$

with

$$\boldsymbol{\gamma}_{i,j}^{(g)} = \left[\gamma_{1,i,j}^{(g)}, \gamma_{2,i,j}^{(g)}, \cdots, \gamma_{M_V^{(0)},i,j}^{(g)}\right]^T, \left(j = 1, 2, \cdots, M_V^{(g)}\right). \tag{A.4}$$

The column vector $\boldsymbol{\gamma}_{i,j}^{(g)}$ has the following property,

$$\begin{aligned}
\left[\boldsymbol{\gamma}_{i,m}^{(g)}\right]^H \cdot \boldsymbol{\gamma}_{i',n}^{(g)} &= \frac{1}{\left[M_V^{(g)}\right]^2} \sum_{q=1}^{M_V^{(0)}} e^{j2\pi \frac{i-i'}{L^{(g)}} q} \sum_{s=1}^{M_V^{(g)}} e^{-j2\pi \frac{n-\frac{q}{L^{(g)}}}{M_V^{(g)}} s} \sum_{t=1}^{M_V^{(g)}} e^{j2\pi \frac{m-\frac{q}{L^{(g)}}}{M_V^{(g)}} t} \\
&= \frac{1}{\left[M_V^{(g)}\right]^2} \sum_{s=1}^{M_V^{(g)}} \sum_{t=1}^{M_V^{(g)}} e^{j2\pi \frac{mt-ns}{M_V^{(g)}}} \sum_{q=1}^{M_V^{(0)}} e^{j2\pi \frac{(t-s)+M_V^{(g)}(i-i')}{L^{(g)}} q} \\
&= \frac{M_V^{(0)}}{\left[M_V^{(g)}\right]^2} \sum_{s=1}^{M_V^{(g)}} \sum_{t=1}^{M_V^{(g)}} e^{j2\pi \frac{mt-ns}{M_V^{(g)}}} \delta\left[(t-s) + M_V^{(g)}(i-i')\right] \qquad \text{(A.5)} \\
&= L^{(g)} \delta(m-n)\, \delta\left(i-i'\right).
\end{aligned}$$

Notice term

$$(t-s) \in \left[1 - M_V^{(g)}, \cdots, -1, 0, 1, \cdots, M_V^{(g)} - 1\right] \qquad \text{(A.6)}$$

and term

$$M_V^{(g)}(i-i') \in \left[\left(1-L^{(g)}\right) M_V^{(g)}, \cdots, -M_V^{(g)}, 0, M_V^{(g)}, \cdots, \left(L^{(g)}-1\right) M_V^{(g)}\right] \qquad \text{(A.7)}$$

Thus, the fourth equality in equation (A.5) is valid as

$$\delta\left[(t-s) + M_V^{(g)}(i-i')\right] = \delta(t-s) \cdot \delta(i-i'). \qquad \text{(A.8)}$$

From equation (A.5), it can be shown

$$\left[\boldsymbol{\Gamma}_i^{(g)}\right]^H \boldsymbol{\Gamma}_{i'}^{(g)} = \begin{cases} L^{(g)} \mathbf{I}^{M_V^{(g)}} & i = i' \\ \mathbf{0} & i \neq i' \end{cases}. \qquad \text{(A.9)}$$

Therefore

$$\left[\widetilde{\boldsymbol{\theta}}_{k,i}^{(g)}\right]^H \widetilde{\boldsymbol{\theta}}_{k,i'}^{(g)} = \frac{1}{L^{(g)}} \left[\mathbf{c}_k^{(g)}\right]^T \left[\left[\boldsymbol{\Gamma}_i^{(g)}\right]^H \boldsymbol{\Gamma}_{i'}^{(g)}\right] \mathbf{c}_k^{(g)} = \left[\mathbf{c}_k^{(g)}\right]^T \mathbf{c}_k^{(g)} \delta(i-i'). \qquad \text{(A.10)}$$

Property B: In the Rayleigh fading channel, the transformed spreading codes corresponding to different bits remain orthogonal.

Proof: In a Rayleigh fading channel, $\widetilde{\boldsymbol{\theta}}_{k,i}^{(g)}$ can be rewritten as,

$$\widetilde{\boldsymbol{\theta}}_{k,i}^{(g)} = \boldsymbol{\Gamma}_{i}^{(g)} \mathbf{H}_{k}^{(g)} \mathbf{c}_{k}^{(g)}, \tag{A.11}$$

where

$$\mathbf{H}_{k}^{(g)} = diag\left(h_{k,1}^{(g)}, h_{k,2}^{(g)}, \cdots, h_{k,M_V^{(g)}}^{(g)} \right). \tag{A.12}$$

Therefore, utilizing the result in AWGN channel expressed in equation (A.10), it can be obtained that

$$\begin{aligned} \left[\widetilde{\boldsymbol{\theta}}_{k,i}^{(g)}\right]^{H} \widetilde{\boldsymbol{\theta}}_{k,i'}^{(g)} &= \frac{1}{L^{(g)}} \left[\mathbf{c}_{k}^{(g)}\right]^{T} \left[\mathbf{H}_{k}^{(g)}\right]^{H} \left[\left[\boldsymbol{\Gamma}_{i}^{(g)}\right]^{H} \boldsymbol{\Gamma}_{i'}^{(g)}\right] \mathbf{H}_{k}^{(g)} \mathbf{c}_{k}^{(g)} \\ &= \left[\mathbf{c}_{k}^{(g)}\right]^{T} \left[\mathbf{H}_{k}^{(g)}\right]^{H} \mathbf{H}_{k}^{(g)} \mathbf{c}_{k}^{(g)} \delta\left(i - i'\right). \end{aligned} \tag{A.13}$$

Thus, even in a Rayleigh fading channel, no SI will be produced in the VSL scheme.

APPENDIX B

SPREADING CODE SELECTION IN THE VSL SCHEME

In the VSL scheme, for the k^{th} user of group g, it employs an $M_V^{(g)}$−point IDFT as modulator but an $M_V^{(0)}$−point DFT as demodulator. By mathematical manipulations shown in equation (2.48), at the lowest rate bit interval $\left[(i-1)\,T^{(0)}, iT^{(0)}\right)$, $L^{(g)}$ transformed spreading codes $\widetilde{\boldsymbol{\theta}}_{k,l}^{(g)}$ are produced, each corresponding to the higher rate bit $b_{k,l}^{(g)}(i)$ transmitted at the l^{th} subinterval $\left[(i-1)\,T^{(0)} + (l-1)T^{(g)}, (i-1)\,T^{(0)} + lT^{(g)}\right)$. It is not difficult to notice that these different transformed spreading codes are produced in the following way:

1) After modulation, the original code $\mathbf{c}_k^{(g)}$ is transformed to $\overline{\mathbf{c}}_k^{(g)}$, which is the $M_V^{(g)}$-IDFT of $\mathbf{c}_k^{(g)}$,

$$\overline{\mathbf{c}}_k^{(g)} = IDFT_{M_V^{(g)}}\left(\mathbf{c}_k^{(g)}\right). \tag{B.1}$$

2) Produce a $\left(1 \times M_V^{(0)}\right)$vector $\widehat{\mathbf{c}}_{k,l}^{(g)}$by padding $L^{(g)} - 1$ zero blocks, each with the same size as $\overline{\mathbf{c}}_k^{(g)}$ and put $\overline{\mathbf{c}}_k^{(g)}$ at the l^{th} sub-block,

$$\widehat{\mathbf{c}}_{k,l}^{(g)} = \left(\overbrace{\left[\mathbf{0}, \cdots, \mathbf{0}, \overline{\mathbf{c}}_k^{(g)T}, \mathbf{0} \cdots, \mathbf{0}\right]^T}^{total\ L^{(g)}\ subblocks} \right). \tag{B.2}$$

$$\Uparrow$$

$$the\ l^{th}\ subblock$$

3) The transformed spreading code corresponding to the l^{th} higher rate bit $\widetilde{\boldsymbol{\theta}}_{k,l}^{(g)}$ is obtained by performing $M_V^{(0)}$-DFT on $\widehat{\mathbf{c}}_{k,l}^{(g)}$,

$$\widetilde{\boldsymbol{\theta}}_{k,l}^{(g)} = DFT_{M_V^{(0)}}\left(\widehat{\mathbf{c}}_{k,l}^{(g)}\right). \tag{B.3}$$

For the k^{th} lowest rate user, since it employs the same $M_V^{(0)}$−point IDFT and DFT as modulator and demodulator, the transformed spreading code is the same as the

original code. The IDFT of the original code $\mathbf{c}_k^{(0)}$ is denoted by $\overline{\mathbf{c}}_k^{(0)}$,

$$\overline{\mathbf{c}}_k^{(0)} = IDFT_{M_V^{(0)}}\left(\mathbf{c}_k^{(0)}\right). \tag{B.4}$$

Since Fourier transform is an orthogonal transform, to obtain a set of orthogonal transformed spreading codes $\left[\widetilde{\mathbf{C}}^{(0)}, \underline{\widetilde{\mathbf{\Theta}}}^{(1)}, \underline{\widetilde{\mathbf{\Theta}}}^{(2)}, \cdots, \underline{\widetilde{\mathbf{\Theta}}}^{(G-1)}\right]$ for all K_v virtual users, it is obvious that the set of vectors on which $M_V^{(0)}-$point DFT is performed should be orthogonal. Therefore, for different users in the same group, the original codes should be chosen orthogonal. For users in different groups, for example, the k^{th} user in group m and n, we should choose the original codes $\mathbf{c}_k^{(m)}$ and $\mathbf{c}_k^{(n)}$, which ensure that all vectors $\widehat{\mathbf{c}}_{k,l}^{(m)}, \left(l = 1, 2, \cdots, M_V^{(m)}\right)$ and $\widehat{\mathbf{c}}_{k,l}^{(n)}, \left(l = 1, 2, \cdots, M_V^{(n)}\right)$ are orthogonal.

Due to the good symmetry properties of the orthogonal Walsh-Hadamard codes, which imposes good symmetry conditions on the Fourier transform, by simple tries, it is easy to find an original spreading code set which can eliminate ICI in the ideal non-faded AWGN channel.

APPENDIX C

DERIVATION OF COVARIANCE MATRICES OF $\widehat{\boldsymbol{\eta}}(I)$ AND $\overline{\boldsymbol{\eta}}(I)$

- *Covariance matrix of* $\widehat{\boldsymbol{\eta}}(i)$

  With the definition of covariance matrix, we have

$$\mathbf{R}_{\widehat{\boldsymbol{\eta}}(i)} = E\left[\widehat{\boldsymbol{\eta}}(i) \cdot \widehat{\boldsymbol{\eta}}(i)^H\right]. \tag{C.1}$$

From equation (3.9) and (3.11),

$$\begin{aligned} \widehat{\boldsymbol{\eta}}(i) &= \mathbf{D}^{-2}\boldsymbol{\Gamma}^{-H} \cdot \widetilde{\boldsymbol{\eta}}(i) \\ &= \mathbf{D}^{-2}\boldsymbol{\Gamma}^{-H}\widetilde{\mathbf{C}}^H\boldsymbol{\eta}(i). \end{aligned} \tag{C.2}$$

Substituting (C.2) into (C.1) and with $\mathbf{R}_{\boldsymbol{\eta}(i)} = E\left[\boldsymbol{\eta}(i) \cdot \boldsymbol{\eta}(i)^H\right] = \sigma_n^2\mathbf{I}$, we have

$$\begin{aligned} \mathbf{R}_{\widehat{\boldsymbol{\eta}}(i)} &= E\left[\mathbf{D}^{-2}\boldsymbol{\Gamma}^{-H}\widetilde{\mathbf{C}}^H\boldsymbol{\eta}(i) \cdot \boldsymbol{\eta}(i)^H\,\widetilde{\mathbf{C}}\boldsymbol{\Gamma}^{-1}\mathbf{D}^{-2}\right] \\ &= \sigma_n^2 \cdot \left(\mathbf{D}^{-2}\boldsymbol{\Gamma}^{-H}\widetilde{\mathbf{C}}^H\widetilde{\mathbf{C}}\boldsymbol{\Gamma}^{-1}\mathbf{D}^{-2}\right). \end{aligned} \tag{C.3}$$

Since $\mathbf{R}_c$=$\widetilde{\mathbf{C}}^H\widetilde{\mathbf{C}}$= $\boldsymbol{\Gamma}^H\mathbf{D}^2\boldsymbol{\Gamma}$, (C.3) can be simplified as

$$\begin{aligned} \mathbf{R}_{\widehat{\boldsymbol{\eta}}(i)} &= \sigma_n^2 \cdot \left(\mathbf{D}^{-2}\boldsymbol{\Gamma}^{-H}\mathbf{R}_c\boldsymbol{\Gamma}^{-1}\mathbf{D}^{-2}\right) \\ &= \sigma_n^2\mathbf{D}^{-2}. \end{aligned} \tag{C.4}$$

- *Covariance matrix of* $\overline{\boldsymbol{\eta}}(i)$

  Similarly,

$$\mathbf{R}_{\overline{\boldsymbol{\eta}}(i)} = E\left[\overline{\boldsymbol{\eta}}(i) \cdot \overline{\boldsymbol{\eta}}(i)^H\right]. \tag{C.5}$$

  By multiplying both sides of equation (3.9) $\mathbf{R}_m^{-1}$, we get

$$\mathbf{R}_m^{-1}\mathbf{y}(i) = \mathbf{A}\mathbf{b}(i) + \overleftrightarrow{\boldsymbol{\eta}}(i). \tag{C.6}$$

With (3.16), apparently, $\overline{\boldsymbol{\eta}}(i) = \overline{\boldsymbol{\Gamma}}\overleftrightarrow{\boldsymbol{\eta}}(i)$, hence,

$$\mathbf{R}_{\overline{\eta}(i)} = \overline{\boldsymbol{\Gamma}}\mathbf{R}_{\overleftrightarrow{\eta}(i)}\overline{\boldsymbol{\Gamma}}^{H}. \tag{C.7}$$

Letting $\mathbf{Ab}(i) = \overline{\mathbf{b}}(i)$, we have [49]

$$\mathbf{R}_{\overleftrightarrow{\eta}(i)} = \mathbf{R}_{\overline{\mathbf{b}}(i)} - \mathbf{R}_{\overline{\mathbf{b}}(i),\mathbf{y}(i)} \cdot \mathbf{R}_{\mathbf{y}(i)}^{-1} \cdot \mathbf{R}_{\mathbf{y}(i),\overline{\mathbf{b}}(i)}. \tag{C.8}$$

It is not difficult to get that $\mathbf{R}_{\overline{\mathbf{b}}(i)} = \mathbf{A}^2$, $\mathbf{R}_{\overline{\mathbf{b}}(i),\mathbf{y}(i)} = \mathbf{A}^2\mathbf{R}_c$, $\mathbf{R}_{\mathbf{y}(i),\overline{\mathbf{b}}(i)} = \mathbf{R}_c\mathbf{A}^2$ and $\mathbf{R}_{\mathbf{y}(i)} = \mathbf{R}_c\mathbf{A}^2\mathbf{R}_c^H + \sigma_n^2\mathbf{R}_c$. With these results and noting $\mathbf{R}_c^H = \mathbf{R}_c$, it can be shown that

$$\begin{aligned}
\mathbf{R}_{\overleftrightarrow{\eta}(i)} &= \mathbf{A}^2 - \mathbf{A}^2\mathbf{R}_c\left(\mathbf{R}_c\mathbf{A}^2\mathbf{R}_c^H + \sigma_n^2\mathbf{R}_c\right)^{-1}\mathbf{R}_c\mathbf{A}^2 \\
&= \mathbf{A}^2 - \mathbf{A}^2\mathbf{R}_c\left(\mathbf{R}_c + \sigma_n^2\mathbf{A}^{-2}\right)^{-1}\left(\mathbf{R}_c\mathbf{A}^2\right)^{-1}\mathbf{R}_c\mathbf{A}^2 \\
&= \mathbf{A}^2\mathbf{R}_m\mathbf{R}_m^{-1} - \mathbf{A}^2\mathbf{R}_c\mathbf{R}_m^{-1} \\
&= \mathbf{A}^2\left(\mathbf{R}_c + \sigma_n^2\mathbf{A}^{-2} - \mathbf{R}_c\right)\mathbf{R}_m^{-1} \\
&= \sigma_n^2\mathbf{R}_m^{-1}.
\end{aligned} \tag{C.9}$$

Substituting it into (C.7) and with $\mathbf{R}_m = \overline{\boldsymbol{\Gamma}}^H\overline{\mathbf{D}}^2\overline{\boldsymbol{\Gamma}}$, it can be proved that

$$\mathbf{R}_{\overline{\eta}(i)} = \sigma_n^2\overline{\mathbf{D}}^{-2}. \tag{C.10}$$

APPENDIX D

SOLUTIONS OF KKT OPTIMALITY CONDITIONS UNDER THE STPC

To solve the optimization problem stated in (4.16), Lagrangian multipliers $\boldsymbol{\lambda}_k = [\lambda_{k,1}, \lambda_{k,2}, \cdots, \lambda_{k,l_k}]^T$ are introduced for inequality constraints $a_{k,l}^2 \geq 0 \quad (l = 1, 2, \cdots, l_K)$ and ϑ_k for equality constraint $\frac{1}{l_k}\sum_{l=1}^{l_k} a_{k,l}^2 = \overline{\mathcal{P}}_k$. Hence, the Lagrangian is given by

$$\mathcal{L}\left(\mathbf{a}_k^2, \boldsymbol{\lambda}, \vartheta_k\right) = \overline{p}_{e,k}\left(\mathbf{a}_k^2\right) - \sum_{l=1}^{l_k} \lambda_{k,l} a_{k,l}^2 + \vartheta_k \left(\frac{1}{l_k}\sum_{l=1}^{l_k} a_{k,l}^2\right). \tag{D.1}$$

With the approximation of $Q(x) \approx \frac{1}{2}e^{-\frac{x^2}{2}}$, $\overline{p}_{e,k}\left(\mathbf{a}_k^2\right)$ can be expressed as

$$\begin{aligned} \overline{p}_{e,k}\left(\mathbf{a}_k^2\right) &= \frac{1}{l_k}\sum_{l=1}^{l_k} Q\left(\sqrt{\frac{a_{k,l}^2}{\sigma_n^2 \cdot d_{k,l}^{-2}}}\right) \\ &\approx \frac{1}{l_k}\sum_{l=1}^{l_k} \frac{1}{2} e^{-\frac{a_{k,l}^2}{2\sigma_n^2 \cdot d_{k,l}^{-2}}}. \end{aligned} \tag{D.2}$$

Therefore, the KKT optimality conditions can be expressed as [45]

$$\begin{cases} \frac{1}{l_k}\sum_{l=1}^{l_k} a_{k,l}^{2\dagger} = \overline{\mathcal{P}}_k, a_{k,l}^{2\dagger} \geq 0 \\ \boldsymbol{\lambda}_k^{\dagger} \geq \mathbf{0} \\ \frac{1}{L_k} \cdot \frac{1}{2} e^{-\frac{a_{k,l}^{2\dagger}}{2\sigma_n^2 \cdot d_{k,l}^{-2}}} \cdot \left(-\frac{1}{2\sigma_n^2 \cdot d_{k,l}^{-2}}\right) - \lambda_{k,l}^{\dagger} + \frac{1}{l_k}\vartheta_k^{\dagger} = 0 \\ \lambda_{k,l}^{\dagger} \cdot a_{k,l}^{2\dagger} = 0 \qquad (l = 1, 2, \cdots, l_K). \end{cases} \tag{D.3}$$

The third equation in (D.3) is obtained by differentiating the right side of equation (D.1) with respect to $a_{k,l}^{2\dagger}$ and setting it to be zero. Notice that $\lambda_{k,l}^{\dagger}$ acts as a slack

variable in the third equation, so it can be eliminated, leaving

$$\begin{cases} \frac{1}{l_k}\sum_{l=1}^{l_k} a_{k,l}^{2\dagger} = \overline{\mathcal{P}}_k, a_{k,l}^{2\dagger} \geq 0 \\ \boldsymbol{\lambda}_k^{\dagger} \geq \mathbf{0} \\ \vartheta_k^{\dagger} \geq \frac{1}{2} e^{-\frac{a_{k,l}^{2\dagger}}{2\sigma_n^2 \cdot d_{k,l}^{-2}}} \cdot \frac{1}{2\sigma_n^2 \cdot d_{k,l}^{-2}} \\ a_{k,l}^{2\dagger} \cdot \left(\vartheta_k - \frac{1}{2} e^{-\frac{a_{k,l}^{2\dagger}}{2\sigma_n^2 \cdot d_{k,l}^{-2}}} \cdot \frac{1}{2\sigma_n^2 \cdot d_{k,l}^{-2}} \right) = 0 \qquad (l = 1, 2, \cdots, l_K). \end{cases} \tag{D.4}$$

If $\vartheta_k^{\dagger} < \frac{1}{4\sigma_n^2 d_{k,l}^{-2}}$, the third equation can only hold if $a_{k,l}^{2\dagger} > 0$, which by the last condition implies that $a_{k,l}^{2\dagger} = -2d_{k,l}^{-2}\sigma_n^2 \ln\left(4\vartheta_k^{\dagger} d_{k,l}^{-2}\sigma_n^2\right)$. If $\vartheta_k^{\dagger} \geq \frac{1}{4\sigma_n^2 d_{k,l}^{-2}}$, then $a_{k,l}^{2\dagger} > 0$ is impossible, thus, $a_{k,l}^{2\dagger} = 0$. Therefore, the following results can be obtained that

$$a_{k,l}^{2\dagger} = \begin{cases} -2d_{k,l}^{-2}\sigma_n^2 \ln\left(4\vartheta_k^{\dagger} d_{k,l}^{-2}\sigma_n^2\right) & \vartheta_k^{\dagger} < \frac{1}{4\sigma_n^2 d_{k,l}^{-2}} \\ 0 & \vartheta_k^{\dagger} \geq \frac{1}{4\sigma_n^2 d_{k,l}^{-2}} \end{cases} \tag{D.5}$$

or equivalently

$$a_{k,l}^{2\dagger} = \max\left[0, -2d_{k,l}^{-2}\sigma_n^2 \ln\left(4\vartheta_k^{\dagger} d_{k,l}^{-2}\sigma_n^2\right)\right]. \tag{D.6}$$

Substituting this expression for $a_{k,l}^{2\dagger}$ into the average power constraint condition, we obtain

$$\frac{1}{l_k}\sum_{l=1}^{l_k} \max\left[0, -2d_{k,l}^{-2}\sigma_n^2 \ln\left(4\vartheta_k^{\dagger} d_{k,l}^{-2}\sigma_n^2\right)\right] = \overline{\mathcal{P}}_k. \tag{D.7}$$

The left hand side is a piecewise decreasing function of ϑ_k, with breakpoints at $\frac{1}{4\sigma_n^2 d_{k,l}^{-2}}$, so the equation has a unique solution $\vartheta_k^{\dagger}$ which is readily determined, by which, the optimal power distribution can be obtained.

APPENDIX E

SOLUTIONS OF KKT OPTIMALITY CONDITIONS UNDER THE LTPC

To solve the optimization problem stated in (4.25), the Lagrangian is given by

$$\mathcal{L}\left(\mathbf{a}_k^2, \boldsymbol{\lambda}_k, \vartheta_k\right) = E_h\left[\overline{p}_{e,k}\left(\mathbf{a}_k^2\right)\right] - \sum_{l=1}^{l_k} \lambda_{k,l} a_{k,l}^2 + \vartheta_k \left(E_h\left[\frac{1}{l_k}\sum_{l=1}^{l_k} a_{k,l}^2\right]\right). \tag{E.1}$$

Similarly, the KKT optimality conditions are be expressed as

$$\begin{cases} \frac{1}{l_k}\int \rho_h\left(\mathbf{h}_k\right)\cdot\sum_{l=1}^{l_k} a_{k,l}^{2\dagger} d\mathbf{h}_k = \overline{\mathcal{P}}_k, a_{k,l}^{2\dagger} \geq 0 \\ \boldsymbol{\lambda}_k^{\dagger} \geq \mathbf{0} \\ \frac{1}{l_k}\int \rho_H\left(\mathbf{h}_k\right)\cdot\frac{1}{2}e^{-\frac{a_{k,l}^{2\dagger}}{2\sigma_n^2\cdot d_{k,l}^{-2}}}\cdot\left(-\frac{1}{2\sigma_n^2\cdot d_{k,l}^{-2}}\right)d\mathbf{h}_k - \lambda_{k,l}^{\dagger} + \frac{1}{l_k}\int \rho_H\left(\mathbf{h}_k\right)\cdot\vartheta_k^{\dagger} d\mathbf{h}_k = 0 \\ \lambda_{k,l}^{\dagger}\cdot a_{k,l}^{2\dagger} = 0 \quad (l = 1, 2, \cdots, l_K). \end{cases} \tag{E.2}$$

After eliminating the slack variable $\lambda_{k,l}^{\dagger}$ in the third equation, it can be simplified as

$$\begin{cases} \frac{1}{l_k}\int \rho_H\left(\mathbf{h}_k\right)\cdot\sum_{l=1}^{l_k} a_{k,l}^{2\dagger} d\mathbf{h}_k = \overline{\mathcal{P}}_k, a_{k,l}^{2\dagger} \geq 0 \\ \boldsymbol{\lambda}_k^{\dagger} \geq \mathbf{0} \\ \int \rho_H\left(\mathbf{h}_k\right)\cdot\vartheta_k d\mathbf{h}_k \geq \int \rho_H\left(\mathbf{h}_k\right)\cdot\frac{1}{2}e^{-\frac{a_{k,l}^{2\dagger}}{2\sigma_n^2\cdot d_{k,l}^{-2}}}\cdot\left(-\frac{1}{2\sigma_n^2\cdot d_{k,l}^{-2}}\right)d\mathbf{h}_k \\ a_{k,l}^{2\dagger}\cdot\left\{\int \rho_H\left(\mathbf{h}_k\right)\cdot\left(\vartheta_k - \frac{1}{2}e^{-\frac{a_{k,l}^{2\dagger}}{2\sigma_n^2\cdot d_{k,l}^{-2}}}\cdot\frac{1}{2\sigma_n^2\cdot d_{k,l}^{-2}}\right)d\mathbf{h}_k\right\} = 0 \quad (l = 1, 2, \cdots, l_K). \end{cases} \tag{E.3}$$

With similar analysis as in the Appendix D, a similar result can be obtained, which is

$$a_{k,l}^{2\dagger} = \begin{cases} -2d_{k,l}^{-2}\sigma_n^2 \ln\left(4\vartheta_k^{\dagger} d_{k,l}^{-2}\sigma_n^2\right) & \vartheta_k^{\dagger} < \frac{1}{4\sigma_n^2 d_{k,l}^{-2}} \\ 0 & \vartheta_k^{\dagger} \geq \frac{1}{4\sigma_n^2 d_{k,l}^{-2}} \end{cases} \tag{E.4}$$

or equivalently

$$a_{k,l}^{2\dagger} = \max\left[0, -2d_{k,l}^{-2}\sigma_n^2 \ln\left(4\vartheta_k^{\dagger} d_{k,l}^{-2}\sigma_n^2\right)\right]. \tag{E.5}$$

Substituting this expression for $a_{k,l}^{2\dagger}$ into the average power constraint, the following expression can be obtained:

$$\int \rho_H\left(\mathbf{h}_k\right) \cdot \sum_{l=1}^{l_k} \max\left[0, -2d_{k,l}^{-2}\sigma_n^2 \ln\left(4\vartheta_k^{\dagger} d_{k,l}^{-2}\sigma_n^2\right)\right] d\mathbf{h}_k = \overline{\mathcal{P}}_k, \tag{E.6}$$

from which, $\vartheta_k^{\dagger}$ can be solved[1], by which, the optimal power distribution can be obtained.

[1]To solve the integral, a summation over the ensemble of channel realizations is used as an approximation.

APPENDIX F

PROOF OF THE PROPERTY OF $[\mathbf{A}]_{L,L}^2$ WITH THE MMSE-SIC UNDER THE EQUAL BER PDC

$[\mathbf{A}]_{l,l}^2 \in [0, +\infty)$ $(l = 1, 2, \cdots, L)$ *are monotonically increasing with* $\lambda \in [\sigma^2, +\infty)$

Proof: With the assumption of ignoring decision errors, the l^{th} detected symbol is only interfered by those haven't been detected $((l+1)^{th}, (l+2)^{th}, \cdots, L^{th})$. The SIR of the l^{th} detected symbol can be expressed alternatively as [13]

$$SIR_{L-l+1} = [\mathbf{A}]_{L-l+1,L-l+1}^2 \left[\widetilde{\mathbf{C}}\right]_{L-l+1}^H \mathbf{S}_{L-l+1}^{-1} \left[\widetilde{\mathbf{C}}\right]_{L-l+1}, \tag{F.1}$$

where $\mathbf{S}_{L-l+1} = \sum_{j<l} \left[\widetilde{\mathbf{C}}\right]_{L-j+1} [\mathbf{A}]_{L-j+1,L-j+1}^2 \left[\widetilde{\mathbf{C}}\right]_{L-j+1}^H + \sigma_n^2 \mathbf{I}$. Apparently, in the extreme case of $\lambda = \sigma_n^2$, $[\mathbf{A}]_{l,l}^2 = 0$ $(l = 1, 2, \cdots, L)$.

For the last (L^{th})detected symbol, since all interference has been perfectly cancelled, its SIR can be simplified as

$$SIR_1 = \frac{\lambda}{\sigma_n^2} - 1 = \frac{[\mathbf{A}]_{1,1}^2 \left[\widetilde{\mathbf{C}}\right]_1^H \left[\widetilde{\mathbf{C}}\right]_1}{\sigma_n^2}. \tag{F.2}$$

Clearly, $[\mathbf{A}]_{1,1}^2$ is monotonically increasing with λ. In another word, with $\lambda_1 > \lambda_2$, $[\mathbf{A}]_{1,1|\lambda_1}^2 > [\mathbf{A}]_{1,1|\lambda_2}^2$. For the second last $\left((L-1)^{th}\right)$ detected symbol, its SIR can be rewritten as

$$SIR_2 = \frac{\lambda}{\sigma_n^2} - 1 = [\mathbf{A}]_{2,2}^2 \left[\widetilde{\mathbf{C}}\right]_2^H \mathbf{S}_2^{-1} \left[\widetilde{\mathbf{C}}\right]_2, \tag{F.3}$$

where $\mathbf{S}_2 = \left[\widetilde{\mathbf{C}}\right]_1 [\mathbf{A}]_{1,1}^2 \left[\widetilde{\mathbf{C}}\right]_1^H + \sigma_n^2 \mathbf{I}$. When $\lambda_1 > \lambda_2$, $[\mathbf{A}]_{1,1|\lambda_1}^2 > [\mathbf{A}]_{1,1|\lambda_2}^2$, hence, $\mathbf{S}_{2|\lambda_1} - \mathbf{S}_{2|\lambda_2}$ is positive definite, i.e. $\mathbf{S}_{2|\lambda_1} \succ \mathbf{S}_{2|\lambda_2}$. Obviously, $\left(\mathbf{S}_{2|\lambda_1}\right)^{-1} \prec \left(\mathbf{S}_{2|\lambda_2}\right)^{-1}$ and $\left[\widetilde{\mathbf{C}}\right]_2^H \left(\left(\mathbf{S}_{2|\lambda_1}\right)^{-1} - \left(\mathbf{S}_{2|\lambda_2}\right)^{-1}\right) \left[\widetilde{\mathbf{C}}\right]_2 < 0$. If $[\mathbf{A}]_{2,2|\lambda_1}^2 \leq [\mathbf{A}]_{2,2|\lambda_2}^2$, $\frac{\lambda_1}{\sigma_n^2} - 1 \leq \frac{\lambda_2}{\sigma_n^2} - 1$, which conflicts with $\lambda_1 > \lambda_2$. Therefore, to achieve a higher SIR, $[\mathbf{A}]_{2,2}^2$ must be

increased to compensate for higher interference power, which means, $[\mathbf{A}]_{2,2}^2$ is also monotonically increasing with λ. Similar analysis can be made successively for the other symbols.

APPENDIX G

DERIVATION OF THE SECOND-ORDER TERM $\mathbf{SOT}_L$

With the equation (6.17), the second-order term $\mathbf{SOT}_l$ can be expressed as

$$\begin{aligned}
\mathbf{SOT}_l &= \begin{bmatrix} \Delta\widetilde{\mathbf{f}}_{l,o}^H & \Delta\mathbf{w}_{l,o}^H \end{bmatrix} \begin{bmatrix} \mathbf{R_{bb}} & -\mathbf{R_{bx}} \\ -\mathbf{R_{xb}} & \mathbf{R_{xx}} \end{bmatrix} \begin{bmatrix} \Delta\widetilde{\mathbf{f}}_{l,o} \\ \Delta\mathbf{w}_{l,o} \end{bmatrix} \\
&= \Delta\widetilde{\mathbf{f}}_{l,o}^H \mathbf{R_{bb}} \Delta\widetilde{\mathbf{f}}_{l,o} - \Delta\mathbf{w}_{l,o}^H \mathbf{R_{xb}} \Delta\widetilde{\mathbf{f}}_{l,o} \\
&\quad -\Delta\widetilde{\mathbf{f}}_{l,o}^H \mathbf{R_{bx}} \Delta\mathbf{w}_{l,o} + \Delta\mathbf{w}_{l,o}^H \mathbf{R_{xx}} \Delta\mathbf{w}_{l,o}. \qquad \text{(G.1)}
\end{aligned}$$

To solve $\mathbf{SOT}_l$, $\Delta\widetilde{\mathbf{f}}_{l,o}$ and $\Delta\mathbf{w}_{l,o}$ should be derived first. From equation (6.7) (6.8),

$$\begin{aligned}
\widehat{\mathbf{w}}_{l,o} &= \mathbf{w}_{l,o} + \Delta\mathbf{w}_{l,o} \\
&= \widehat{\mathbf{R}}_{\mathbf{xx}}^{-1} \widehat{\mathbf{R}}_{\mathbf{xb}} \widehat{\widetilde{\mathbf{f}}}_{l,o} \\
&= \left(\mathbf{R_{xx}} + \Delta\mathbf{R_{xx}}\right)^{-1} \left(\mathbf{R_{xb}} + \Delta\mathbf{R_{xb}}\right) \left(\widetilde{\mathbf{f}}_{l,o} + \Delta\widetilde{\mathbf{f}}_{l,o}\right) \\
&= \left(\mathbf{R_{xx}^{-1}} - \mathbf{R_{xx}^{-1}} \Delta\mathbf{R_{xx}} \mathbf{R_{xx}^{-1}}\right) \left(\mathbf{R_{xb}} + \Delta\mathbf{R_{xb}}\right) \left(\widetilde{\mathbf{f}}_{l,o} + \Delta\widetilde{\mathbf{f}}_{l,o}\right) \\
&= \mathbf{R_{xx}^{-1}} \mathbf{R_{xb}} \widetilde{\mathbf{f}}_{l,o} + \mathbf{R_{xx}^{-1}} \Delta\mathbf{R_{xb}} \widetilde{\mathbf{f}}_{l,o} - \mathbf{R_{xx}^{-1}} \Delta\mathbf{R_{xx}} \mathbf{R_{xx}^{-1}} \mathbf{R_{xb}} \widetilde{\mathbf{f}}_{l,o} \\
&\quad -\mathbf{R_{xx}^{-1}} \Delta\mathbf{R_{xx}} \mathbf{R_{xx}^{-1}} \Delta\mathbf{R_{xb}} \widetilde{\mathbf{f}}_{l,o} \\
&\quad +\mathbf{R_{xx}^{-1}} \mathbf{R_{xb}} \Delta\widetilde{\mathbf{f}}_{l,o} + \mathbf{R_{xx}^{-1}} \Delta\mathbf{R_{xb}} \Delta\widetilde{\mathbf{f}}_{l,o} - \mathbf{R_{xx}^{-1}} \Delta\mathbf{R_{xx}} \mathbf{R_{xx}^{-1}} \mathbf{R_{xb}} \Delta\widetilde{\mathbf{f}}_{l,o} \\
&\quad -\mathbf{R_{xx}^{-1}} \Delta\mathbf{R_{xx}} \mathbf{R_{xx}^{-1}} \Delta\mathbf{R_{xb}} \Delta\widetilde{\mathbf{f}}_{l,o}. \qquad \text{(G.2)}
\end{aligned}$$

By ignoring all higher order error terms, the above equation can be simplified as

$$\begin{aligned}
\widehat{\mathbf{w}}_{l,o} &= \underbrace{\mathbf{R_{xx}^{-1}} \mathbf{R_{xb}} \widetilde{\mathbf{f}}_{l,o}}_{\mathbf{w}_{l,o}} + \\
&\quad \underbrace{\mathbf{R_{xx}^{-1}} \Delta\mathbf{R_{xb}} \widetilde{\mathbf{f}}_{l,o} - \mathbf{R_{xx}^{-1}} \Delta\mathbf{R_{xx}} \mathbf{R_{xx}^{-1}} \mathbf{R_{xb}} \widetilde{\mathbf{f}}_{l,o} + \mathbf{R_{xx}^{-1}} \mathbf{R_{xb}} \Delta\widetilde{\mathbf{f}}_{l,o}}_{\Delta\mathbf{w}_{l,o}}, \qquad \text{(G.3)}
\end{aligned}$$

hence,

$$\begin{aligned}\Delta \mathbf{w}_{l,o} &= \mathbf{R}_{\mathbf{xx}}^{-1}\Delta\mathbf{R}_{\mathbf{xb}}\widetilde{\mathbf{f}}_{l,o} - \mathbf{R}_{\mathbf{xx}}^{-1}\Delta\mathbf{R}_{\mathbf{xx}}\mathbf{R}_{\mathbf{xx}}^{-1}\mathbf{R}_{\mathbf{xb}}\widetilde{\mathbf{f}}_{l,o} + \mathbf{R}_{\mathbf{xx}}^{-1}\mathbf{R}_{\mathbf{xb}}\Delta\widetilde{\mathbf{f}}_{l,o} \\ &= \mathbf{R}_{\mathbf{xx}}^{-1}\left(\mathbf{R}_{\mathbf{xb}}\Delta\widetilde{\mathbf{f}}_{l,o} + \Delta\mathbf{R}_{\mathbf{xb}}\widetilde{\mathbf{f}}_{l,o} - \Delta\mathbf{R}_{\mathbf{xx}}\mathbf{R}_{\mathbf{xx}}^{-1}\mathbf{R}_{\mathbf{xb}}\widetilde{\mathbf{f}}_{l,o}\right) \\ &= \mathbf{R}_{\mathbf{xx}}^{-1}\left(\mathbf{R}_{\mathbf{xb}}\Delta\widetilde{\mathbf{f}}_{l,o} + \Delta\mathbf{R}_{\mathbf{xb}}\widetilde{\mathbf{f}}_{l,o} - \Delta\mathbf{R}_{\mathbf{xx}}\mathbf{w}_{l,o}\right). \end{aligned} \tag{G.4}$$

With equation (6.8), similarly, ignoring higher order error terms and using the first-order approximation $\frac{1}{a+\Delta a} = \frac{1}{a} - \frac{\Delta a}{a^2}$,

$$\begin{aligned}\widehat{\mathbf{f}}_{l,o} &= \mathbf{f}_{l,o} + \Delta\mathbf{f}_{l,o} \\ &= \frac{\widehat{\mathbf{R}}_{\Delta,l}^{-1}\mathbf{u}_l}{\mathbf{u}_l^T\widehat{\mathbf{R}}_{\Delta,l}^{-1}\mathbf{u}_l} \\ &= \frac{\left(\mathbf{R}_{\Delta,l} + \Delta\mathbf{R}_{\Delta,l}\right)^{-1}\mathbf{u}_l}{\mathbf{u}_l^T\left(\mathbf{R}_{\Delta,l} + \Delta\mathbf{R}_{\Delta,l}\right)^{-1}\mathbf{u}_l} \\ &= \frac{\left(\mathbf{R}_{\Delta,l}^{-1} - \mathbf{R}_{\Delta,l}^{-1}\Delta\mathbf{R}_{\Delta,l}\mathbf{R}_{\Delta,l}^{-1}\right)\mathbf{u}_l}{\mathbf{u}_l^T\left(\mathbf{R}_{\Delta,l}^{-1} - \mathbf{R}_{\Delta,l}^{-1}\Delta\mathbf{R}_{\Delta,l}\mathbf{R}_{\Delta,l}^{-1}\right)\mathbf{u}_l} \\ &= \left(\mathbf{R}_{\Delta,l}^{-1}\mathbf{u}_l - \mathbf{R}_{\Delta,l}^{-1}\Delta\mathbf{R}_{\Delta,l}\mathbf{R}_{\Delta,l}^{-1}\mathbf{u}_l\right)\cdot \\ &\quad \left(\frac{1}{\mathbf{u}_l^T\mathbf{R}_{\Delta,l}^{-1}\mathbf{u}_l} + \frac{\mathbf{u}_l^T\mathbf{R}_{\Delta,l}^{-1}\Delta\mathbf{R}_{\Delta,l}\mathbf{R}_{\Delta,l}^{-1}\mathbf{u}_l}{\left(\mathbf{u}_l^T\mathbf{R}_{\Delta,l}^{-1}\mathbf{u}_l\right)^2}\right) \\ &\approx \underbrace{\frac{\mathbf{R}_{\Delta,l}^{-1}\mathbf{u}_l}{\mathbf{u}_l^T\mathbf{R}_{\Delta,l}^{-1}\mathbf{u}_l}}_{\mathbf{f}_{l,o}} \underbrace{- \frac{\mathbf{R}_{\Delta,l}^{-1}\Delta\mathbf{R}_{\Delta,l}\mathbf{R}_{\Delta,l}^{-1}\mathbf{u}_l}{\mathbf{u}_l^T\mathbf{R}_{\Delta,l}^{-1}\mathbf{u}_l} + \frac{\mathbf{R}_{\Delta,l}^{-1}\mathbf{u}_l\mathbf{u}_l^T\mathbf{R}_{\Delta,l}^{-1}\Delta\mathbf{R}_{\Delta,l}\mathbf{R}_{\Delta,l}^{-1}\mathbf{u}_l}{\left(\mathbf{u}_l^T\mathbf{R}_{\Delta,l}^{-1}\mathbf{u}_l\right)^2}}_{\Delta\mathbf{f}_{l,o}}, \end{aligned} \tag{G.5}$$

hence

$$\begin{aligned}\Delta\mathbf{f}_{l,o} &= \frac{\mathbf{R}_{\Delta,l}^{-1}\mathbf{u}_l\mathbf{u}_l^T\mathbf{R}_{\Delta,l}^{-1}\Delta\mathbf{R}_{\Delta,l}\mathbf{R}_{\Delta,l}^{-1}\mathbf{u}_l}{\left(\mathbf{u}_l^T\mathbf{R}_{\Delta,l}^{-1}\mathbf{u}_l\right)^2} - \frac{\mathbf{R}_{\Delta,l}^{-1}\Delta\mathbf{R}_{\Delta,l}\mathbf{R}_{\Delta,l}^{-1}\mathbf{u}_l}{\mathbf{u}_l^T\mathbf{R}_{\Delta,l}^{-1}\mathbf{u}_l} \\ &= \mathbf{R}_{\Delta,l}^{-1}\mathbf{u}_l\left(\mathbf{f}_{l,o}^H\Delta\mathbf{R}_{\Delta,l}\mathbf{f}_{l,o}\right) - \mathbf{R}_{\Delta,l}^{-1}\Delta\mathbf{R}_{\Delta,l}\mathbf{f}_{l,o}. \end{aligned} \tag{G.6}$$

Substituting (G.4) into (G.1),

$$\begin{aligned}
\mathbf{SOT}_l &= \Delta\widetilde{\mathbf{f}}_{l,o}^H\mathbf{R}_{\mathbf{bb}}\Delta\widetilde{\mathbf{f}}_{l,o} - \Delta\widetilde{\mathbf{f}}_{l,o}^H\mathbf{R}_{\mathbf{bx}}\mathbf{R}_{\mathbf{xx}}^{-1}\mathbf{R}_{\mathbf{xb}}\Delta\widetilde{\mathbf{f}}_{l,o} \\
&\quad -\widetilde{\mathbf{f}}_{l,o}^H\Delta\mathbf{R}_{\mathbf{bx}}\mathbf{R}_{\mathbf{xx}}^{-1}\mathbf{R}_{\mathbf{xb}}\Delta\widetilde{\mathbf{f}}_{l,o} + \mathbf{w}_{l,o}^H\Delta\mathbf{R}_{\mathbf{xx}}\mathbf{R}_{\mathbf{xx}}^{-1}\mathbf{R}_{\mathbf{xb}}\Delta\widetilde{\mathbf{f}}_{l,o} \\
&\quad -\Delta\widetilde{\mathbf{f}}_{l,o}^H\mathbf{R}_{\mathbf{bx}}\mathbf{R}_{\mathbf{xx}}^{-1}\mathbf{R}_{\mathbf{xb}}\Delta\widetilde{\mathbf{f}}_{l,o} - \Delta\widetilde{\mathbf{f}}_{l,o}^H\mathbf{R}_{\mathbf{bx}}\mathbf{R}_{\mathbf{xx}}^{-1}\Delta\mathbf{R}_{\mathbf{xb}}\widetilde{\mathbf{f}}_{l,o} \\
&\quad +\Delta\widetilde{\mathbf{f}}_{l,o}^H\mathbf{R}_{\mathbf{bx}}\mathbf{R}_{\mathbf{xx}}^{-1}\Delta\mathbf{R}_{\mathbf{xx}}\mathbf{w}_{l,o} + \Delta\widetilde{\mathbf{f}}_{l,o}^H\mathbf{R}_{\mathbf{bx}}\mathbf{R}_{\mathbf{xx}}^{-1}\mathbf{R}_{\mathbf{xb}}\Delta\widetilde{\mathbf{f}}_{l,o} \\
&\quad +\widetilde{\mathbf{f}}_{l,o}^H\Delta\mathbf{R}_{\mathbf{bx}}\mathbf{R}_{\mathbf{xx}}^{-1}\mathbf{R}_{\mathbf{xb}}\Delta\widetilde{\mathbf{f}}_{l,o} - \mathbf{w}_{l,o}^H\Delta\mathbf{R}_{\mathbf{xx}}\mathbf{R}_{\mathbf{xx}}^{-1}\mathbf{R}_{\mathbf{xb}}\Delta\widetilde{\mathbf{f}}_{l,o} \\
&\quad +\Delta\widetilde{\mathbf{f}}_{l,o}^H\mathbf{R}_{\mathbf{bx}}\mathbf{R}_{\mathbf{xx}}^{-1}\Delta\mathbf{R}_{\mathbf{xb}}\widetilde{\mathbf{f}}_{l,o} - \Delta\widetilde{\mathbf{f}}_{l,o}^H\mathbf{R}_{\mathbf{bx}}\mathbf{R}_{\mathbf{xx}}^{-1}\Delta\mathbf{R}_{\mathbf{xx}}\mathbf{w}_{l,o} \\
&\quad + \left(\widetilde{\mathbf{f}}_{l,o}^H\Delta\mathbf{R}_{\mathbf{bx}} - \mathbf{w}_{l,o}^H\Delta\mathbf{R}_{\mathbf{xx}}\right)\mathbf{R}_{\mathbf{xx}}^{-1}\left(\Delta\mathbf{R}_{\mathbf{xb}}\Delta\widetilde{\mathbf{f}}_{l,o} - \Delta\mathbf{R}_{\mathbf{xx}}\mathbf{w}_{l,o}\right) \\
&= \left(\widetilde{\mathbf{f}}_{l,o}^H\Delta\mathbf{R}_{\mathbf{bx}} - \mathbf{w}_{l,o}^H\Delta\mathbf{R}_{\mathbf{xx}}\right)\mathbf{R}_{\mathbf{xx}}^{-1}\left(\Delta\mathbf{R}_{\mathbf{xb}}\Delta\widetilde{\mathbf{f}}_{l,o} - \Delta\mathbf{R}_{\mathbf{xx}}\mathbf{w}_{l,o}\right) \\
&\quad +\Delta\widetilde{\mathbf{f}}_{l,o}^H\mathbf{R}\Delta\widetilde{\mathbf{f}}_{l,o}. \qquad \text{(G.7)}
\end{aligned}$$

Also, with equation (G.6), the second term in the above equation can be derived as

$$\begin{aligned}
&\Delta\widetilde{\mathbf{f}}_{l,o}^H\mathbf{R}\Delta\widetilde{\mathbf{f}}_{l,o} \\
&= \Delta\mathbf{f}_{l,o}^H\mathbf{R}_{\Delta}\Delta\mathbf{f}_{l,o} \\
&= \left(\mathbf{R}_{\Delta,l}^{-1}\mathbf{u}_l\left(\mathbf{f}_{l,o}^H\Delta\mathbf{R}_{\Delta,l}\mathbf{f}_{l,o}\right) - \mathbf{R}_{\Delta,l}^{-1}\Delta\mathbf{R}_{\Delta,l}\mathbf{f}_{l,o}\right)^H\mathbf{R}_{\Delta}\cdot \\
&\quad \left(\mathbf{R}_{\Delta,l}^{-1}\mathbf{u}_l\left(\mathbf{f}_{l,o}^H\Delta\mathbf{R}_{\Delta,l}\mathbf{f}_{l,o}\right) - \mathbf{R}_{\Delta,l}^{-1}\Delta\mathbf{R}_{\Delta,l}\mathbf{f}_{l,o}\right) \\
&= \mathbf{f}_{l,o}^H\Delta\mathbf{R}_{\Delta,l}\mathbf{R}_{\Delta,l}^{-1}\Delta\mathbf{R}_{\Delta,l}\mathbf{f}_{l,o} - \left(\mathbf{f}_{l,o}^H\Delta\mathbf{R}_{\Delta,l}\mathbf{f}_{l,o}\right)^2\mathbf{u}_l^T\mathbf{R}_{\Delta,l}^{-1}\mathbf{u}_l \\
&= \mathbf{f}_{l,o}^H\Delta\mathbf{R}_{\Delta,l}\mathbf{R}_{\Delta,l}^{-1}\Delta\mathbf{R}_{\Delta,l}\mathbf{f}_{l,o} - \frac{\left(\mathbf{f}_{l,o}^H\Delta\mathbf{R}_{\Delta,l}\mathbf{f}_{l,o}\right)^2}{\mathbf{MMSE}_l}. \qquad \text{(G.8)}
\end{aligned}$$

Therefore, the $\mathbf{SOT}_l$ can be expressed as

$$\begin{aligned}
\mathbf{SOT}_l &= \left(\widetilde{\mathbf{f}}_{l,o}^H\Delta\mathbf{R}_{\mathbf{bx}} - \mathbf{w}_{l,o}^H\Delta\mathbf{R}_{\mathbf{xx}}\right)\mathbf{R}_{\mathbf{xx}}^{-1}\left(\Delta\mathbf{R}_{\mathbf{xb}}\widetilde{\mathbf{f}}_{l,o}^H - \Delta\mathbf{R}_{\mathbf{xx}}\mathbf{w}_{l,o}\right) \\
&\quad +\mathbf{f}_{l,o}^H\Delta\mathbf{R}_{\Delta,l}\mathbf{R}_{\Delta,l}^{-1}\Delta\mathbf{R}_{\Delta,l}\mathbf{f}_{l,o} - \frac{\left(\mathbf{f}_{l,o}^H\Delta\mathbf{R}_{\Delta,l}\mathbf{f}_{l,o}\right)^2}{\mathbf{MMSE}_l}. \qquad \text{(G.9)}
\end{aligned}$$

APPENDIX H

DERIVATION OF THE MEMSE UNDER A GIVEN CHANNEL REALIZATION

It has been shown that

$$\begin{aligned}\mathbf{SOT}_l &= \left(\widetilde{\mathbf{f}}_{l,o}^H \Delta\mathbf{R}_{\mathbf{bx}} - \mathbf{w}_{l,o}^H \Delta\mathbf{R}_{\mathbf{xx}}\right) \mathbf{R}_{\mathbf{xx}}^{-1} \left(\Delta\mathbf{R}_{\mathbf{xb}} \widetilde{\mathbf{f}}_{l,o}^H - \Delta\mathbf{R}_{\mathbf{xx}} \mathbf{w}_{l,o}\right) \\ &\quad + \mathbf{f}_{l,o}^H \Delta\mathbf{R}_{\Delta,l} \mathbf{R}_{\Delta,l}^{-1} \Delta\mathbf{R}_{\Delta,l} \mathbf{f}_{l,o} - \frac{\left(\mathbf{f}_{l,o}^H \Delta\mathbf{R}_{\Delta,l} \mathbf{f}_{l,o}\right)^2}{\mathbf{MMSE}_l}. \end{aligned} \tag{H.1}$$

First, consider the first term of $\mathbf{SOT}_l$. Using equation (6.9), (6.22), (6.24) and (6.25), it can be shown that

$$\begin{aligned} & \widetilde{\mathbf{f}}_{l,o}^H \Delta\mathbf{R}_{\mathbf{bx}} - \mathbf{w}_{l,o}^H \Delta\mathbf{R}_{\mathbf{xx}} \\ = \; & \widetilde{\mathbf{f}}_{l,o}^H \Delta\mathcal{H}^H - \mathbf{w}_{l,o}^H \left(\mathcal{H}\Delta\mathcal{H}^H + \Delta\mathcal{H}\mathcal{H}^H\right) \\ = \; & \left(\widetilde{\mathbf{f}}_{l,o} - \mathcal{H}^H \mathbf{w}_{l,o}\right)^H \Delta\mathcal{H}^H - \mathbf{w}_{l,o}^H \Delta\mathcal{H}\mathcal{H}^H \\ = \; & \mathbf{g}_{l,o}^H \Delta\mathcal{H}^H - \mathbf{w}_{l,o}^H \Delta\mathcal{H}\mathcal{H}^H \\ = \; & \Delta\mathfrak{h}^H \mathcal{G}_{l,o} - \Delta\mathfrak{h}^H \mathcal{W}_{l,o} \mathcal{H}^H, \end{aligned} \tag{H.2}$$

thus, the first term of $\mathbf{SOT}_l$ can be expressed as

$$\mathbf{SOT}_{l,1} = \Delta\mathfrak{h}^H \underbrace{\left(\mathcal{G}_{l,o} - \mathcal{W}_{l,o}\mathcal{H}^H\right)}_{\Psi_1} \mathbf{R}_{\mathbf{xx}}^{-1} \left(\mathcal{G}_{l,o}^H - \mathcal{H}\mathcal{W}_{l,o}^H\right) \Delta\mathfrak{h}. \tag{H.3}$$

The second term of $\mathbf{SOT}_l$ can be expressed as

$$\begin{aligned}
\mathbf{SOT}_{l,2} &= \mathbf{f}_{l,o}^H \Delta\mathbf{R}_{\Delta,l} \mathbf{R}_{\Delta,l}^{-1} \Delta\mathbf{R}_{\Delta,l} \mathbf{f}_{l,o} \\
&= \mathbf{f}_{l,o}^H \left[\mathbf{0}_{(L-l+1)\times(l-1)}, \mathbf{I}_{L-l+1}\right] \Delta\mathbf{R} \begin{bmatrix} \mathbf{0}_{(l-1)\times(L-l+1)} \\ \mathbf{I}_{L-l+1} \end{bmatrix} \mathbf{R}_{\Delta,l}^{-1} \cdot \\
&\quad \left[\mathbf{0}_{(L-l+1)\times(l-1)}, \mathbf{I}_{L-l+1}\right] \Delta\mathbf{R} \begin{bmatrix} \mathbf{0}_{(l-1)\times(L-l+1)} \\ \mathbf{I}_{L-l+1} \end{bmatrix} \mathbf{f}_{l,o} \\
&= \widetilde{\mathbf{f}}_{l,o}^H \Delta\mathbf{R} \boldsymbol{\Xi} \Delta\mathbf{R} \widetilde{\mathbf{f}}_{l,o}, \qquad \text{(H.4)}
\end{aligned}$$

where

$$\boldsymbol{\Xi} = \begin{bmatrix} \mathbf{0}_{(l-1)\times(L-l+1)} \\ \mathbf{I}_{L-l+1} \end{bmatrix} \mathbf{R}_{\Delta,l}^{-1} \left[\mathbf{0}_{(L-l+1)\times(l-1)}, \mathbf{I}_{L-l+1}\right]. \qquad \text{(H.5)}$$

Using equation (6.4), (6.15) and (6.24),

$$\begin{aligned}
\mathbf{SOT}_{l,2} &= \left(\mathbf{w}_{l,o}^H \Delta\mathcal{H}\mathbf{R} + \mathbf{g}_{l,o}^H \Delta\mathcal{H}^H \mathbf{R}_{\mathbf{xx}}^{-1} \mathbf{R}_{\mathbf{xb}}\right) \boldsymbol{\Xi} \cdot \\
&\quad \left(\mathbf{R}\Delta\mathcal{H}^H \mathbf{w}_{l,o}^H + \mathbf{R}_{\mathbf{bx}} \mathbf{R}_{\mathbf{xx}}^{-1} \Delta\mathcal{H} \mathbf{g}_{l,o}\right). \qquad \text{(H.6)}
\end{aligned}$$

Similarly, with equation (6.22) and (6.25),

$$\mathbf{SOT}_{l,2} = \Delta\mathfrak{h}^H \underbrace{\left(\mathcal{W}_{l,o}\mathbf{R} + \mathcal{G}_{l,o}\mathbf{R}_{\mathbf{xx}}^{-1}\mathbf{R}_{\mathbf{xb}}\right)\boldsymbol{\Xi}}_{\Psi_2} \left(\mathbf{R}\mathcal{W}_{l,o}^H + \mathbf{R}_{\mathbf{bx}}\mathbf{R}_{\mathbf{xx}}^{-1}\mathcal{G}_{l,o}^H\right) \Delta\mathfrak{h}. \qquad \text{(H.7)}$$

Finally, for the third term in $\mathbf{SOT}_l$, the square root of the numerator can be expressed as,

$$\begin{aligned}
&\mathbf{f}_{l,o}^H \Delta\mathbf{R}_{\Delta,l} \mathbf{f}_{l,o} \\
&= -\mathbf{f}_{l,o}^H \left(\mathbf{R}_{\mathbf{bx}}\mathbf{R}_{\mathbf{xx}}^{-1}\Delta\mathcal{H}\mathbf{R} + \mathbf{R}\Delta\mathcal{H}^H\mathbf{R}_{\mathbf{xx}}^{-1}\mathbf{R}_{\mathbf{xb}}\right) \mathbf{f}_{l,o} \\
&= -\mathbf{w}_{l,o}^H \Delta\mathcal{H}\mathbf{g}_{l,o} - \mathbf{g}_{l,o}^H \Delta\mathcal{H}^H \mathbf{w}_{l,o} \\
&= -\Delta\mathfrak{h}^H \mathcal{W}_{l,o}\mathbf{g}_{l,o} - \mathbf{g}_{l,o}^H \mathcal{W}_{l,o}^H \Delta\mathfrak{h}, \qquad \text{(H.8)}
\end{aligned}$$

hence, the $\mathbf{SOT}_{l,3}$ is given by

$$\mathbf{SOT}_{l,3} = \Delta\mathfrak{h}^H \underbrace{4\mathcal{W}_{l,o}\mathbf{g}_{l,o}\mathbf{g}_{l,o}^H\mathcal{W}_{l,o}^H}_{\Psi_3}\Delta\mathfrak{h}. \tag{H.9}$$

Therefore, in conclusion,

$$\mathbf{MEMSE}_{l|\mathcal{H}} = Tr\left(\mathcal{S}_l \cdot \mathbf{R}_{\Delta\mathfrak{h}}\right). \tag{H.10}$$

In the above equation, $\mathcal{S}_l \triangleq \Psi_1\mathbf{R}_{\mathbf{xx}}^{-1}\Psi_1^H + \Psi_2\Xi\Psi_2^H - \frac{\Psi_3}{\mathbf{MMSE}_l}$, in which $\Psi_1 = \mathcal{G}_{l,o} - \mathcal{W}_{l,o}\mathcal{H}^H$, $\Psi_2 = \mathcal{W}_{l,o}\mathbf{R} - \mathcal{G}_{l,o}\mathbf{R}_{\mathbf{xx}}^{-1}\mathbf{R}_{\mathbf{xb}}$, $\Xi = \begin{bmatrix} \mathbf{0}_{(l-1)\times(L-l+1)} \\ \mathbf{I}_{L-l+1} \end{bmatrix} \mathbf{R}_{\Delta,l}^{-1}\left[\mathbf{0}_{(L-l+1)\times(l-1)}, \mathbf{I}_{L-l+1}\right]$ and $\Psi_3 = 4\mathcal{W}_{l,o}\mathbf{g}_{l,o}\mathbf{g}_{l,o}^H\mathcal{W}_{l,o}^H$.

BIBLIOGRAPHY

[1] T. Ojanpera and R. Prasad, "An overview of air interface multiple access for IMT-2000/UMTS," *IEEE Commun. Mag.*, vol. 36, pp. 82–86, 91–95, Sept. 1998.

[2] J. Huber, D. Weiler, and H. Brand, "UTMS, the mobile multimedia vision for IMT-2000: A focus on standardization," *IEEE Commun. Mag.*, vol. 38, pp. 129–136, Sept. 2000.

[3] T. Ottosson and A. Svensson, "On schemes for multirate support in DS-CDMA systems," *Wireless Personal Communications*, vol. 6, pp. 265–287, March 1998.

[4] E. A. Sourour and M. Nakagawa, "Performance of orthogonal Multicarrier CDMA in a multipath fading channel," *IEEE Trans. on Commun.*, vol. 44, pp. 356–367, March 1996.

[5] J. Bingham, "Multicarrier modulation for data transmission: An idea whose time has come.," *IEEE Commun. Mag.*, pp. 5–14, May 1990.

[6] Z. Wang and G. B. Giannakis, "Wireless multicarrier communications where Fourier meets Shannon," *IEEE Signal Processing Mag.*, pp. 29–48, May 2000.

[7] S. Hara and R. Prasad, "Overview of multicarrier CDMA," *IEEE Commun. Mag.*, vol. 35, pp. 126–133, Dec. 1997.

[8] S. Hara and R. Prasad, "Design and performance of multicarrier CDMA system in frequency-selective Rayleigh fading channels," *IEEE Trans. on Vehic. Tech.*, vol. 48, pp. 1584–1595, Sept. 1999.

[9] S. Kondo and L. B. Milstein, "Performance of multicarrier DS CDMA systems," *IEEE Trans. on Commun.*, vol. 44, pp. 238–246, Feb 1996.

[10] R. Nogueroles, M. Bossert, A. Donder, and V. Zyablov, "Improved performance of a random OFDMA mobile communication system," *Proc. IEEE VTC*, vol. 3, pp. 2502–2506, May 1998.

[11] K. Fazel and G. P. Fettweis, *Multicarrier Spreading-Spectrum.* Kluwer Academic Publishers, 1997.

[12] N. Yee, J.-P. Linnartz, and G. Fettweis, "Multi-carrier CDMA in indoor wireless radio networks," *Proc. IEEE PIMRC*, pp. 109–113, Sept. 1993.

[13] M. Tan, P. Zong, and Y. Bar-Ness, "Multi-rate access schemes for MC-CDMA," *Wireless Personal Communications*, vol. 27, pp. 149–182, 2003.

[14] P. Zong, Y. Bar-Ness, and J. Chan, "Performance analysis of a dual-rate synchronous MC-CDMA system," *Proc. IEEE GLOBECOM*, vol. 3, pp. 1380–1384, 2000.

[15] P. Zong, K. Wang, and Y. Bar-Ness, "Performance improvement for low-rate signal in a dual-rate MC-CDMA system with frequency-selective Rayleigh fading channel," *Proc. WPMC*, Sept. 2001.

[16] M. Tan, C. Ibars, and Y. Bar-Ness, "Rate-adaptive convolutional coded fixed spreading length (CCFSL) multi-rate transmission schemes for MC-CDMA," *Proc. WPMC*, vol. 2, pp. 663–667, Oct. 2002.

[17] M. Tan and Y. Bar-Ness, "Maximum spectral utilization efficiency multi-code FSL scheme for multi-rate MC-CDMA," *Proc. 3G Wireless*, 2002.

[18] M. Tan and Y. Bar-Ness, "Performance comparison of the multi-code fixed spreading length (MFSL) scheme and variable spreading length (VSL) scheme for multi-rate MC-CDMA," *Proc. IEEE ISSSTA*, vol. 1, pp. 108–112, Sept. 2002.

[19] P. Zong and Y. Bar-Ness, "Performance of a variable spreading length (VSL) dual-rate MC-CDMA system," *Proc. CISS*, 2001.

[20] A. J. Viterbi, "Very low rate convolutional codes for maximum theoretical performance of spread-spectrum multi-access channels," *IEEE J. Select Areas Commun.*, vol. 8, pp. 641–649, May 1990.

[21] A. Duel-Hallen, "Performance of multiuser zero-forcing and MMSE decision-feedback detectors for CDMA channels," *Proc. IEEE GLOBECOM*, pp. 82–86, 1993.

[22] P. K. I., K. T. E., S. I., and H. J. M., "Practical implementation of successive interference cancellation in DS/CDMA system," *Proc. Universal Personal Communications*, vol. 1, pp. 321–325, Sept. 1996.

[23] R. M. Buehrer, "Equal BER performance in linear successive interference cancellation for CDMA systems," *IEEE Trans. on Commun.*, vol. 49, pp. 1250–1258, July 2001.

[24] G. Mazzini, "Equal BER with successive interference cancellation DS-CDMA systems on AWGN and Ricean channels," *Proc. IEEE PIMRC*, pp. 727–731, July 1995.

[25] A. J. Goldsmith and P. P. Varaiya, "Capacity of fading channels with channel side information," *IEEE Trans. on Inform. Theory*, vol. 43, pp. 1986–1992, Nov. 1997.

[26] M. Tan, C. Ibars, and Y. Bar-Ness, "Optimal power distribution control for multicode MC-CDMA with zero-forcing successive interference cancellation," *to appear in the EURASIP Journal on Applied Signal Processing*, 2004.

[27] M. Tan and Y. Bar-Ness, "Optimal power distribution control for multicode MC-CDMA with zero-forcing successive interference cancellation," *Proc. IEEE WCNC'04*, 2004.

[28] M. Tan and Y. Bar-Ness, "Equal BER power distribution control for multicode MC-CDMA with MMSE successive interference cancellation," *to appear in the IEEE International Conference on Communications (ICC)*, 2004.

[29] M. Tan and Y. Bar-Ness, "Equal BER power control for uplink MC-CDMA with MMSE successive interference cancellation," *to appear in IEEE Commun. Lett.*, 2004.

[30] M. Tan and Y. Bar-Ness, "Effect of channel estimation errors on the performance of MMSE-SIC with equal BER power control," *submitted to the IEEE VTC'04*, March.

[31] A. P. Liavas, "On the robustness of finite-length MMSE-DFE with respect to channel and second-order statistics estimation errors," *IEEE Trans. on Signal Processing*, vol. 50, pp. 2866–2874, Nov. 2002.

[32] A. Leon-Garcia, *Probability and Random Processes for Electrical Engineering.* Addison-Wesley, 1994.

[33] W. C. Jackes, *Microwave Mobile Communications.* New York, Wiley, 1974.

[34] M. Saquib, R. Yates, and N. Mandayan, "Decorrelating detectors for a dual rate synchronous DS/CDMA channel," *Wireless Personal Communications*, pp. 197–216, 1999.

[35] J. Chen and U. Mitra, "Analysis of decorrelator-based receivers for multi-rate DS/CDMA communications," *IEEE Trans. on Vehic. Tech.*, vol. 48, pp. 1966–1983, 1999.

[36] U. Mitra, "Comparison of maximum-likelihood-based detection for two multirate access schemes for CDMA system," *IEEE Trans. on Commun.*, vol. 47, pp. 64–77, Jan. 1999.

[37] P. Viswanath, V. Anantharam, and D. N. C. Tse, "Optimal sequences, power control, and user capacity of synchronous CDMA systems with linear MMSE multiuser receivers," *IEEE Trans. on Inform. Theory*, vol. 45, pp. 1968–1983, Sept. 1999.

[38] J. G. Proakis, *Digital Communications.* McGraw-Hill, Inc., 1995.

[39] J. Hagenauer, N. Seshadri, and C.-E. Sundberg, "The performance of rate-compatible punctured convolutional codes for digital mobile radio," *IEEE Trans. on Commun.*, vol. 38, pp. 966–980, July 1990.

[40] C. Ibars and Y. Bar-Ness, "The principle of time-frequency duality of DS and MC CDMA," *Proc. CISS*, 2002.

[41] J. G. Proakis and D. G. Manolakis, *Digital Signal Processing Principles, Algorithms, and Applications.* Prentice Hall, 1996.

[42] T. Guess, "Optimal sequences for CDMA with decision-feedback receivers," *IEEE Trans. on Commun.*, vol. 49, pp. 886–900, Apr. 2003.

[43] M. K. Varanasi, "Decision feedback multiuser detection: A systematic approach," *IEEE Trans. on Inform. Theory*, vol. 45, pp. 219–240, Jan. 1999.

[44] G. K. Kaleh, "Channel equalization for block transmission systems," *IEEE J. Select Areas Commun.*, vol. 13, pp. 110–121, Jan. 1995.

[45] D. G. Luenberger, *Optimization by Vector Space Methods.* Wiley, 1969.

[46] S. Verdú, *Multiuser Detection.* Cambridge University Press, 1998.

[47] N. Al-Dhahir and J. M. Cioffi, "MMSE decision-feedback equalizers: Finite-length results," *IEEE Trans. on Inform. Theory*, vol. 41, pp. 961–975, July 1995.

[48] H. Cheon and D. Hong, "Effect of channnel estimation errors in OFDM-based WLAN," *IEEE Commun. Lett.*, vol. 6, pp. 190–192, Nov. 2002.

[49] L. Scharf, *Statistical Signal Processing: Detection, Estimation and Time Series Analysis.* Addison-Wesley, 1990.